Identification of Aged Cell Types in Mouse Skeletal Muscles

by
Jiwon Seo
B.S., John Jay College of Criminal Justice, 2016
A.S., Queensborough Community College, 2013

Submitted as partial fulfillment of the requirements for the degree of Doctor of Philosophy in the Molecular Biology, Cell Biology, and Biochemistry Graduate Program in the Division of Biology and Medicine at Brown University

May 2024

This dissertation by Jiwon Seo is accepted in its present form by the Department of Molecular Biology, Cell Biology, and Biochemistry as satisfying the dissertation requirement for the degree of Doctor of Philosophy.

Date _____ _____
John M. Sedivy, Ph.D., Advisor

Recommended to the Graduate Council

Date _____ _____
Mark Johnson, Ph.D., Committee Chair

Date _____ _____
Michelle Dawson, Ph.D., Reader

Date _____ _____
Jill Kreiling, Ph.D., Reader

Date _____ _____
Paul Robbins, Ph.D., Reader

Approved by the Graduate Council

Date _____ _____
Thomas A. Lewis, Ph.D.,
Interim Dean of the Graduate School

Jiwon Seo

EDUCATION

Brown University, Providence, RI
PhD, Molecular biology, cell biology, and biochemistry**,** May 2024 (expected)

John Jay College of Criminal Justice, New York, NY
BS, Forensic Science: Molecular Biology and Toxicology Dual-Track, May 2016

Queensborough Community College, Bayside, NY
AS, Liberal Arts & Science – Forensics Dual-Joint, 2013

RESEARCH EXPERIENCE

Brown University
Graduate Study with Dr. John M. Sedivy 2016-2024
Identifying aged cell types in mouse skeletal muscles

- Explored methods such as Basescope, Rnascope Hiplex, Stellaris FISH, and FACs to identify and isolate different muscle resident cell types.
- Developed methods to identify and quantify aged cells in muscles.
- Created probes specific to LINE-1 polymorph sequences.
- Created ORF1 and ORF1 reporter expressing cell lines.

Harvard University
Summer Intern with Dr. Victoria D'Souza Summer 2015
Study of VEGF-Ax translational recoding

- Synthesized RNA elements with varying lengths of upstream nucleotides to be studied.
- Conducted dual-luciferase reporter assay to assess the effects of upstream nucleotides on readthrough.
- Optimized 2D NOESY NMR sample to study the structural change of the Ax element in the presence and absence of hnRNP A2/B1.

John Jay College of Criminal Justice
Undergraduate Researcher with Dr. Shu-Yuan Cheng 2013-2016
Study of cytotoxic effects of fungicides in the context of neurodegenerative diseases

- Optimized the protocols and conducted flow cytometry to study the effects of common fungicides on rat pheochromocytoma (PC12) and human neuroblastoma (SHSY5Y) cells.
- Performed quantitative and qualitative senescence associated β-galactosidase assays to investigate senescence induction after fungicides exposure.
- Conducted a time-course study to evaluate the increased cytotoxic response after prolonged exposure to fungicide and following various recovery periods after exposure.

Research Assistant with Dr. Elise Champei 2014-2015
Mechanism study of chemotherapeutic agents in the context of p53 deficiency

- Synthesized chemotherapeutic agents: mitomycin C and 10-decarbomitomycin C.

- Conducted flow cytometry to assess the cytotoxic effects on p53 preserved and deficient cell lines: MCF-7 and K562.
- Isolated DNA inter-strand crosslinks (ICLs) to examine association of ICLs with cytotoxic responses.
- Conducted flow cytometry to examine the changed response to the drugs after p53 knockdown on MCF-7 with short hairpin RNA.

TEACHING EXPERIENCE

RICKC Youth Group (Rhode Island Central Korean Church)

Director 2018-2024

- Preached for middle and high school students twice a week.
- Provided music classes to form the youth group praise team.
- Served in Operation Committee for the church.
- Found and led the Rides Team; organizing two shuttles and multiple cars to transport college students to church twice a week.
- Found and led Media Team; created a broad caste system to live stream the services. Created church website and developed various free software to aid church services which are currently used by hundreds of churches in USA and Korea. Documented training guides for new sound engineers.
- Served in Praise Team as keyboard.
- Served in Translation Team for Friday young adults' service.

Teacher 2016-2018

- Led Bible Study groups on Sundays.
- Organized various church events.
- Organized summer SAT classes for the community.

Korea Food for the Hungry in Cambodia Summer 2016

Teacher

- Child Development Program: Light International Kindergarten primary teacher for age 5. Assisted in science projects and taught English, Korean, and Music.
- Youth Development Program: English reading, writing, and conversation classes for high school and college students.

HVPC Korean School 2015-2016

Director

- Founded a Korean school for local Korean-American students.
- Earned the sponsorship of Heavenly Voice Presbyterian Church.
- Established cooperative learning relationship with Hyoseong Elementary School in Korea.
- Searching for a publication company to let students translate story books.

HVPC Sunday School

Teacher 2011-2016

- Led Bible Study groups on Sundays.
- Organized various church events and summer camps.

SAT Prep Course 2012-2014

Director

- Organized private classes for middle and high school students.
- Primary focus in SAT I but also extended to SAT II and AP history, literature, and sciences.
- Private tutoring upon individual requests.

NY EduPIA 2011-2012

Co-director

- Executed a digital initiative project: all lessons recorded on video and uploaded to institutional website, all students given private eNook for enhanced learning experience, and real-time parents-teacher online feedback exchange during certain classes.
- Designed K-12th grade math curriculum and all math worksheets.
- Reviewed resumes and invited qualified candidates for interviews.

Galilee After School Summer 2013

Teacher

- Developed SAT program and restructured other programs at this institution.
- Implemented new curriculums and teaching styles for middle and high school students.
- Built active parental involvement through regular progress reports and feedbacks.

HONORS & AWARDS

- Pfizer SOT Undergraduate Award (2015)
- ABRCMS Poster Presentation Award (2015)
- SOT Travel Award (2014)
- ABRCMS Travel Award (2014)
- Kimbo Scholarship (2014)
- CUNY Community Service Scholarship (2012)
- President's Volunteer Service Award (2010)

CONFERENCE PRESENTATIONS

Seo, J., Huang, B.T., Cheng, S.Y., and Champeil, E. p53-independent activation of p21 in response to mitomycin C and decarbamoylmitomycin C. To be presented at Annual Meeting of the Society of Toxicology, New Orleans, LA, March, 2016. Manuscript in preparation.

Seo, J., Wagner, N., and D'Souza M.V., The effects of upstream nucleotides on the readthrough rate of VEGF-Ax. Presented at Annual Biomedical Research Conference for Minority Students, Seattle, WA, November, 2015

Seo, J., Wagner, N., and D'Souza M.V., The effects of upstream nucleotides on the readthrough rate of VEGF-Ax. Presented at Leadership Alliance National Symposium, Stamford, CT, July, 2015.

Seo, J., Ta, C., and Cheng, S.Y. Mancozeb induced cell cycle arrest and senescence via RTP801. Presented at Annual Meeting of the Society of Toxicology, San Diego, CA, March 2015.

Seo, J., Cheng, S.Y., and Champeil, E. Mitomycin C and 10-decarbamoyl mitomycin C activity study on p53 wild-type and deficient cancer cells using flow cytometry. Presented at Annual Biomedical Research Conference for Minority Students, San Antonio, TX, November, 2014.

Acknowledgements

First, I would like to thank wonderful researchers of the Sedivy lab. Dr. Marco De Cecco for helping me fit into the Sedivy laboratory, guiding me in my initial development of the projects, and teaching me the secrets of the RI Food Fights which helped me and my wife gain about twenty pounds before our marriage. Dr. Takahiro Ito for training me with the viral transfections and challenging me with his demonstration of unyielding devotion to his research. Dr. Anna Petrashen for teaching various deadly techniques such as mouse dissection and tissue grinding. My good friend, Dr. Trenton Woodham for continuing the legacy of the RI Food Fights with me, providing incredible insights on burgers, pizzas, and wings. The Xbox and game collections he left with me helped me through my darkest times. Dr. Amy Elias, who taught me how to dance. The music still rings in my head when I shower! The ever humble and considerate, Dr. Alberto Caligiana for teaching me his secret transfection tips. Maxfield Kelsey, a fellow warrior of the StarCraft with lots of wisdom, taught me the joy of casual, small talks. Radha Kalekar, who is always kind and never stops asking if I am okay. I would also like to thank our formidable lab technicians. Gale Golom-Mello, who always knew the whereabouts of any supply I inquired. Bianca Kun, the fierce reformist who changed many of the old and inefficient systems of the lab. Jess Anderson, who is somehow executing a million different tasks in the midst of the lab relocation.

Second, I would like to thank my mentors. Dr. Mark Johnson, the current chair of my committee, was the face of the MCB program when I began my study here at Brown. He led all graduate events and seminars, and I was truly touched by the commitments he showed to the students. It was clear that he puts the students before anything, and uncoincidentally, whenever

I email something to my committee, he is the first person to respond. That alone demonstrates his care and attention, and I was greatly encouraged.

I am truly blessed with having another very committed mentor, Dr. Ashley Webb. She was the previous chair of my committee who now works at the Buck Institute for Research on Aging. I had heard how detailed her advice are on developing and presenting the research, and I could see that during the committee meetings. What came as a surprise was the concerns and kindness she showed outside the meetings. She had heard of my medical crisis and shared her personal stories. I could feel how deeply troubled she was for me, and I am truly grateful for her words of comfort. She reached out to me even after resigning from the committee to check and make sure I was okay. I wanted to somehow express my gratitude but couldn't find the right opportunity before her relocation. So, I say now. Thank you.

Dr. Michelle Dawson is not only a reader of my committee but my previous adviser. I was one of her first rotation students when she joined Brown. She probably had a lot of things to deal with after the move, but she always allocated a time to talk with me one to one. She showed genuine interest in helping me develop my career and made me feel like I can depend on her if anything went wrong. Even though my time at her lab was very short, strangely, one advice during this time stuck with me. As a busy rotation student, I was always "running like a headless chicken" as Marco phrased. She had Deepraj (the postdoc who trained me) tell me I could create an air movement that contaminates the cells in the hood. I had never thought about this, but it made a lot of sense and I kept this in mind. Years later, I was trained to do peritoneal dialysis at home, and it was all about how to avoid contamination. One chapter of the training was dedicated to controlling the air flow; how I must shut down all windows, close all doors, turn off the AC, and make slow movements to not disturb the air around the open port. As I must do this every night, I slowly perform the tasks while replaying Deepraj's advice in my head: do not rush; do not disturb

the air! I have a feeling this advice will never be forgotten (Shout-out to Deepraj, my current apartment neighbor and a fellow K-drama lover).

Dr. Jill Kreiling only recently joined my committee, but I probably spent the most time with her. As her lab is right next to ours, I often bump into her during my work and over the years I learned that if I have any question, and if I want to make sure I get the right answer, I should ask her. From things like finding a supply to an expert advice on a technique, she always give me the best answers. I could think of no better person to invite to my committee when Ashley left.

Dr. John Sedivy is my adviser. I was still an undergraduate researcher at a small college when I got introduced to his wife, Dr. De Long, at an undergraduate research symposium. My research at the time was on senescence and cancer, and I was interested with the works of Dr. Sedivy. I was simply expressing this interest to Barbara Khan, who was the graduate coordinator of the symposium I happened to get friendly with, when she said she was also from Brown University and led me to Dr. De Long. I had no idea at the time that Dr. De Long would be teaching me the graduate core a year later and that I would be working with Dr. Sedivy two years later. I still don't understand how I could join his laboratory. It was a thrilling privilege and an undeserved fortune. As a renowned scientist, I expected him to be too busy to spend much time on mentoring me. He was always on call with other scientists and somehow had more paper works on his desk than what's on our desks combined. But this did not stop him from focusing on my projects when we met. In my earliest email communications with him, I included random references and supplementary data just in case we get into discussing some of them. When we met, I realized I was wrong. Dr. Sedivy read every fine print attached to my email. Even things on a disorganized supplementary data had not escaped his scrutiny and I felt guilty for making him go through everything. I was deeply touched by the amount of attention he pours in mentoring me and was also motivated to be a thorough reader. I was always determined to do the best to repay for the opportunity and trust I received. It's regrettable that an illness occurred to severely limit my

capacity in recent years. It only took a few months for me to realize that I am not going to recover, and my work output could only be a fraction of what it used to be. I thought about what the best course of action in my current circumstance would be. Should I quit work now that I can't fully do what I am paid for? Should I carry on until I produce at least one paper so the resource and time he invested are not wasted? I decided to wait for him to assess my condition and start the discussion in one way or the other. Weeks went by. Months passed. The year changed. But only thing he asks me when we meet is, "how are you feeling?" He was okay with me taking things easy and working at my pace. He was extremely understanding and considerate of my circumstances. I actually have multiple email drafts in my inbox that say I am quitting graduate school. I had a few appointments with my social worker to talk about transitioning out of the graduate school. I even told my primary care doctor one time that I am quitting school next week. There were many weekends I finally made up the mind to give up everything because I felt so weak and tired. Somehow, he must have read my mind, because he would cancel the meeting before I say anything, and I get another week to think about my decision. In the end, what kept me going was this: I am not giving up until he does. If he is willing to support me and continue to mentor me despite all this, I have no right to give up. I still didn't believe I could finish the graduate study, but I decided to continue one more week at a time since he expected to see me the next week. Our weekly meetings are what sustained my life, and I am grateful for the relentless support and unbelievable patience Dr. Sedivy demonstrated. He was on this very difficult journey right next to me.

I would like to thank my medical team. The kind and skilled nurses who brought me back to life several times when I lost consciousness during hemodialysis. You always complained how the company don't fix the water equipment and make you clean the flood all the time, but you never complained when I vomited and created a mess on the floor. Barbara, my first PD nurse, who trained me with extreme zeal. Shawna who rescued me from the yearlong cough by

suggesting Allegra. Eve who out of kind heart, tries to distract my mind by going over the drug list while I am needled (to tell you the truth, it never worked). Charles for giving me strength to go on when I was deeply distressed by my conditions. Lisa the RN for her morning calls reminding appointments, and Lisa the RD for keeping close watch over my ice-cream consumptions. Dr. Dragomire who shows great interest in my research and makes the best calls with the treatments. Kind, elderly folks at East Side Providence Dialysis Center who adopted me as their new grandson from day one and made sure the nurses take extra good care for me. Last but not least, Dr. George Lee. You have literally saved my life with your urgent calls. You rushed to my side even on weekend mornings to personally check my condition even when I am surrounded with other doctors and nurses. You were always kind in answering questions I had on my disease and readily got into in depth discussions on various treatment options. I was comforted and really looked forward to seeing you every week. It somehow put my mind at ease when I am with you. I felt assured and safe. I had said this when you told me you are retiring, but I really meant it. You are a good doctor, and I am deeply touched by everything you did for me. Had I met you earlier in my life, I would have aspired to be a medical doctor just like you.

Lastly, I would like to thank my family and friends at church. My mother, who had offered her kidney. We had went through a lot together past few years, more than what can be described in words. I feel like I learned you more in the few years that we struggled together than in any other time and I am glad I had this experience. You had been my shelter and steady stronghold. I could forget about the worries about my life by listening to your chats over the phone. When we talk, magically, everything seems fine. I am happy to be born your son. My father, who is also fighting his fight. You got diagnosed with cancer a month before my illness, but you kept this from me. You were all alone in your fight so I can focus on my fights, and that’s how you’ve always expressed your love to the family. You always put the family before you, and I am sorry I couldn’t be of help when you were struggling. You are a father I can proudly boast, and I am lucky to be

your son. My brother, I know I had neglected you past few years. When our father was ill and mother distressed, I was not there to do anything. You had to face it all. Watch it and deal with it in your daily life. I am sorry I couldn't be the good elder brother. I had never expressed but I am thankful that you are keeping our mother in company. You being there so she is not alone is such an assurance. I know it can be a burden and I do wish to take if off your shoulder as soon as possible. My father-in-law, I always feel guilty in front of you. When I asked for your daughter, you made me promise just one thing: be healthy. I took your words lightly as I was confident with my health and did not expect to be ill a year later. Knowing your character, I expected your rage, but I was surprised to see your tears instead. You offered your kidney when my mother was disqualified and actively looked for ways to make it happen despite living in different countries and having different blood types. I now know what it means to be part of a new family. We have not known each other for long, but my heart is filled with compassion towards you just like how it does toward my father. My mother-in-law who is on my side more than your own daughter's side. Your kind words of wisdoms and comforts have a soothing effect on me and Hyeon. There is a mystical power in your voice. I love eavesdropping as Hyeon talks to you over the phone. It gives hope that things will get better soon. It untangles our minds. We are at peace knowing your prayers. Jin and Perry, my sister and brother-in-law, we are a thousand miles apart, but I feel like we live in the same apartment. I come home every day with your voice on the phone and they go on until the bedtime. We have only met a few times in person, but I somehow know just about everything: how you thought you lost the bracelet Hyeon sent you, how Perry's friends came over to watch LoL Championship, and how our baby nephew is growing so fast. These casual talks really keep Hyeon alive and bring cheerful energy in our home. Thank you for being a good sister for her.

Hyeon, my wife. I see that you went into the room so I can write this in private. Well, I actually don't have much to say about you. But I do, out of good consciousness, must

acknowledge your contributions to this work. For a year when I was too weak to walk to the lab, you became my Uber driver dropping and picking me up multiple times a day whenever I called. For half a year when I couldn't move my right arm after a surgery, you sneaked into the lab with me at night and performed all those TC works and cloning under my supervision. I still wonder why some of the single cell clones ended up being heterozygous but without your aid, none of this could have happened. Every night you help set up the dialysis, throw out trash bags larger than your size, refill the humidifier, and turn on the heat, all so that I can sleep. You jump up at night when I moan and stay by my side when the pain keeps me awake. I make fun of how you like to nap during the day, but I know it's my fault that you are awake at night. You complain how you don't have the time to do your work, but you were always available to help make figures for this paper. This paper really deserves your name and not mine. You were my hands and my feet, but I can't do the same for you. So, take my heart as yours. It's yours forever.

"Trust in the LORD with all your heart
and lean not on your own understanding;
in all your ways submit to him,
and he will make your paths straight."
(Proverbs 3:5-6)

God be Glorified.

Table of Contents

Signature Page ……iii

Curriculum Vitae ……iv

Acknowledgements ……vii

Table of Contents ……xiv

List of Tables ……xviii

List of Figures ……xix

Chapter 1: Introduction ……1

The debate over senescence in muscle aging ……2

Sarcopenia: age-associated loss of muscle mass and function ……2

Senescence in skeletal muscles ……2

Searching for the origin of muscle aging ……4

The mitotic muscle resident cells ……4

LINE-1 retrotransposable element as a potential aging marker in muscles ……7

Reference ……9

Chapter 2: Identifying Aged Cells ……14

Background ……15

Methods ……17

Dissecting mouse hind limb muscles ……17

Measuring the cross-sectional area of mouse myofibers ……18

Senescence associated beta galactosidase assay ……18

Creating etoposide induced senescent human lung fibroblasts ……19

Immunofluorescence labeling of senescence markers ……19

Transfection of MT302 LINE-1 overexpression plasmid in HeLa ……19

Stellaris L1 mRNA FISH ……19

Designing p16 mRNA probe ……20

Basescope Assay with p16 ……20

Consecutive muscle sectioning and signal validation ……21

Basescope Duplex assay with p16 and p21 ……21

ORF1 staining ……22

Results ……23

Performing SA-β-gal assay on mouse geriatric muscles ……23

Inducing senescent LF1 ……24

Using Stellaris L1 mRNA probe to identify aged cells ……24

Using Basescope Assay to analyze aged muscles ……26

Using ORF1 as an aging marker in muscles ……29

Discussion ……31

Reference ……36

Chapter 3: Identifying Muscle Resident Cell Types ……..…37

Background ……38

Methods ……40

GentleMACS muscle digestion ……40

TRIzol RNA extraction ……40

FACS ……41

The RNAscope Hiplex Assay ……41

Quantifying cell types ……42

Results ……44

Digesting mouse muscles into single cells ……44

FACS on mouse hind limb muscles ……44

RNA extraction on individual cell types ……48

The RNAscope HiPlex Assay ……49

Discussion ……53

Reference ……56

Chapter 4: Identifying Aged Cell Types in Muscles ……57

Background ……58

Methods ……59

Co-Detection ……59

Consecutive cryosections and thickness optimization ……60

Analysis of the triplet assays ……60

Results ……62

RNAscope integrated Co-Detection Assay ……62

Combining ORF1 IF with the HiPlex ……63

Combining p21 Basescope Assay with the HiPlex ……65

Combining p21 Basescope Assay and ORF1 IF with the HiPlex ……66

Discussion ……69

Reference ……72

Chapter 5: Discussions ……73

Summary ……74

Limitations ……76

Future Direction ……77

Appendix A: Addressing the Autofluorescence ……80

Appendix B: Quantifying Basescope Results in Muscles ……83

Appendix C: Detecting LINE-1 Polymorph Sequences ……90

Supplementary Data ……97

List of Tables

Table 3.1. Surface markers and conjugates used for the FACS ……..……46

Table 3.2. Percentages of different cell types collected by FACS ……46

Table 3.3. Cell counts for each cell type collected out of hind limb muscles of 2 mice …..48

Table 3.4. RNA extractions from muscle digests before FACS ……48

Table 3.5. Muscle digest before FACS is serially diluted before RNA extractions ……49

Table 3.6. Muscle resident cell types investigated with corresponding markers …….49

List of Figures

Fig. B1. RNAscope Probes ……..……..……..……16

Fig. 2.1. Senescence associated beta galactosidase assay on mouse geriatric muscles …….23

Fig. 2.2. Etoposide induced senescence in human lung fibroblasts (LF1) ……24

Fig. 2.3. Using Stellaris L1 mRNA probe as a new aging marker ……..25

Fig. 2.4. Development and validation of the p16 Basescope probe ……..27

Fig. 2.5. Analyzing aged muscles with Basescope ……...28

Fig. 2.6. Using ORF1 as an aging marker in muscles ……..29

Fig. B2. RNAscope HiPlex procedure ……40

Fig. 3.1. Preparing mouse muscle samples …….45

Fig. 3.2. FACS on mouse muscle digest ……47

Fig. 3.3. RNAscope HiPlex Assay on 29 months mouse quadriceps muscles ……..50

Fig. 3.4. Initial muscle distribution data with HiPlex on 29 months muscles ……52

Fig. 4.1. Co-detection of RNA and proteins ……63

Fig. 4.2. Combining ORF1 protein detection with HiPlex ……64

Fig. 4.3. Combining p21 mRNA detection with Basescope and the cell type identification with HiPlex …..65

Fig. 4.4. Cross referencing HiPlex results with p21 and ORF1 staining of the same cells ……67

Fig. 4.5. Comparing the results from the triplet combination experiments of the young and old muscles …68

Fig. 5.1. CINtec p16 Histology for human p16 protein detection ……78

Fig. 5.2. Speculated look of the reference data ……79

Fig. A1.1. Addressing the autofluorescence ……....82

Fig. A2.1. Various illustrations to show RNA signals and nuclei arrangements ……85

Fig. A2.2. Working with the real data to find the distance maximum ……87

Fig. A2.3. Matrix of RNA signals vs. nuclei signals ……88

Fig. A2.4. Applying the script to ten fields of views ……...89

Fig. A3.1. L1 polymorph sequences against human and baboon fibroblasts ……92

Fig. A3.2. Testing distinguishing powers of L1 probes with transfected 3T3 ……...94

Fig. A3.3. Attempts at making stably expressing 3T3 ……...96

Supp. Data 1. L1HS Stellaris probes sequences ……98

Supp. Data 2. L1 polymorph specific Basescope probes design ……..99

Supp. Data 3. Mathematical determination of two sources of the false positives ……...100

CHAPTER 1:

Introduction

The debate over senescence in muscle aging

Sarcopenia: age-associated loss of muscle mass and function

About half of the geriatric population suffers from sarcopenia, an age-associated loss of skeletal muscle mass and function[1]. Sedentary life style of the elderly contributes to some loss of the muscle mass, but fails to explain the sudden acceleration of the muscle loss that occurs by the eighth decade of life[2]. An early study in muscle aging identified reduced number of muscle stem cells, known as the satellite cells, as the major cause of the reduced muscle mass[3]. However, a more recent study revealed that the reduced satellite cell count alone does not trigger sarcopenia: the features of sarcopenia is only observed in the geriatric mice (28-32 months) whose satellite cell count is similar to the old mice (20-24 months)[4]. Further investigation with geriatric satellite cells demonstrated markedly diminished capacity to proliferate, which in addition to other markers, indicated cellular senescence[4].

Senescence in skeletal muscles

Cellular senescence is a state of irreversible cell cycle arrest caused by various cellular stresses including DNA damage, oncogene activation, oxidative stress, and telomere erosion[5,6]. Biomarkers of senescence include upregulation of p16 and p21, appearance of telomere induced foci, DNA damage markers, senescence-associated heterochromatin foci (SAHF), and senescence-associated beta-galactosidase activity[7]. More recently, senescence-associated secretory phenotype (SASP) is recognized as important biomarker and functional effector of senescence[8]; senescent cells secrete soluble factors that can modulate extracellular matrix, trigger immune response, and promote or inhibit proliferation[8]. Accumulation of senescent cells with age results in chronic inflammation that contributes to the age-associated tissue dysfunction[9]. The causal role of cellular senescence in aging is increasingly being recognized. Senescent cells are shown to reduce both the lifespan and healthspan[10], and selective removal of senescent cells

are shown to restore juvenile traits in normal[10] and progeria mouse models[11]. Clearance of senescent cells or inhibition of SASP ameliorated symptoms of various age-related diseases such as atherosclerosis and osteoarthritis[12].

The role of senescence in sarcopenia had also been explored in the past, but the initial studies failed to affirm the effects of senescence in muscle aging[13,14]; use of crude muscle homogenates and nuclear fraction at the time may not have given sensitivity necessary to detect transcriptional changes observed in specific cells. Recently, senescent satellite cells became popular research subject of the muscle aging field. With improved isolation techniques, the presence and functional defects of senescent satellite cells were clearly demonstrated by the Rando group[4]. Furthermore, introduction of active satellite cells greatly enhanced muscle regeneration and compensated for the volumetric muscle loss from injury[15]. These studies, however, lack direct connection with muscle aging. An awakening paper by Fry et al.[16] shows that near complete depletion of satellite cells in young adult mice eradicated muscle regenerative capacity but this did not lead to reduction in muscle volume as in sarcopenia. Hence, the loss of muscle regeneration by lack of satellite proliferation cannot fully explain age-associated loss of muscle mass.

What had escaped the scrutiny of the Rando group are the many effects of senescence beyond the cell cycle arrest. Chronic inflammation is a well-known associate of sarcopenia and commonly reported inflammation factors include notable SASP proteins: IL-6 and TNF-α[17,18,19]. In rats, reduction of chronic inflammation by ibuprofen treatment for five months ameliorated age-associated decline of muscle mass[20], suggesting causal relationship between the chronic inflammation and sarcopenia. In addition, IL-6 and TNF- α are known to be regulated by NF-κB, activation of which caused inflammation and inhibition resulted in the improved muscle mass[21,22]. Skeletal muscle NF-κB activation is known to increase with age and with sedentary lifestyle[23]. As increased activity of NF-κB is also a well-known characteristic of senescence[6,8], senescent

muscle cells may be driving sarcopenia by SASP induced inflammation. In fact, selective removal of p16 positive cells in progeria mouse have shown to increase muscle fiber diameter and enhance performance in treadmill exercises[24]. Together with the data reported by Fry et al.[16], it can be speculated that the presence of senescent satellite cells rather than the absence of active satellite cells triggers sarcopenia.

The traditional definition of the senescence is a state of cellular arrest due to the aging. However, recent studies demonstrate that post mitotic cells are also undergoing age related changes, express typical senescence biomarkers, and influence other cells through SASP [52, 53, 54]. We had been using cellular arrest as the primary metric of the senescence because it is readily identifiable feature of an aged cell. However, the halted replication is not the cause of the various molecular changes associated with the senescence. Rather, it is one of the many effects of the characteristic molecular changes seen in the aged cells. Old cells accumulate DNA damage, and this triggers the increased expressions of a set of genes which includes CDK inhibitors like p21/p53 and p16. These changes in the gene expression promotes cell cycle arrest for the mitotic cells. For the post mitotic cells, it would still have the same cell cycle suppression effects, but it is not noticed because the cells had not been replicating. We call a set of aged cells that demonstrate certain changes in the gene expression as senescent, but these senescent cells should not be limited to the mitotic cells that stopped replicating. The real causes of the senescent phenotypes are in the changed gene expression due to DNA damage and environmental stress, and the real impact of the senescent cells in aging is with their inflammatory state. Therefore, we should now define senescent cells as a set of aged cells exposed to enough DNA damage and stress to exhibit a well characterized set of aged gene expressions and secrete inflammatory factors. It is already known that some post mitotic cells such as neurons and myofibers do demonstrate senescence like changes in the gene expression (increased CDK inhibitors), secrete SASP, and also are responsive to SASP [52, 54]. Therefore, in our new definition of the senescence,

the post mitotic cells like the skeletal muscles can also be senescent. Further research is needed to identify the changes in the gene expression that best define the senescent population. For now, we propose increased expression of CDK inhibitors p16 and p21 to best reconcile the traditional and evolved definitions of the senescence as they both relate to the changes leading to the cell cycle arrest.

Searching for the origin of the muscle aging

The mitotic muscle resident cells

If the primary contribution of senescent satellite cells is in the secretion of inflammatory factors rather than the halted myogenesis, other senescent cells in muscle are likely to make equal, if not greater, contribution. Endothelial cell, fibro/adipogenic progenitor (FAP), and leukocytes are other cell types in skeletal muscle that may enter senescence. These cells constitute considerable part of the skeletal muscle and their role in muscle aging is increasingly being recognized. For instance, a subpopulation of the FAPs cells is reported to show high expression of p16 along with other senescence related genes. Interestingly, p21 is another potential hallmark of muscle aging, expression of which is shown to increase in most muscle types, but not from the mitotic muscle resident cells[39]. This suggests that while p16 is a good aging marker for the FAPs cells, p21 is the better marker for the myofibers. In other words, even within the same tissue environment, different cell types exhibit different aging phenotypes and it's important to find the right aging marker suitable for the study of each cell type. Notable cell types within skeletal muscles include the myofibers, the endothelial cells, the fibro/adipogenic progenitor cells, the satellite cells, the leukocytes, the neurons, and the tenocytes.

Endothelial cells are juxtaposed to the satellite cells and secrete soluble factors such as IGF-I, HGF, bFGF, PDGF-BB, and VEGF, which stimulate satellite cell growth[25]. Myogenesis is drastically impaired without endothelial cells, affirming its critical role in muscle development and

repair[25]. The cross talks between endothelial cells and stem cells through soluble factors are well established in hippocampus[26] and in bone marrow[27], and is increasingly being recognized in muscle[28]. In terms of aging, when endothelial cells are exposed to TNF-α *in vitro*, endothelial cells enter senescence through NF-κB activation and display SASP[29]. This strongly suggests that the increased level of TNF-α by age-associated chronic inflammation can promote senescence in endothelial cells, which in turn amplify SASP effects. Altered metabolism of senescent endothelial cells may also contribute to the muscle aging by disrupting normal secretion of the myogenic factors[30].

Fibro/adipogenic progenitors (FAP) reside in the interstitial space of muscle tissue but they are not part of the muscle lineage. FAPs are unable to generate myofibers, and instead have high tendency to differentiate as adipocytes[31]. When given appropriate stimuli, they are able to generate osteoblasts, smooth muscle, and fibroblasts, as well[32]. These characteristics are also seen with the muscle-derived mesenchymal stem cells (MSC), which are isolated by a slightly different set of surface markers[33]. To this date, functional difference between FAP and MSC is unclear and they are often considered alike. FAPs are known to create favorable environment for the satellite expansion and play critical role in muscle regeneration[31]. Loss of regenerative capacity in dystrophic muscles coincides with impaired ability of FAPs to support satellite expansion[34]. FAPs also respond to the immune signals and aid in the clearance of necrotic cells by phagocytosis[35]. With age, FAPs become committed to fibro-adipogenic lineage and lose its ability to promote satellite expansion[35]. This contributes to the reduced regenerative capacity, increased fibrosis, and increased fat deposition in the aged skeletal muscle. Interestingly, adipocytes derived from FAPs are less sensitive to the insulin compared to those derived from the adipose stroma cells, and increased adipocyte commitment of FAPs may contribute to the age-associated insulin resistance[36]. Senescence of FAPs had not been investigated, but a study in the muscle dystrophy mouse model discussed functional impact of age associated epigenetic

changes in FAPs[34,37]. Senescence in mesenchymal stem cells (MSC) of other tissues, on the other, is well documented[38].

LINE-1 retrotransposable element as a potential aging marker in muscles

While detailed characterization of senescent cells in skeletal muscle is lacking, senescence studies *in vitro* provide valuable insights to what may also occur in the muscle. Whole genome analysis of cultured senescent human diploid fibroblasts (HDF) revealed global relaxation of chromatin: while senescent cells are known to display distinct heterochromatin foci, many other regions become more permissive[40]. Notably, repetitive sequences such as LINE-1 are de-repressed in senescent cells[40], which suggests that the increased LINE-1 transcription with age[41] is due to accumulating senescent cells. LINE-1, or long interspersed nuclear element 1, is a transposable element comprising approximately 17% of the human genome[42]. LINE-1 is more specifically classified as retrotransposable elements, because like a retro virus, its transcript is reverse transcribed and inserted back into the genome[43]. Only a fraction of these elements in human genome retains high transposition efficiency *in vitro*[44], but successful LINE-1 insertion into key genes can lead to destructive consequences[45,46]. Recently, increased retrotransposition is identified as possible cause of markedly shorter lifespan in a social insect[47], reinforcing the increasing recognition of LINE-1 contribution to aging.

Senescent cells are also noted to exhibit decreased level of TREX1, which degrades single-stranded DNA in cytosol[48]. Decreased TREX1 is associated with increased accumulation of cytosolic LINE-1 cDNA[49]. Treatment of cells with genotoxic agents is also shown to increase cytosolic DNA, which may be derived from retrotransposable elements[50]. Cytosolic DNA is detected by cyclic GMP-AMP synthase (cGAS), which triggers the activation of Stimulator of Interferon Genes (STING)[51]. cGAS-STING response leads to the activation of immune genes such as type-I interferon (INF-I)[51,49,50]. IFN-I, in turn, provokes SASP and inflammation: hepatic stellate cells of mice lacking STING gene expressed substantially less SASP factors[48]. It is,

therefore, conceivable that the increased LINE-1 transcription in senescent cells by epigenetic de-repression, together with decreased TREX1 cytosolic DNA degradation enzyme, leads to the LINE-1 cDNA accumulation in the cytosol. This in turn elicits IFN-I response, which seems to be essential for mature SASP. Nearby cells would also enter senescence by the paracrine effect and amplify SASP. Persistent inflammatory cytokines thus secreted cause age-associated chronic inflammation. Use of LINE-1 as an aging marker in muscle may reveal the mechanism by which a small population of specific muscle resident cell types drives the decline of muscle mass and function with age.

REFERENCE

1. Arthur, S. T. & Cooley, I. D. The effect of physiological stimuli on sarcopenia; Impact of Notch and Wnt signaling on impaired aged skeletal muscle repair. Int. J. Biol. Sci. 8, 731–760 (2012).

2. Doherty, T. J. Invited review: Aging and sarcopenia. J. Appl. Physiol. 95, 1717–27 (2003).

3. Renault, V., Thorne, L.-E., Eriksson, P.-O., Butler-Browne, G. & Mouly, V. Regenerative potential of human skeletal muscle during aging. Aging Cell 1, 132–9 (2002).

4. Sousa-Victor, P. et al. Geriatric muscle stem cells switch reversible quiescence into senescence. Nature 506, 316–321 (2014).

5. Rufini, A., Tucci, P., Celardo, I. & Melino, G. Senescence and aging: The critical roles of p53. Oncogene 32, 5129–5143 (2013).

6. Watanabe, S., Kawamoto, S., Ohtani, N. & Hara, E. Impact of senescence-associated secretory phenotype and its potential as a therapeutic target for senescence-associated diseases. Cancer Sci. 108, 563–569 (2017).

7. Jesus, B. B. De & Blasco, M. A. Assessing Cell and Organ Senescence Biomarkers. Circ. Res. 111, 97–109 (2016).

8. Salama, R., Sadaie, M., Hoare, M. & Narita, M. Cellular senescence and its effector programs Cellular senescence and its effector programs. cold spring Harb. Lab. Press 99–114 (2014). doi:10.1101/gad.235184.113

9. Freund, A., Orjalo, A.V., Desprez, P., Campisi, J. Inflammatory networks during cellular senescence: causes and consequences. trends Mol. Med. 40, 1301–1315 (2012).

10. Baker, D. J. et al. Naturally occurring p16 Ink4a-positive cells shorten healthy lifespan. Nature 530, 184–189 (2016).

11. Baar, M. P. et al. Targeted Apoptosis of Senescent Cells Restores Tissue Homeostasis in Response to Chemotoxicity and Aging. Cell 169, 132–147.e16 (2017).

12. Childs, B. G. et al. Senescent cells: An emerging target for diseases of ageing. Nat. Rev. Drug Discov. 16, 718–735 (2017).

13. Sakuma, K. & Yamaguchi, A. Sarcopenia and cachexia: The adaptations of negative regulators of skeletal muscle mass. J. Cachexia. Sarcopenia Muscle 3, 77–94 (2012).

14. Sakuma, K., Aoi, W. & Yamaguchi, A. Current understanding of sarcopenia: possible candidates modulating muscle mass. Pflugers Arch. Eur. J. Physiol. 467, 213–229 (2014).

15. Quarta, M. et al. Bioengineered constructs combined with exercise enhance stem cell-mediated treatment of volumetric muscle loss. Nat. Commun. 8, 1–17 (2017).

16. Fry, C. S. et al. inducible depletion of satellite cells in adult, sedentary mice impairs muscle regeneration capacity but does not contribute to sarcopenia. Nat. Med. 21, 76–80 (2015).

17. Beyer, I., Mets, T. & Bautmans, I. Chronic low-grade inflammation and age-related sarcopenia. Curr. Opin. Clin. Nutr. Metab. Care 15, 12–22 (2012).

18. Bian, A. L. et al. A study on relationship between elderly sarcopenia and inflammatory factors IL - 6 and TNF - α. Eur. J. Med. Res. 4–11 (2017). doi:10.1186/s40001-017-0266-9

19. Schaap, L. A. et al. Higher Infl ammatory Marker Levels in Older Persons : Associations With 5-Year Change in Muscle Mass and Muscle Strength. J. Gerontol. Med. Sci. 64, 1183–1189 (2018).

20. Rieu, I. et al. Reduction of low grade inflammation restores blunting of postprandial muscle anabolism and limits sarcopenia in old rats. J. Physiol. 22, 5483–5492 (2009).

21. Li, H., Malhotra, S., Kumar, A. Nuclear Factor-kappa B Signaling in Skeletal Muscle Atrophy. J. Mol. Med. 86, 1113–1126 (2009).

22. Mourkioti, F. et al. Targeted ablation of IKK2 improves skeletal muscle strength , maintains mass , and promotes regeneration. J. Clin. Invest. 116, (2006).

23. Buford, T. W., Cooke, M. B., Manini, T. M., Leeuwenburgh, C. & Willoughby, D. S. Effects of age and sedentary lifestyle on skeletal muscle nf-κb signaling in men. Journals Gerontol. - Ser. A Biol. Sci. Med. Sci. 65 A, 532–537 (2010).

24. Baker, D. J. et al. Clearance of p16 Ink4a-positive senescent cells delays ageing-associated disorders. Nature 479, 232–236 (2011).

25. Christov, C., Chretien, F., Abou-Khalil, R., Bassez, G., Vallet, G., Authier, F., Bassaglia, Y., Vasily, S., Shahragim, T., Chazaud, B., Gherardi, R. K. Muscle satellite cells and endothelial cells: close neighbors and privilaged partners. Mol. Biol. Cell 18, 1397–1409 (2007).

26. Palmer, T. D., Willhoite, A. R. & Gage, F. H. Vascular niche for adult hippocampal neurogenesis. J. Comp. Neurol. 425, 479–494 (2000).

27. Suda, T., Arai, F. & Hirao, A. Hematopoietic stem cells and their niche. Trends Immunol. 26, 426–433 (2005).

28. Dinulovic, I., Furrer, R., Handschin, C. Plasticity of the muscle stem cell microenvironment. Adv. Exp. Med. Biol. 1041, 141–169 (2017).

29. Khan, S. Y. et al. Premature senescence of endothelial cells upon chronic exposure to TNFα can be prevented by N-acetyl cysteine and plumericin. Sci. Rep. 7, 1–13 (2017).

30. Coppé, J.-P. et al. Senescence-Associated Secretory Phenotypes Reveal Cell-Nonautonomous Functions of Oncogenic RAS and the p53 Tumor Suppressor. PLoS Biol. 6, e301 (2008).

31. Joe, A.W.B., Yi, L., Natarajan, A., Le Grand, F., So, L., Wang, J., Rudnicki, M.A., Rossi, F. M. V. muscle injury activates resident fibro/adipogenic progenitors that facilitate myogenesis. Nat. Cell Biol. 70, 773–779 (2016).

32. Malecova, B. Mix of Mics- Phenotypic and Biological Heterogeneity of Multipotent Muscle Interstitial Cells (MICs). J. Stem Cell Res. Ther. 01, 1–6 (2012).

33. Uezumi, A., Fukada, S. I., Yamamoto, N., Takeda, S. & Tsuchida, K. Mesenchymal progenitors distinct from satellite cells contribute to ectopic fat cell formation in skeletal muscle. Nat. Cell Biol. 12, 143–152 (2010).

34. Mozzetta, C. et al. Fibroadipogenic progenitors mediate the ability of HDAC inhibitors to promote regeneration in dystrophic muscles of young, but not old Mdx mice. EMBO Mol. Med. 5, 626–639 (2013).

35. Heredia, J. E. et al. Type 2 innate signals stimulate fibro/adipogenic progenitors to facilitate muscle regeneration. Cell 153, 376–388 (2013).

36. Arrighi, N. et al. Characterization of adipocytes derived from fibro/adipogenic progenitors resident in human skeletal muscle. Cell Death Dis. 6, (2015).

37. Farup, J., Madaro, L., Puri, P. L. & Mikkelsen, U. R. Interactions between muscle stem cells, mesenchymal-derived cells and immune cells in muscle homeostasis, regeneration and disease. Cell Death Dis. 6, e1830-13 (2015).

38. Li, Y. et al. Senescence of mesenchymal stem cells (Review). Int. J. Mol. Med. 39, 775–782 (2017).

39. Zhang, X. et al. Characterization of cellular senescence in aging skeletal muscle. Nat. Aging. 7, 601-615 (2022).

40. De Cecco, M. et al. genomes of replicatively senescent cells undergo global epigenetic changes leading to gene silencing and activation of transposable elements. Aging Cell 12, 247–256 (2013).

41. De Cecco, M. et al. Transposable elements become active and mobile in the genomes of aging mammalian somatic tissues. Aging (Albany. NY). 5, 867–883 (2013).

42. Lander, E. S. et al. Initial sequencing and analysis of the human genome. Nature 409, 860–921 (2001).

43. Kopera, H. C., Moldovan, J. B., Morrish, T. A., Garcia-Perez, J. L. & Moran, J. V. Similarities between long interspersed element-1 (LINE-1) reverse transcriptase and telomerase. Proc. Natl. Acad. Sci. 108, 20345–20350 (2011).

44. Brouha, B. et al. Hot L1s account for the bulk of retrotransposition in the human population. Proc. Natl. Acad. Sci. 100, 5280–5285 (2003).

45. St. Laurent III, G., Hammell, N., McCaffrey, T. A. A LINE-1 componenet of human aging: do LINE elements exact a longevity cost for evolutionary advantage? Mech Ageing Dev 131, 299–305 (2010).

46. Maxwell, P. H., Burhans, W. C. & Curcio, M. J. Retrotransposition is associated with genome instability during chronological aging. Proc. Natl. Acad. Sci. 108, 20376–20381 (2011).

47. Elsner, D., Meusemann, K. & Korb, J. Longevity and transposon defense , the case of termite reproductives. PNAS (2018). doi:10.1073/pnas.1804046115

48. Takahashi, A. et al. Downregulation of cytoplasmic DNases is implicated in cytoplasmic DNA accumulation and SASP in senescent cells. Nat. Commun. 9, 1–12 (2018).

49. Thomas, C. A. et al. Modeling of TREX1-Dependent Autoimmune Disease using Human Stem Cells Highlights L1 Accumulation as a Source of Neuroinflammation. Cell Stem Cell 21, 319–331.e8 (2017).

50. Shen, Y. J. et al. Genome-derived cytosolic DNA mediates type I interferon-dependent rejection of B cell lymphoma cells. Cell Rep. 11, 460–473 (2015).

51. Dhanwani, R., Takahashi, M., Sharma, S. cytosolic sensing of immuno-stimulatory DNA, the enemy within. Curr Opin Immunol 50, 82–87 (2018).

52. Chou, S. et al. Neuronal senescence in the aged brain. Aging Dis. 5, 1618-1632 (2023).

53. Jurk, D. et al. Postmitotic neurons develop a p21-dependent senescence-like phenotype driven by a DNA damage response. Aging Cell. 6, 996-1004 (2012).

54. Englund, D. et al. Skeletal muscle aging, cellular senescence, and senotherapeutics: current knowledge and future directions. Mech Ageing Dev. 200, 111595 (2021).

CHAPTER 2:

Identifying Aged Cells

Background

Muscle aging is largely a mysterious phenomenon. Mechanisms of reduced regenerative capacity in the old, injured muscles had been well studied but they do not clearly explain the reduced muscle mass and functions with age[1]. In order to investigate the mechanisms of muscle aging, it is imperative to identify suitable aging markers in muscles. Senescence-associated beta galactosidase (SA-β-gal) assay is a well-established marker to identify aged cells. Some studies report SA-β-gal activity in aged muscles[2], but most studies failed to identify SA-β-gal+ cells in muscles. As most studies use 20 -25 months old mice as the aged group, perhaps the use of older mice (30+ months) may reveal SA-β-gal activity in muscles.

It is possible that the muscles have a unique biology that deters SA-β-gal activity their aged cells. This would require us to identify different aging marker to use for the muscles. Our previous study had found LINE-1 retrotransposable element as the potential aging marker in muscles: bulk RNA analysis revealed that LINE-1 mRNA expression is greatly enhanced in the liver and muscle tissues of geriatric mice[3]. Using RNA FISH, we may be able to pin-point the origin of this LINE-1 expression in aged muscles.

p16 is another well established senescence marker that had been shown to increase in aged muscles[3]. In the past, we had successfully used antibodies to show p16 in human senescent cells, but p16 antibodies for the mice had not been very reliable[4]. One strategy to address this issue is to target the p16 RNA instead. Based on the activity study on p16, the most ideal target would be 62-456 region[5]. However, p16 have splice variants of almost identical sequences and traditional RNA FISH technologies are unable to differentiate between the variants. The most notable variant is called $p14^{ARF}$ (variant 4) in human and $p19^{ARF}$ (variant 1) in mouse; $p16^{CDKN2a}$ is variant 1 in human and variant 2 in mouse. p16 and ARF have different reading frame and code

for completely different proteins but as they share their sequences, RNA FISH probe for p16 would inevitably detect the ARF sequence as well. The only difference between the two mRNA are their first exon junction. ARF mRNA is made by splicing exon 1β with exon 2 while p16 mRNA is made by splicing exon 1α with exon 2 (Fig.2.4A). This creates a small region of the mRNA where the two sequences show difference.

RNAscope is a new RNA FISH technology with a unique probe design. It utilizes Z shaped oligo probe complementary to ~25 nucleotides (Fig. B1.1A) that must bind in consecutive pair to support its amplifying tree (Fig. B1.1B). The signal elements of choice bind to the amplifying tree for highly sensitive RNA detection (Fig. B1.1C), and because this detection is only made for consecutively bound oligo probes, false positivity by unspecific binding is greatly reduced. As a result, we get highly sensitive and specific detection of RNA targets. Multiple pairs of RNAscope probes tile along the target sequence of about 500 nucleotides for detection of individual RNA target (Fig. B1.D).

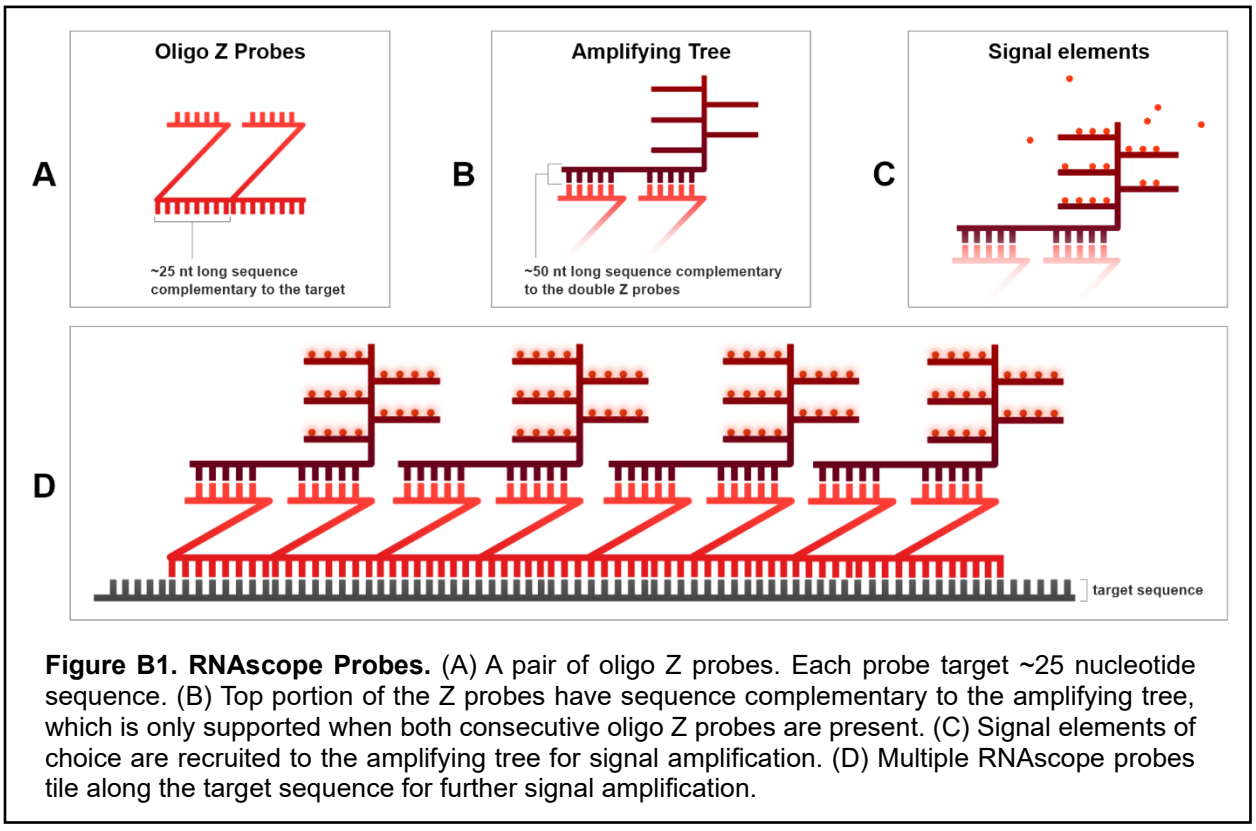

Figure B1. RNAscope Probes. (A) A pair of oligo Z probes. Each probe target ~25 nucleotide sequence. (B) Top portion of the Z probes have sequence complementary to the amplifying tree, which is only supported when both consecutive oligo Z probes are present. (C) Signal elements of choice are recruited to the amplifying tree for signal amplification. (D) Multiple RNAscope probes tile along the target sequence for further signal amplification.

Basescope is a variant technology that utilizes one or just a few pairs of the oligo Z probes to allow detection of much smaller targets (~50 nt). The use of smaller number of probes per target reduces total signal strength per target but this is complemented by adding more amplification power per probe. This is expected to slightly increase the false positivity rate, but the outcome is still very good and reliable. One application of the Basescope technology is targeting exon junctions to differentiate between transcript variants. In order to test this technology, we ordered stock p16 Basescope probe targeting the exon junction at 425-465 (NM_000077.4). We then designed p16 mRNA Basescope for mouse by applying the same principle.

p21 is increasingly recognized potential aging marker in muscles[6] and its Basescope probe was readily available. Combining two Basescope detections require the use of the Duplex kit. In Basescope Duplex, the top portion of the oligo Z probe contains sequence information for a specific channel. This sequence recruits the channel specific amplifying tree and develops signals specific to the assigned channel.

Methods

Dissecting mouse hind limb muscles

C57BL/6 mice were aged in house until appropriate months are reached. The mouse anesthesia is done by intraperitoneal injection of 21.5 ul ketamine and 28.5 ul xylazine. Once knocked out, the cervical dislocation was performed. The mouse was generously sprayed with ethanol to keep the furs down. A horizontal incision is made at a side of the belly and the skin is ripped across the full diameter of the body. Gently holding down the chest of the mouse, the bottom half of the ripped skin is pulled all the way down to clearly reveal the hind limb muscles. One leg at a time, the hind limb was lifted up and the distal tendon of the gastrocnemius is articulated with a blunt probe. A tweezer is inserted underneath the tendon and allowed to expand to detach gastrocnemius from the bone. The tendon is severed and held with the tweezer. A probe was used

to articulate the red soleus muscle at the back of the gastrocnemius. Both ends of the soleus were cut to remove this muscle. The tendon is closely inspected to identify two tendons. Each is held with a tweezer and pulled apart to reveal two sets of the muscles. The smaller muscle located closer to the center of the mouse is PLA. The larger muscle is the gastrocnemius. The gastrocnemius is then cut behind the knee and either transferred to a petri dish for mechanical digestion or lightly coated with OCT and snap frozen in isopentane cooled with liquid nitrogen and air dried on dry ice for at least 20 minutes. Quadriceps are harvested by probing between the top of the knee and the pelvis. Taking caution not to disturb the blood vessel, the muscle is removed and treated like the gastrocnemius.

Measuring the cross-sectional area of mouse myofibers

OCT coated snap frozen muscle is vertically fixed on a cryo-plate with additional OCT and trimmed to the thickest portion of the muscle. 10 um thick cryosection is made. The sample is fixed with 4% PFA for 10 minutes at room temperature, washed with PBS and mounted with ProLong Gold. The lateral cross section of the muscle is imaged with microscope. The image is opened in Photoshop and area measurement tool is activated. Individual myofiber is selected to amass a list of myofiber areas in the given field of view and the average cross sectional area of the myofiber is calculated. The areas are also sorted by the bin of 1,000 um^2 and their frequencies are represented in a bar graph. The process was repeated on different age groups.

Senescence associated beta galactosidase assay

10 um thick cryosection of the muscle is fixed for 5 min at room temperature and washed with PBS three times. The sample is immersed in SA-β-gal solution overnight at 37 °C and counterstained with 0.5% eosin with 1:100 acetic acid. The fixative solution is made by adding 2% formaldehyde and 0.2% glutaraldehyde in PBS. SA-β-gal solution is prepared by mixing 1 ml of 1

mg/ml Xgal, 4 ml of citric acid/sodium phosphate solution, 1ml of 100mM potassium ferrocyanide, 1 ml of 100 mM potassium ferricyanide, 0.6 ml of 5 M NaCl, 0.04 ml of 1M $MgCl_2$, filled up to 20 ml with distilled water, prepared fresh before each use. Citric acid/sodium phosphate solution is made by mixing 36.85 ml of 0.1M citric acid with 63.15 ml of 0.2 M sodium phosphate and pH adjusted to 6.0.

Creating etoposide induced senescent human lung fibroblasts

Lung fibroblast (LF) 1 cells are treated with 20 uM etoposide for 3 days. The cells are allowed to recover for 4 days and treated with a second round of 20 uM etoposide for 3 days. At this point the cells are marked as day-0 senescence and monitored for a week in the growth media to confirm that they do not replicate.

Immunofluorescence labeling of senescence markers

Cryosection muscle samples or harvested cells are fixed in 4% PFA for 15 minutes at room temperature. The sample is washed with PBS twice and blocked with a buffer containing 5% donkey serum and 0.3% Triton X-100 in PBS for 60 minutes at room temperature. The blocking buffer is replaced with the primary antibody diluted 1:100 in 1% BSA, 0.3% Triton X-100 in PBS. The sample is carefully placed in the fridge or a cold room set to 4°C overnight. On following day, the sample is washed three times with PBS and incubated for an hour with the secondary antibody diluted 1:1000 in 1% BSA, 0.3% Triton X-100 in PBS. The sample is washed three times with PBS, counter stained with DAPI for 25 minutes at room temperature and washed twice with PBS. The sample is mounted with ProLong Gold and allowed to cure overnight.

Transfection of MT302 LINE-1 overexpression plasmid in HeLa

For each well of the six wells plate, 1.5 ug of MT302 plasmid is mixed with 6.8 ul Fugene HD, which is previously vortexed and left at room temperature before use, in 100 ul Opti-MEM. The mixed solution is left at room temperature for 10 minutes and given to cells in serum free media

for 24 hours. The transfection medium is removed and normal growth media with 1ug/ml puromycin is given for 48 hours. 0, 0.1, 1.0, and 2 ug/ul of doxycycline is given for 24 hours to induce L1 expression.

Stellaris L1 mRNA FISH

Stellaris FISH was performed according to the manufacturer's protocol. In short, cells are fixed with 4% PFA for 10 minutes at room temperature, permeabilized with 70% ethanol for at least 1 hour at 4°C. The cells are incubated in Wash Buffer A for 5 minutes and placed in a humidified chamber. 100 uL of Hybridization Buffer containing fresh deionized formamide and the probe is dispensed and incubated at dark for 4 hours at 37 °C. Wash Buffer A is given and incubated at dark for another 30 minutes at 37 °C. DAPI stained for 30 minutes and washed with Wash Buffer B for 5 minutes. The exact sequences of the L1HS Stellaris probes are listed in Supp. Data 1.

Designing Basescope probes

Human p16 mRNA Basescope was available as stock probes. We chose BA-Hs-CDKN2A-tv1-E1E2 (catalog number 711131) as this probe targets the exon 1 and exon 2 junction and avoids most prominent splice variants. Variant 5 is also expected to be detected by this probe (NM_001195132.1) but this had not been an issue for our analysis. As for the mouse p16 mRNA, there was no stock probe available which targets the exon 1 and exon 2 junction. We custom ordered this probe by supplying the sequence information and desired target region. The resulting probe is now available as a stock: BA-Mm-Cdkn2a-tv2-E1-E2. For the p21 mRNA probes, stocks were available but we still made the custom order to allow simultaneous detections with our p16 mRNA probes. The probes we made are BA-Mm-Cdkn1a-tv1-1zz-st for the mouse and BA-Hs-CDKN1A-tv1-E2E3 for human. The sequence information for all probes are available in ACDbio's catalog probes page.

Basescope Assay with p16

Cells or tissues were fixed with 4% PFA for 30 minutes at room temperature and dehydrated with 50, 70, and 100% ethanol 1 minute each. The sample was then stored in fresh 100% ethanol at -20°C for at least a day. Within one or two weeks, the sample was retrieved and air dried. Hydrophoic barrier was drawn around the sample. RNAscope Hydrogen Peroxide solution was given to the sample for 10 minutes at room temperature. Basescope probes and protease were warmed in the water bath for 10 minutes during this time. Enough RNAscope Protease IV was given to cover the whole sample and kept for 30 minutes at room temperature in a humidified chamber. Basescope probe was diluted to proper strength and given to the samples. The samples were put into HybEZ oven set to 40°C for 2 hours. The samples were washed with agitation two minutes for two times. Amp 1 to Amp 6 were given as instructed, each time followed by the two minutes of agitated wash two times. Amp 7 was incubated for 2 hours instead of 30 minutes for increased signal strength, followed by Amp 8 and signal development with Fast RED. 50% hematoxylin counter stain and Ecomount were performed. For the tissue samples, images were taken with 40x objectives on Nikon-Ti2-E fluorescence microscope with DS-RI2 camera and stitched together to allow full cross-sectional view of the muscles.

Consecutive muscle sectioning and signal validation

Four consecutive muscle cryosections of 10 um thickness were made. Sections 1 and 3 were stained with DapB, negative control, while sections 2 and 4 were stained with p16 mRNA. Resulting images were cross referenced to check whether p16 signal is observed also in DapB stained control, which would mean false positive, and whether p16 signal of sections 2 and 4 show matching pattern, which would mean true positive.

Basescope Duplex assay with p16 and p21

The first half of the duplex protocol is identical to the single-plex assay described above. After the signal development with FAST RED, Amp 9 to Amp 10 were performed as instructed. For Amp 11,

incubation time was increased to 2 hours instead of 30 minutes for increased signal strength, followed by Amp 12 and signal development with the Duplex Green. The sample was cleaned with Xylene and mounted with toluene instead of Ecomount because the green signals fade when exposed to aqueous based mount.

ORF1 staining

Muscles were cut in 10 um section and fixed with 4% PFA for 15 minutes at room temperature. After two agitated wash with PBS for two minutes each, the sample was dehydrated with 50, 70, and 100% ethanol one minute each and immersed in fresh 100% ethanol for each least a day. The sample was retrieved and air dried. A hydrophobic barrier was drawn around the muscle and left to dry for five minutes. A blocking buffer was applied for 30 minutes at room temperature, consisting of 10% donkey serum and 0.3% Triton X-100 in PBS. ORF1 (EPR21844) antibody was diluted in 3% donkey serum, 0.3% Triton X-100, PBS at 1:100 and applied to the sample. The sample was washed with PBS, with agitation, two minutes each. Secondary antibody (Alexa fluor 647) was diluted 1:1000 in the dilution buffer described previously and applied for 1 hour at room temperature. The sample was washed with PBS twice as before and counter stained with DAPI.

Results

Performing SA-β-gal assay on mouse geriatric muscles

Quadricep muscles from 5, 25, and 36 months old male mice were harvested. The muscles were cut in 10 μm sections and looked under the microscope. Using the area measurement function in the Photoshop, we collected cross sectional areas of the myofibers and represented the data across 1,000 μm^2 bins (Fig. 2.1A). At 5 months, the area distribution showed a bell-shaped curve around 3,000 μm^2. By 25 months, there was a drastic shift in the distribution towards 1,000 and 2,000 μm^2. We observed that this trend continued to 36 months old muscles, which showed even more skew towards 1,000 μm^2. This suggests that the age associated changes in mouse muscles continue from 25 to 36 months. We tested whether SA-β-gal activity can be observed from 36 months old mice. 36 months old mice did not show any SA-β-gal activity (Fig. 2.1B, middle). This was in contrast to the 36 months old liver that showed strong SA-β-gal activity indicated by green signal developments (Fig. 2.1B, right).

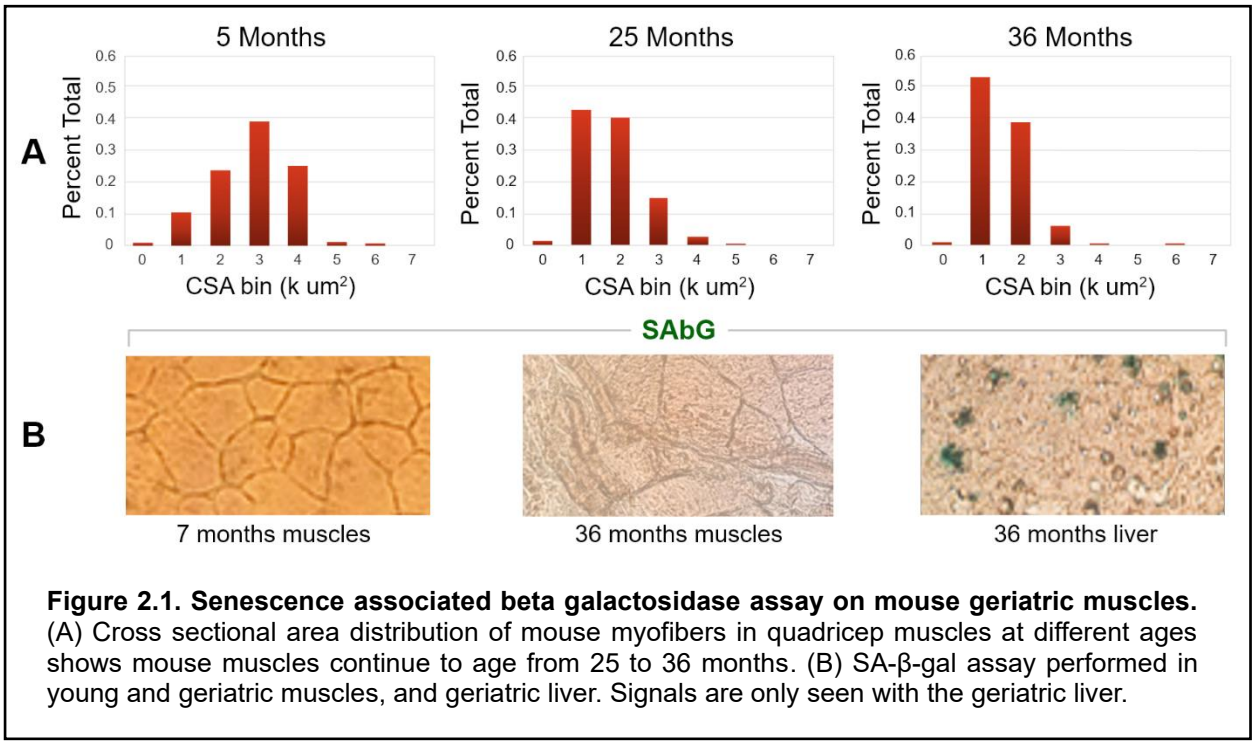

Figure 2.1. Senescence associated beta galactosidase assay on mouse geriatric muscles. (A) Cross sectional area distribution of mouse myofibers in quadricep muscles at different ages shows mouse muscles continue to age from 25 to 36 months. (B) SA-β-gal assay performed in young and geriatric muscles, and geriatric liver. Signals are only seen with the geriatric liver.

Inducing senescent LF1

Human lung fibroblasts (LF1) were treated with etoposide for two weeks and given normal growth media. After 4 weeks of confirming no further proliferation, the cells were stained with various senescence markers. The etoposide treated LF1 showed positive results for all senescence markers tested (Fig. 2.2A). We also mixed these cells with actively proliferating LF1 at 1:9 ratios and checked to see if p16 can be used to identify the rare senescent cells in largely proliferating population. Fig. 2.2B is a representative image which captures three LF1 cells in which only one is p16 positive. $p16^{+}$ cell also shows the large cell body which is a known feature of a senescent cell.

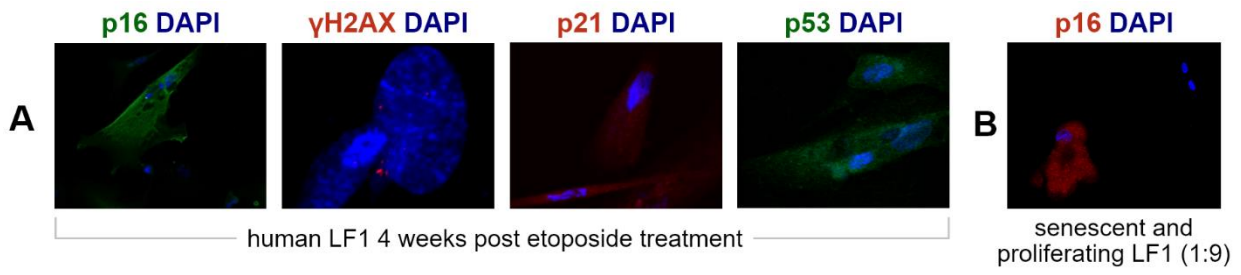

Figure 2.2. Etoposide induced senescence in human lung fibroblasts (LF1). (A) Traditional immunofluorescence markers for senescent cells tested on LF1 4 weeks post etoposide treatment. (B) Seeding senescent LF1 with proliferating LF1 at 1:9 ratio and performing p16 staining to locate the rare senescent cells.

Using Stellaris L1 mRNA probe to identify aged cells

Previous studies in our laboratory demonstrated increased L1 activity in aged murine muscles[3]. We ordered Stellaris probes that would bind to the known human L1 mRNA sequence. In order to check whether this probe really binds to the L1 mRNA sequence, we performed a pilot experiment on HeLa cells. Two positive controls were used: GAPDH is the positive control for the cytosolic expression (Fig. 2.3A, left) and MALAT1 is the positive control for the nuclear expression (Fig. 2.3A, right). HeLa cells were stably transfected with MT302-GFP LINE-1 overexpressing plasmids (Fig. 2.3B), which can be conditionally turned on with doxycycline. We treated the HeLa cells with varying concentrations of doxycycline and observed L1 signal intensity proportional to

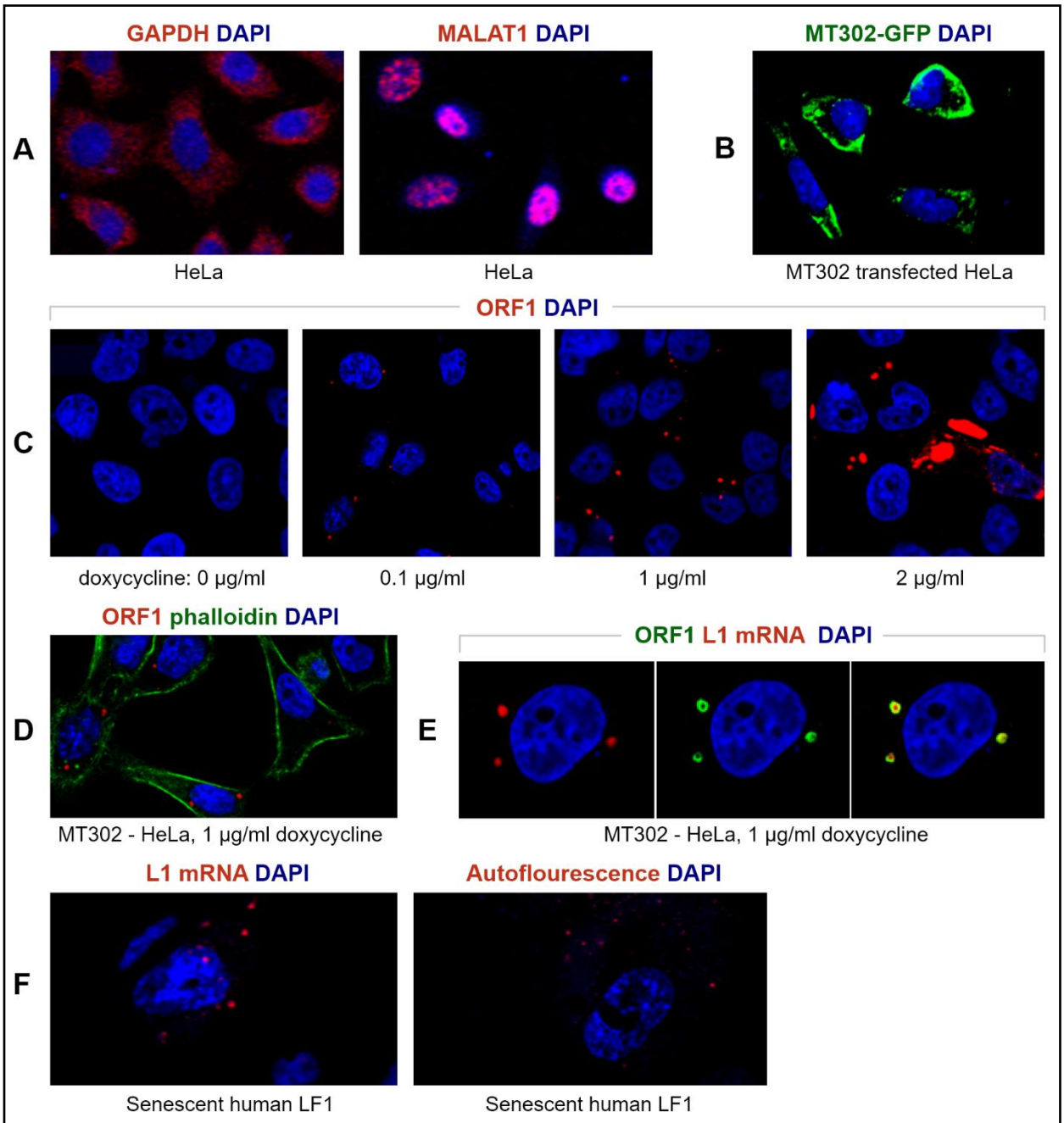

Figure 2.3. Using Stellaris L1 mRNA probe as a new aging marker. (A) Stellaris GAPDH positive cytosolic expression (left) and Stellaris MALAT1 positive nuclear expression (right) on HeLa. (B) GFP signals in HeLa cells indicative of MT302 L1 overexpressing plasmids. (C) Stellaris L1 mRNA probes detecting increasing amount of L1 mRNA according to the given concentrations of doxycycline from 0 to 2 ug/ml in MT302-HeLa. (D) HeLa cells with L1 overexpression stained with phalloidin to show that L1 mRNA signals originate from the cell bodies. (E) Co-staining of Stellaris L1 mRNA and ORF1 protein in MT302-HeLa. (F) Senescent LF1 stained with (left) and without (right) Stellaris L1 mRNA probe.

the concentrations of doxycycline (Fig. 2.3C). To make sure these stains are not random artifacts outside the cell bodies, we took the cells treated with 1 ug/ml doxycycline and re-stained with phalloidin to show the cytoplasmic boundary (Fig. 2.3D). We also tried co-staining ORF1 protein with Stellaris L1 mRNA. At least in HeLa cells with L1 overexpressing plasmids, L1 mRNA is detected as fine points outside the nuclei with ORF1 surrounding L1 mRNA (Fig. 2.3E). Finally, we tested Stellaris L1 mRNA in previously made senescent LF1. This also resulted in fine points outside the nuclei but to our surprise similar results were seen with our negative control that did not receive any stellaris probe. Further investigation revealed that the signals from stellaris L1 mRNA look very similar to the autofluorescence of the senescent cells (Appendix A) and therefore not suitable for our study.

Using Basescope Assay to analyze aged muscles

We designed new human and mouse p16 Basescope probes targeting ~40 nucleotides around its exon junction (Fig. 2.4A) and tested on senescent human LF1 (Fig. 2.4B) and geriatric mouse muscles (Fig. 2.4C).

To maker sure that the stains from the Basecope assay were not just random signal developments, we prepared four consecutive muscle sections of 10 um thick each and alternated between p16 and DapB (negative control) staining. The red signals only developed for the p16 stained sections and the staining patterns were mostly preserved across the consecutive sectioning. As shown in Figure 2.4D, while the nuclei pattern is slightly different between sections 2 and 4, their p16 staining is very similar.

We then performed p16 Basescope assay on 2 and 36 months old mouse quadriceps and noted that p16 mRNA signals are only detected in the 36 months old muscle (Fig. 2.5A). We also tried human p16 probe on young and old human muscle samples, and noted that p16 signals very low and seen only with the oldest human muscle samples (Fig. 2.5B). Even with the oldest

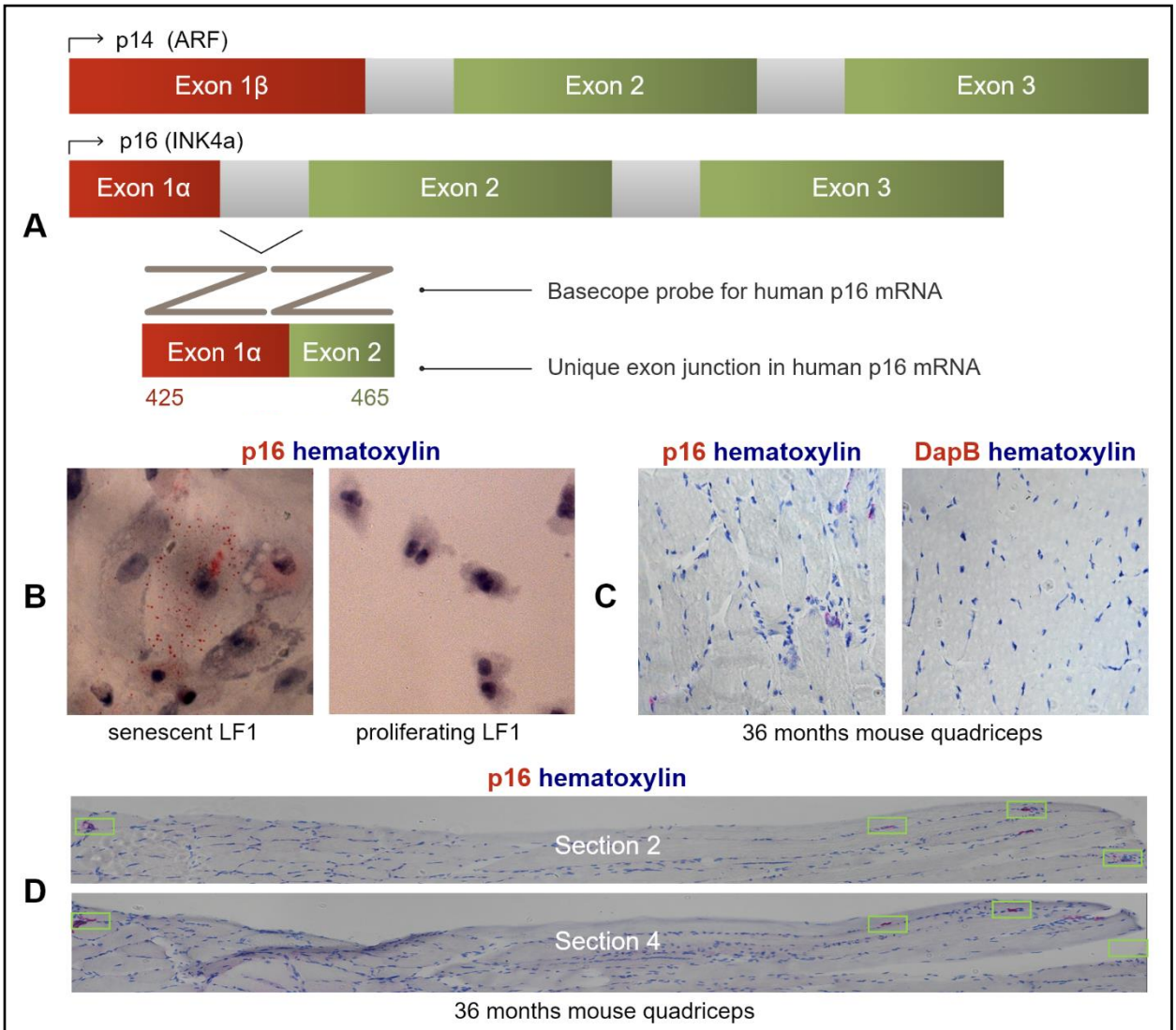

Figure 2.4. Development and validation of the p16 Basescope probe. (A) Illustration of two human transcript variants of almost identical sequences (p14 and p16) and the need for targeting the short and unique exon junction. (B) p16 Basescope probe staining senescent (left) and proliferating (right) human LF1 cells. (C) 36 months mouse quadriceps stained with p16 Basescope probe (left) and DapB negative control probe (right). (D) Two of the four consecutive cuts of 36 months mouse quadriceps showing consistent p16 Basescope staining pattern indicated by green boxes.

sample, p16 signals were not very common. To see if this is a technical limitation of the assay, we tried co-staining with p21, which is another potential aging marker in muscles that is expected to be more abundant. For this we utilized the Basescope Duplex kit, which develops green and red colorimetric signals to allow simultaneous detection of two RNA targets. We first tested p16 and p21 duplex staining on etoposide induced senescent LF1, 2 weeks post treatment. Figure 2.5C shows the result of the staining. We observed several p16 signals indicated by green dots and

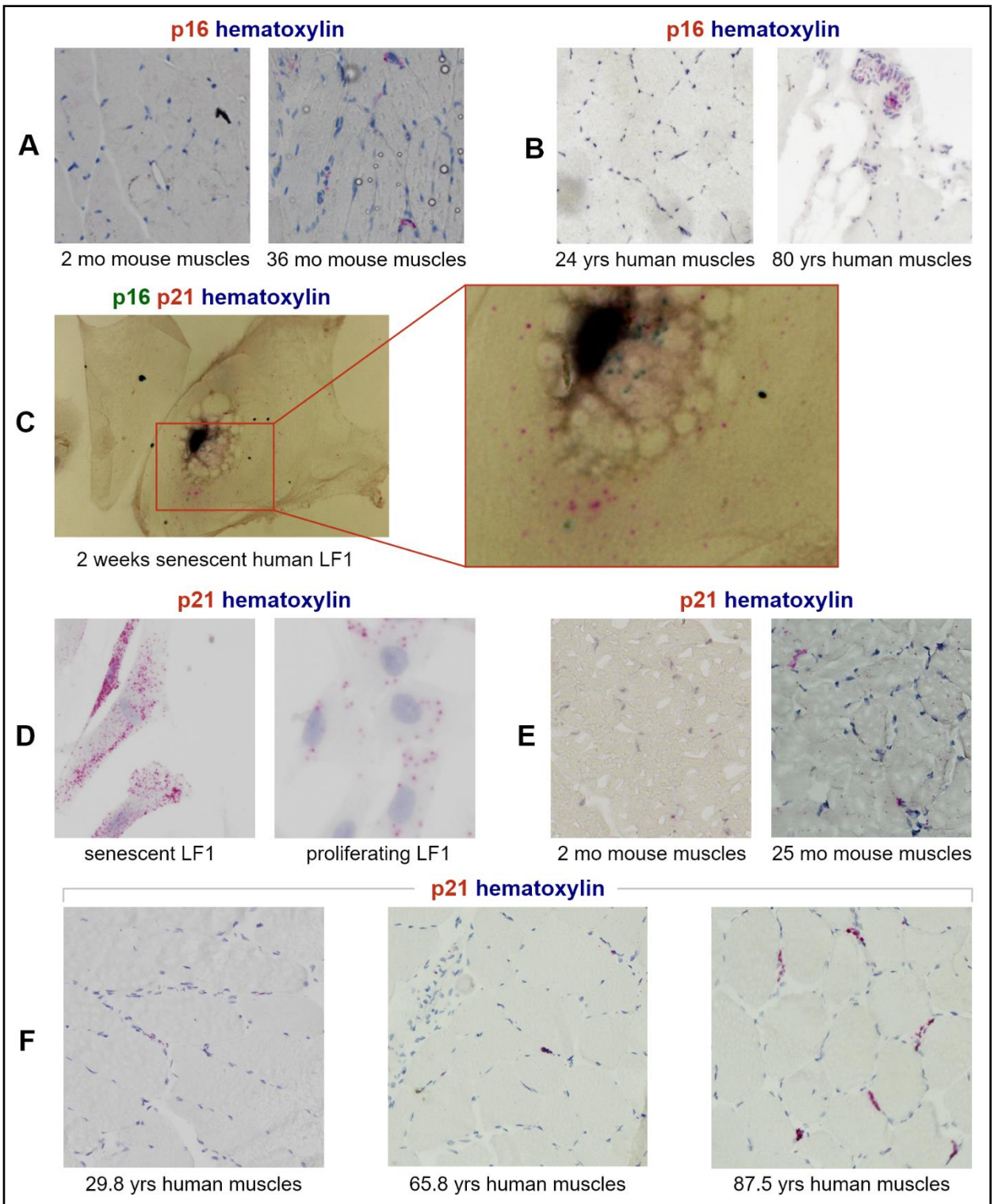

Figure 2.5. Analyzing aged muscles with Basescope. (A) p16 Basescope Assay on 2 and 36 months old mouse muscles. (B) p16 Basescope Assay on 24 and 80 years old human muscles. (C) p16 and p21 Basescope Duplex Assay on human LF1, 2 weeks post etoposide treatment. (D) p21 Basescope Assay on senescent and proliferating human LF1. (E) p21 Basescope Assay on 2 and 25 months mouse muscles. (F) p21 Basescope Assay on human muscles of varying ages.

much more abundant p21 signals indicated by red dots. P21 signals were seen even with the proliferating LF1 but its abundance was drastically increased when the cells enter senescence (Fig. 2.5D). Finally, we tested p21 Basescope probe on mouse (Fig. 2.5E) and human (Fig. 2.5F) muscles at various ages and saw a clear age-related increase in the signal abundance.

Using ORF1 as an aging marker in muscles

ORF1 is one of the two proteins encoded by LINE-1. It was only with EPR21844 (abcam ab 216324) that we detected ORF1 in mouse muscles with consistent success. Figure 2.6A shows 25 months old mouse quadricep muscle stained with ORF1. The signal is bright and clear and is found near a nucleus. To confirm that this is a real signal and not a staining artifact, we tested the antibody with two different secondary channels (488 and 647). We also stained two consecutive muscle sections of 10 um apart and saw that ORF1 stains the same cells across the sections (Fig. 2.6B). We then tried staining the entire cross section of 29 months old mouse quadricep muscle and noted ORF1 staining throughout the geriatric muscle (Fig. 2.6C). In order to test the age related increase in the ORF1 signal we stained 2 and 29 months old wild type muscles along with a 2 months old D2-mdx dystrophy muscle given by the Robbins laboratory of the University of Minnesota. As the dystrophy muscle sample showed unusually large number of nuclei (Fig. 2.6D), we normalized the ORF1 signal to the cross-sectional area of the muscles. We saw an increased ORF1 signals when comparing the young and old WT muscles and saw even greater ORF1 signals with the dystrophy muscle sample (Fig. 2.6E).

Figure 2.6. Using ORF1 as an aging marker in muscles. (A) 25 months old mouse quadriceps stained with ORF1 (EPR21844). (B) 29 months mouse quadricep muscles are cut into two consecutive sections of 10 um thickness and stained with ORF1 coupled with Alexa fluor 488 or 647. (C) 29 months mouse quadriceps stained with ORF1. Signals allowed to saturate for bird's-eye view on the distribution pattern. (D) ORF1 staining on 2 and 29 months wildtype mouse muscles and 2 months old D2-mdx mouse muscles. (E) ORF1 signals of the young, old, and dystrophy muscle samples normalized to the cross-sectional area of the muscle represented in 100 m pixels.

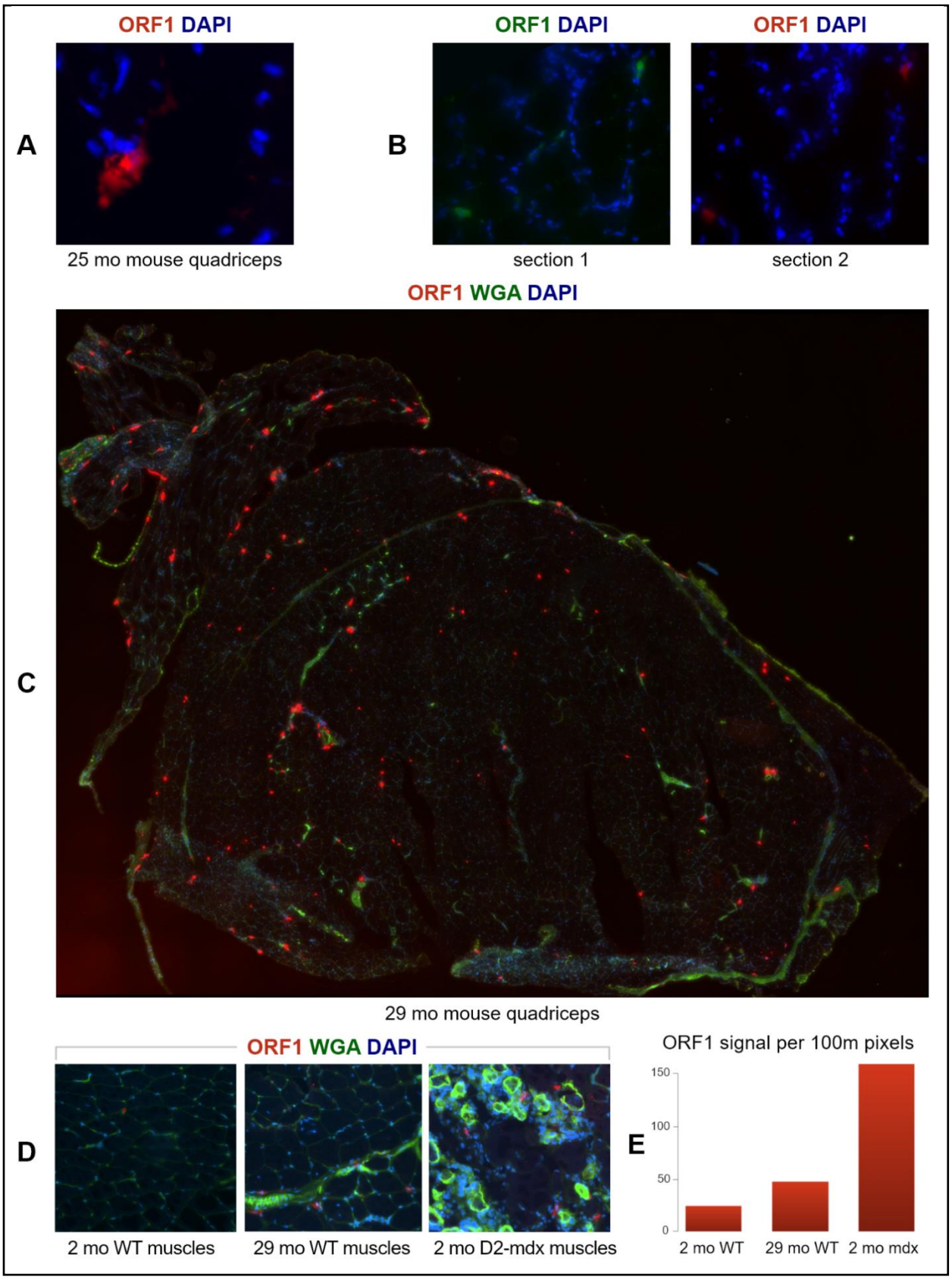
A
ORF1 DAPI
25 mo mouse quadriceps
B
ORF1 DAPI
section 1
ORF1 DAPI
section 2
C
ORF1 WGA DAPI
29 mo mouse quadriceps
D
ORF1 WGA DAPI
2 mo WT muscles
29 mo WT muscles
2 mo D2-mdx muscles
E
ORF1 signal per 100m pixels
150
100
50
0
2 mo WT
29 mo WT
2 mo mdx

Discussion

Mice can reproduce when they reach 35 days of age and are considered fully mature when they reach 3 months of age. They are still considered young until 6 months of age. A middle-aged mice would be somewhere between 10 and 14 months of age while old mice are generally referred to those in 18 to 24 months of age. After this point, the mortality rate of the mice rapidly increases and they rarely survive past 36 months of age. In the senescence study of the mice, 3-6 months are used as the reference of a healthy adult mice while 18-24 months are used as aged group affected by the senescence. As most facilities require mice to be euthanized when they start to show the severe aging phenotypes, studies on the geriatric mice who are between 25 and 36 months old are lacking. In most studies, the senescence in the old murine muscles had not been detected, but this may be because they did not look at the older muscles. Our myofiber cross sectional area analysis in Figure 2.1A demonstrates that the age associated decline of the myofiber size continue past 25 months. The frequency of the smallest myofibers noticeably increased in the 36 months when compared to the 25 months, and this suggests that the molecular markers of the aging in the geriatric muscles could be different from the old muscles. Although our study with the young, old, and geriatric muscles did not show any increase in the SA-β-gal activity (Fig. 2.1B), there may be other biomarkers of aging which onsets in the geriatric muscles. We should, therefore, try to include the geriatric mice in our aging studies, but this also comes with a caution. As not many mice are able to survive until 36 months, these geriatric mice may be special “centenarian” mice. Biomarkers observed in these mice may not be a demonstration of what happens when they age, but rather what allowed them to survive so long.

The inclusion of the geriatric mice in the aging studies comes with a number of challenges. For example, as the mortality rate rapidly increases in mice after 25 months, experiments must account for the mice that unexpectedly die. Having to wait longer for the analysis is also an

unwelcoming inconvenience. To facilitate the study of the muscle aging, the earliest experiments should employ the *in vitro* tools. We decided to induce senescence in human, baboon, and mouse fibroblasts using etoposide. Etoposide is a chemotherapeutic drug that induces DNA damage by inhibiting Topoisomerase II[7]. At the right concentration, this drug can permanently halt the cell cycle and induce senescence. We performed two rounds of etoposide treatment with a recovery period in between to induce senescence in the human lung fibroblasts (LF1). These cells showed morphological features of the senescent cells such as enlarged cell body and nucleus and we monitored its growth for a month to confirm no further division occurred. As few incompletely halted cells can quickly dominate the culture, it was very important to make sure all cells had entered senescence before proceeding with the experiments. These cells exhibited all senescence phenotypes tested: p16, γH2AX, p21, and p53 (Fig. 2.2A). We also performed a mock experiment of identifying the rare senescent cell in an actual tissue environment by diluting the senescent LF1 with the suspension of the proliferative LF1 at 1:10 ratio, which is the expected frequency of senescent cells in the muscles. At this ratio, we could readily identify the aged cells as they were larger and stained strongly with our p16 antibody (Fig. 2.2B). Although this may not be the case in the actual muscle tissues, it was enough to explore various potential aging markers for the muscles.

The first marker we investigated was LINE-1 (L1) retrotransposable elements. The transcription of LINE-1 elements is increased with age and muscles showed especially high expression of LINE-1 with age[3]. In order to detect LINE-1 in muscles, we first designed Stellaris probes against L1HS (Supp. Data 1). These probes tile along the unique sequence of LINE-1 with high sensitivity. As we were interested in sequences in and out of the nuclei, we first tested reference targets in and out of the nuclei. GAPDH is a house keeping gene found in the cytoplasm while MALAT1 is one found inside the nuclei (Fig. 2.3A). To see if our probes do detect LINE-1, we first transfected LINE-1 overexpression plasmid MT302 to HeLa cells and made stable

expression clones (Fig. 2.3B). The MT302 expressing HeLa cells were then subject to various dosage of doxycycline and stained with Stellaris L1 probes (Fig. 2.3C). We confirmed that the signals from our Stellaris L1 probes are only detected when L1 expression is induced with doxycycline and the signal frequency correlated with the greater induction of L1 expression by higher doxycycline dosage. As the signals started to saturate in cells induced with 2 μg/ml doxycycline, we decided to use 1 μg/ml doxycycline for our experiments. To further validate our probe, we co-stained our cells with Stellaris L1 probes and ORF1 antibody. ORF1 is one of the two proteins encoded by LINE-1 retrotransposable element and is used to mark the LINE-1 expression. With LINE-1 overexpressing HeLa cells, we observed distinct LINE-1 RNA signals outside the nucleus encased by circular ORF1 signals (Fig. 2.3E). When the focal point is set to the center of LINE-1 signal, we even see a donut shaped ORF1 signal with hollow center, suggesting that the signals are not overlapped due to limited resolution, but ORF1 protein is indeed surrounding LINE-1 RNAs. We should note that the expression level of LINE-1 in MT302 HeLa cells is much higher than what is normally found in aged cells. Peculiar behavior of these LINE-1 and ORF1 in the cytoplasm may only occur at extremely high LINE-1 concentrations. To see the expressions of endogenous LINE-1, we stained previously developed senescent LF1 cells with the Stellaris L1 probes. We still saw the distinct signals in the cytoplasm at dimmer intensity. However, similar dim signals were also observed in our negative control cells that had not been stained with L1 probes. It turned out that the senescent LF1 cells have autofluorescence at a wide spectrum and they are very similar to the results of the Stellaris L1 staining (Appendix A). We tried different methods to quench the autofluorescence but in the end had to conclude that Stellaris L1 probes are not suitable as markers of senescence.

The next aging marker we investigated was p16 mRNA. We had a few antibodies against the p16 protein, but the signals from the staining was very weak and difficult to identify over the autofluorescence, especially in mouse muscles. We thought about targeting p16 mRNA instead,

but this posed greater challenge than anticipated. It turned out that p16 RNA is spliced into multiple transcript variants with similar sequences. Any RNA FISH probe targeting p16 mRNA would also target the unprocessed RNAs of multiple transcript variants. For instance, ARF protein, which is called p14 in human, is a transcript variant of p16 with almost identical RNA sequence (Fig. 2.4A). We employed a Basescope probe to target the unique sequence found at its first exon junction and this probe successfully distinguished between senescent and proliferative LF1 (Fig 2.4B). It could also differentiate young and old murine muscles (Fig. 2.5A). We also tried staining the young and old human muscles and found out that no p16 mRNA is detected with the young muscles while few p16 mRNA signals are detected with the very old (80 yrs) muscles (Fig. 2.5B). The image on the right of the Figure 2.5B is one of only two fields of views where we could see p16 mRNA in the entire cross section of the muscle. There is a cluster of nuclei in the top right portion of the image where multiple p16 signals are found, but as this is towards the edge of the muscle and potentially a folded region, they may be staining artifacts. At a closer inspection, there are few more p16 signals at the bottom left of the image and they are more likely to be the true signals. In any case, p16 mRNA signals were very rare even with the geriatric samples and would only have limited usage in identifying aged cells in muscles. We needed an aging marker than can be used to analyze muscles that are relatively young and be able to track the progression of age for longer periods. p21 was a good potential aging marker on this regard as p21 is known to be expressed in young cells but its expression increases with age. We began by making basescope probe for p21 that can be used with our p16 probe. Using Basescope Duplex kit, we successfully stained senescent LF1 with p16 and p21 mRNA probes (Fig. 2.5C). We observed greater number of p21 signals per senescent cell and the change in p21 expression level with senescence was apparent (Fig. 2.5D). This increase in p21 expression level was demonstrated with young and old muscles as well (Fig. 2.5E &F).

Now that we have a good aging marker, we wanted to compare this with other potential aging markers in mice. Although we couldn't get LINE-1 Stellaris probes to work, ORF1 antibodies had shown some promises. When we tried ORF1 staining on murine muscles, however, we were not completely satisfied as the signals were not very strong and very infrequent (data not shown). It was hard to tell whether these extremely rare signals are true ORF1 signals. While testing ORF1 antibodies from different vendors, we stumbled upon EPR21844, which had extremely bright and unambiguous signals (Fig. 2.6A). We usually saw very dim signals that required 1 second exposure and post image processing. With the new ORF1 antibody, however, we had to take the images at 200 – 400 ms exposure to prevent saturation. To make sure these are real signals and not random unspecific binding, we made consecutive muscle sections and stained both with ORF1 coupled with different secondary antibodies. Signals appeared with the same cells in both sections and channels (Fig. 2.6B). Taking advantage of the high signal intensity, we allowed ORF1 signals to saturate and took an image of the entire geriatric muscle section to show the distribution pattern of ORF1 in muscles (Fig. 2.6C). ORF1 signals were spread out evenly throughout the muscle, and we noticed that the signals usually appeared next to what looks like blood vessels. WGA depicts, in green, circular structures some of which show features of the large blood vessels. Others look like the ends of muscle spindles, but additional staining is required to confirm their identity. We next tried staining murine muscles of different conditions: young, old, and dystrophy. 29 months old muscles had about twice as many ORF1 signals compared to the 2 months old muscles. And this difference was dwarfed by the dramatic increase in ORF1 signals in the dystrophy muscles. This demonstrates that the presence of many ORF1 signals may be an indication of aging or diseased state of the muscles. Future study should focus on finding the identity of ORF1 expressing cells and their contribution to the muscle aging.

REFERENCE

1. Sousa-Victor, P. et al. Geriatric muscle stem cells switch reversible quiescence into senescence. Nature 506, 316–321 (2014).

2. Wu J. et al. Ginsenoside Rg1 supplementation clears senescence-associated β-galactosidase in exercising human skeletal muscle. J Ginseng Res. 43, 580-588 (2019).

3. De Cecco, M. et al. Transposable elements become active and mobile in the genomes of aging mammalian somatic tissues. Aging (Albany. NY). 5, 867–883 (2013).

4. Herbig, U. et al. Telomere shortening triggers senescence of human cells through a pathway involving ATM, p53, and p21 CIP1, but not p16 INK4a. Mol. Cell 14, 501-513 (2004).

5. Hara, E. et al. Regulation of p16CDKN2 expression and its implications for cell immortalization and senescence. Mol. Cell Biol. 16, 859-867 (1996).

6. Zhang X. et. al. Characterization of cellular senescence in aging skeletal muscle. Nat. Aging. 2, 601-615 (2022)

7. Burden, D.A. et. al. Topoisomerase II etoposide interactions direct the formation of drug-induced enzyme-DNA cleavage complexes. J. Biol. Chem. 271, 29238-29244 (1996).

CHAPTER 3:

Identifying Muscle Resident Cell Types

Background

As the largest tissue in our body, skeletal muscle makes up 40% of human body mass[1]. Unlike other tissues that are mostly formed of various cell bodies, muscles are mostly composed of functional proteins (myosin and actin) and regulatory proteins (tropomyosin, and troponin), composing 50-75% of all body proteins[1]. Another interesting feature of the muscle is that the tissue is composed of a long fiber like structures called myofibers. These myofibers are formed by fusion of multiple myoblast cells and are at their terminally differentiated state[2]. While these multinucleated cells make up the core of the muscle tissue, each bundle of myofibers also contain other non-muscle cell types such as immune cells and endothelial cells. Some of these cells are shown to closely interact with the muscles to regulate the growth and regeneration of the tissue[3]. The role of individual cell type in the muscle biology is being actively studied[4] and recent technological advancement is allowing detailed categorization and characterization of various muscle resident cell types[5].

Identification of these various muscle resident cells are critical prerequisite in studying the mechanisms of muscle aging. One way to scrutinize specific muscle resident cell type, is to use fluorescence-activated cell sorting (FACS) to isolate the cell type of interest and perform in-depth RNA analysis. Comparing the results of the young and old muscle samples might reveal the important driving factors of the muscle aging.

Another strategy to study the role of various cell types in muscle aging is to try identifying different cell types under the microscope. There may be a change in the distribution or frequency of different cell types depending on the age of the muscle. If we could find appropriate markers to distinguish various cell types and their subpopulations, we can visualize how the tissue composition gradually change with different age groups. If there is a systematic method of creating the reliable markers for the cell of any desired characteristic, we would be able to differentiate and detect even the slightest changes in the muscles' cell composition with age.

A common limitation in studying many cell types is in the maximum number of simultaneous detection possible for the technology. IHC labeling of the various cell types, for instance, is limited to how many different but compatible enzymatic signal developments exist. IF labeling of the cell types is limited to how many channels are utilized in given range of wavelengths without creating spillover effects. Currently, at least 13 different cell types are identified in skeletal muscles[5,6], and each is being studied to reveal a number of important sub populations relevant to muscle aging. In a field of ever-expanding subjects of interest, a tool that can be easily and consistently adapted to any new target while offering almost unlimited maximum number of simultaneously analyzed targets is highly desired.

RNAscope HiPlex offers simultaneous detection and visualization of many RNA targets of interest. As this technology targets the RNA instead of the protein, the development of a new probe is a rapid, reliable and well-established process that simply requires quiring the RNA sequences. The technology employs the oligo Z probes of the RNAscope but each probe comes with one of twelve channels associated with the major fluorescence channels (488, 550, 650, and 750). After each round of signal amplification, the results are imaged, and fluorophores are chemically cleaved to allow signal development from the next set of probes (Fig. B2.1). In theory this process can be repeated infinitely for simultaneous detection of infinite number of targets, but in practice, the tissue integrity is lost with repeated washing and cleaving, and the noise gradually accumulates. Still, with careful execution of the protocol, the detection of about a dozen different RNAs is easily achieved and if desired multiple consecutive sections can be analyzed and overlaid for much greater number of simultaneous detections.

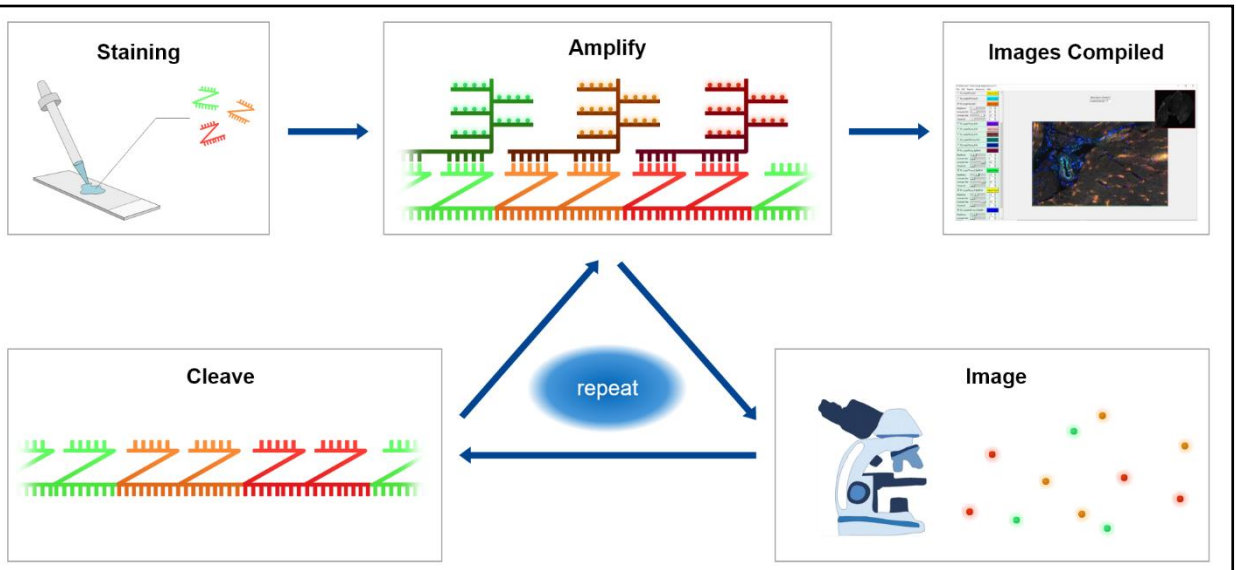

Figure B2. RNAscope HiPlex procedure. After staining and initial amplification steps, individual signal amplification for the first round of probes are done. The results are imaged and the probes are cleaved. Second set of probes are amplified and imaged. The process is repeated as many times as needed and resulting images are complied in the Image Registration Software.

Methods

GentleMACS muscle digestion

Harvested muscles were mechanically digested with scissors (repeatedly cut for 5 minutes by which time the product became a dry slurry). The sample was then digested with collagenase II in Ham's F10 solution for 1.5 hours and washed. The sample was further digested with a mix of collagenase II and dispase for 30 more minutes and washed. The sample is then moved to the gnetleMACS dissociator and placed in the instrument for additional digestion. At the end of the digest, the sample is strained through 40 um filter two times and stored in ice until FACS.

TRIzol RNA extraction

1 mL TRIzol solution was added to FACS tube and cells were sorted directly into this tube. 0.2 mL chloroform was added and thoroughly mixed by shaking. The tube was allowed to sit for 2 minutes

and spinned down for 15 minutes at 12,000 x g at 4°C. The clear supernatant was transferred to a new tube for the RNA analysis.

FACS

1 mL of mouse hind limb muscle digest from two mice was carefully loaded on top of 9 mL of 25% Percoll. The tube was spinned down at 15,000 x g for 10 minutes at 4°C. Resulting pellet was resuspended in 100 uL PBS and given 10 uL of 10 ug/mL propidium iodine and 1 uL each of the following antibodies: CD45 (30-F11) APC-eFluor 780 (ThermoFisher 47-0451-82), CD31 (PECAM-1) PE-Cyanine 7 (ThermoFisher 25-0311-82), CD34 Alexa Fuor 647 (BioLegend 119314), Ly06A/E Sca-1 PE (BioLegend 108107). The sample was incubated at dark for one minute. FACS was performed with *BD FACSAria III.* FSC vs SSC plot was used to filter out the debris. The singlet population was selected in FSC-H vs FSC-A. PI negative cells were selected as viable cells. CD45 positive cells were collected as immune cells. CD31 positive cells were collected as endothelial cells. CD45 negative cells were examined for CD34 and Sca1. CD34+ and Sca1+ cells were collected as FAPs cells while CD34+ and Sca1- cells were collected as satellite cells.

The RNAscope HiPlex Assay

The HiPlex Assay was performed according to manufacturer's protocol. In short, muscle cryosections were immediately fixed with 4% PFA for 1 hour at room temperature to ensure that the tissue is not detached during multiple washing steps. The sample was then dehydrated with 50, 70, and 100% ethanol and stored in fresh 100% ethanol for at least overnight, at -20°C. The sample was retrieved and air dried. In a humidifying chamber, enough Protease IV solution was given to cover the whole tissue and incubated for 30 minutes at room temperature. The HiPlex probe mix was prepared during this time. The probes were applied and the sample was placed in an oven set to 40°C for 2 hours. After two 2 minutes wash with rigorous agitation in the washing

buffer, Amplification solution 1 to 3 was given, each with 30 minutes of incubation in 40°C followed by two 2 minutes wash with agitation. At this point, the sample was stored in 5xSSC solution overnight at room temperature. On following day, the sample was briefly rinsed and counter stained with DAPI and imaged to obtain background signals for all channels (if DAPI stain was already performed in prior day, the DAPI signals may be feint and require re-staining at some point). Fluoro T4-T6 was applied to the sample and incubated for 15 minutes at 40°C. The sample was washed twice for two minutes with agitation. A drop of ProLong Gold was given and the sample was covered with a coverslip. The slide was placed on ice and carried to the microscope. Images were taken for all channels while keeping the sample as close to its prior position as possible. After taking the images, the sample was immediately placed back on ice and brought to the work bench. The sample was soaked in 4X SSC at room temperature for at least 20 minutes and the coverslip was gently removed with a probe. The slide was rinsed with fresh 4X SSC. A fresh glass of ampoule containing cleavage solution was broken and diluted 1:10 in 4X SSC. The diluted cleavage solution was applied to the sample in a humidifying chamber and incubated for 15 minutes at room temperature. The sample was washed with PBST (0.5% Tween) for 2 minutes with agitation, twice. The diluted cleavage solution was applied one more time and incubated as before. The sample was washed with PBST as before. Next, Fluoro T1-T3 was applied to the sample. Incubation, washing, imaging, and cleavage procedure were repeated as before. The WGA counter staining was performed on the sample and images were taken.

Quantifying cell types

From the raw image file of entire muscle cross section, one field of view was selected and magnified at 50% in NIS-Elements software. The DAPI channel was opened and LUTS value was adjusted for the clear depiction of nuclei. A notable DAPI stain pattern (A group of DAPI signals forming a memorable shape) was selected and their position was marked on the screen. Without modifying the field of view, a screenshot of every channel was taken and each posted on

Window's Paint program. In the property section of the Paint, the width and length of the canvas was changed to something slightly smaller than the original and saved to a folder. Next raw image file was opened in NIS-Elements software. The field of view was set to 50% magnification and moved to the same region as before. DAPI channel was opened and adjusted appropriately, and the notable DAPI pattern previously identified was located again. Using the mark on the screen, the notable DAPI pattern was aligned as close to the previous file as possible. Screenshots of the channels were taken and posted on the Paint as before. The size of the image on Paint was changed to the same width and length used with previous set of pictures and saved to the same folder. Failure to match the size of these images prevent the use of the compiling program. This process was repeated for every raw image file. Next, all images of the matching size were added to the Image Registration Software. All DAPI images were selected and registered as DAPI images, which creates transformation matrix after every additional DAPI image. The matrix was applied to all channel images of the same imaging round. Images of the same channel were selected and the background was subtracted with the background image (image taken right after DAPI before any Fluoro application) of the channel. This resulted in final raw images. One DAPI image was selected and one of the five Fluoro image was selected. Blue color was assigned to the DAPI channel and red color was assigned to the Fluoro image for best visualization. Signal for the Fluoro image was raised until background noise started to appear or until the signals became too saturated and merged. A screen shot was taken and opened in ImageJ. The estimate of DAPI count was made by making the image binary with appropriate threshold and applying watershed and particle analysis. Cell type count was done by manual cell counting function of ImageJ. To identify the unaccounted cells, a screenshot was taken from the Image Registration Software after selecting all Fluoro images and DAPI. In ImageJ, the nucleus not associated with any red signal was identified as the unaccounted cells. The counts from every cell type and the unaccounted cells were combined to obtain the total cell count.

Results

Digesting mouse muscles into single cells

The workflow for the muscle sample preparation is shown in Figure 3.1A. In short, mouse hind limb muscles from two 7 months mice were pooled and digested through mechanical and enzymatic methods along with *gentleMACS* tissue digestion protocol. The digest was strained through 40 um filter two times. Resulting muscle digest contained successfully separated single cells and long-fiber like debris. These debris did not have any nucleus and was less dense than healthy single cells. To filter out the debris from the single cells, we performed *Percoll* gradient centrifuge. To find an optimal concentration of *Percoll*, we split the muscle digest into several 100 ul aliquots and carefully dispensed each on a 200 ul *Percoll* of varying concentrations ranging from 10 to 100%. Figure 3.1B (right), shows the result of the 100% *Percoll* gradient where debris and cells all collected at the interphase because they were not as dense as the 100% *Percoll*. We show representative images from 60 to 20% *Percoll* in Figure 3.1C. Images from the interphase is shown on the top row while images from the pellet, if any formed, is shown on the bottom row. We did not observe any pellet when *Percoll* concentration was 60% or greater. The best separation occurred at 25% *Percoll*. From 20% *Percoll*, debris also started to collect at the bottom of the tube. Having found the optimal concentration, we used 1 ml muscle digest on a 9 ml of 25% Percoll solution to obtain clean, single cell muscle digest.

FACS on mouse hind limb muscles

Resulting single cell muscle digest was stained with PI and cell type specific markers shown in Table 3.1 for analysis with *BD FACSAria III*. FSC vs SSC plot was used to filter out the debris. The singlet population was selected in FSC-H vs FSC-A. FSC-A vs PI plot was used to select PI^- population which represents the viable cells. The live, viable cells were then passed through multiple gating to isolate individual cell type as shown in Figure 3.2A.

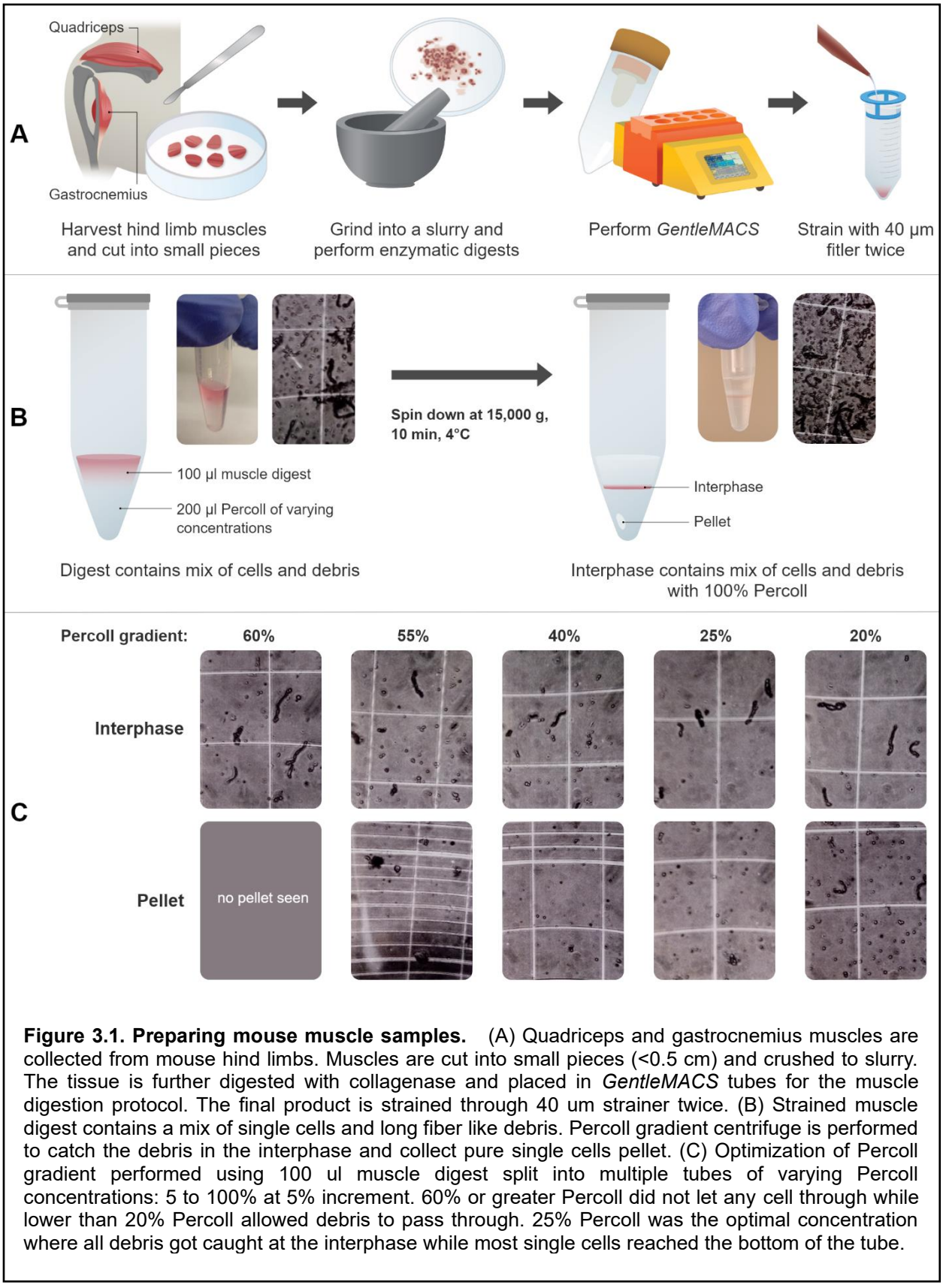

Figure 3.1. Preparing mouse muscle samples. (A) Quadriceps and gastrocnemius muscles are collected from mouse hind limbs. Muscles are cut into small pieces (<0.5 cm) and crushed to slurry. The tissue is further digested with collagenase and placed in *GentleMACS* tubes for the muscle digestion protocol. The final product is strained through 40 um strainer twice. (B) Strained muscle digest contains a mix of single cells and long fiber like debris. Percoll gradient centrifuge is performed to catch the debris in the interphase and collect pure single cells pellet. (C) Optimization of Percoll gradient performed using 100 ul muscle digest split into multiple tubes of varying Percoll concentrations: 5 to 100% at 5% increment. 60% or greater Percoll did not let any cell through while lower than 20% Percoll allowed debris to pass through. 25% Percoll was the optimal concentration where all debris got caught at the interphase while most single cells reached the bottom of the tube.

Marker	Signal
CD45	APC-Cy7
CD31	PE-Cy7
Sca1	PE
CD34	APC

Table 3.1. Surface markers and conjugates used for the FACS. Four popular surface markers for muscle cell typing coupled with appropriate conjugates for the minimum spill over effects.

Actual plots for gastrocnemius and quadricep muscles are shown in Figure 3.2B. Total of 79,095 viable, single cells were collected from gastrocnemius muscles of two mice (viability = 79.1%). 13,026 viable, single cells were collected from quadriceps of the same two mice (viability = 74.9%). Percentages of different muscle resident cell types collected from these viable cells are listed in Table 3.2.

	Gastrocnemius	Quadriceps
Leukocytes	1.19%	1.01%
Endothelial cells	14.82%	12.52%
Satellite cells	2.3%	5.08%
FAPs	0.2%	0.16%
Mature muscle	<81.49%	<81.23%

Table 3.2. Percentages of different cell types collected by FACS. Similar percentages observed from two different hind limb muscles. The most abundant type collected was endothelial cells. Did not get much FAPs cells with our sorting strategy.

Endothelial cells were the most abundant non-muscle cell type, ranging from 12.52 and 14.82% of the total viable, single cells. The satellite cells were 2 to 5% and leukocytes were about 1% of the live cells. We did not get much FAPs cells with our gating strategy (<0.2%). Finally, we assumed most of the non-identified cells would be myofibers and indicated the maximum possible percentage in the table. As there are other rare cell types we did not investigate, actual myofiber population is expected to be smaller than what is estimated. As a confirmatory test for isolated cells, we performed the cytospin with the collected cell suspension and stained each collection with different cell type specific antibody. Figure 3.2C shows the most successful isolation which was CD31+ endothelial cells.

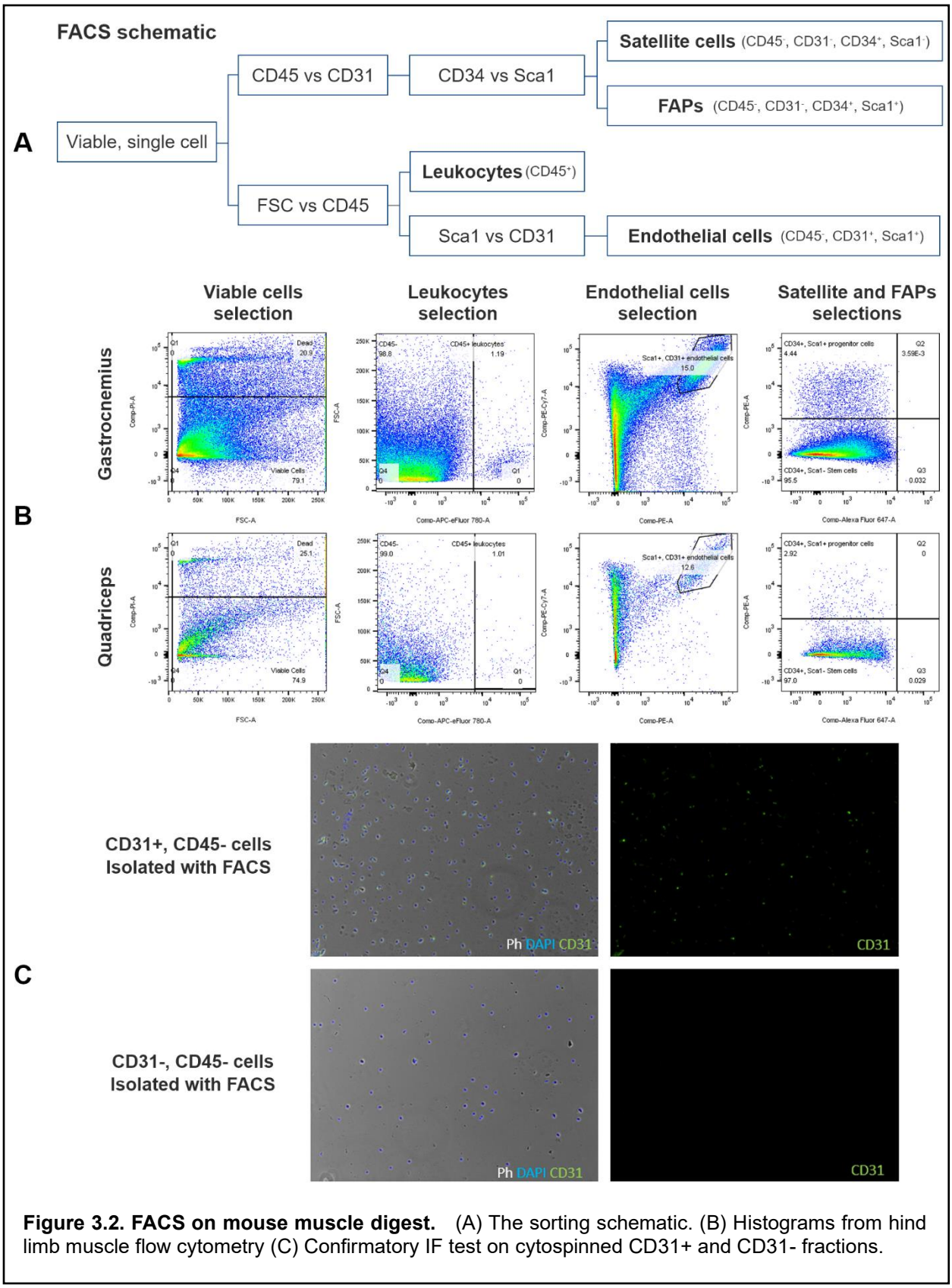

Figure 3.2. FACS on mouse muscle digest. (A) The sorting schematic. (B) Histograms from hind limb muscle flow cytometry (C) Confirmatory IF test on cytospinned CD31+ and CD31- fractions.

RNA extraction on individual cell types

Total of 500,000 endothelial cells had been collected, which is the maximum amount possible in a single run through of the *FACSAria III*. For other cell types, we could only collect a couple of thousands (Table 3.3). These isolates were each sorted directly into 1mL TRIzol and extracted on the same day. RIN socre of the endothelial cells was poor (2.6) while RNA concentrations from other cell types were too low to be analyzed.

	Cell Counts	RNA conc.	RIN
Endothelial cells	500,000 (max)	<20ng/ml	2.6
MSC	25,734	<20ng/ml	N/A
Satellite cells	21,948	<20ng/ml	N/A
Fibroblast	10,154	<20ng/ml	N/A

Table 3.3. Cell counts for each cell type collected out of hind limb muscles of 2 mice. While endothelial cells reached single collection limit of half million cells, other cell types were only in tens of thousands. The quality of extracted RNA was also very poor.

To make sure this is not a technical problem with TRIzol extraction, we performed the same assay on unsorted muscle digest from four mice over two different experiments. The digest from each mouse was diluted 1:3 to get roughly 500,000 cell count before the extraction. Resulting RNA concentrations ranged from 188 to 301 ng/ml. Two samples were chosen at random to test the quality of the extract and we got the RIN scores of 8.4 and 8.7 (Table 3.4).

	Cell Counts	RNA conc.	RIN
Exp 1 mouse 1	~500,000	246 ng/ml	not tested
Exp 1 mouse 2	~500,000	273 ng/ml	8.4
Exp 2 mouse 1a	~500,000	188 ng/ml	not tested
Exp 2 mouse 1b	~500,000	301 ng/ml	not tested
Exp 2 mouse 2a	~500,000	200 ng/ml	8.7
Exp 2 mouse 2b	~500,000	229 ng/ml	not tested

Table 3.4. RNA extractions from muscle digests before FACS. Half a million cells from each of four mice over two independent experiments were used for TRIzol RNA extraction. We obtained about 200 ng/ml RNA from each sample with RIN score greater than 8.

These results show that the integrity of the RNA is well preserved before the FACS, but the quality of RNA is quickly degraded right after the FACS. We were also worried that we might not have

enough cells for a successful RNA extraction by TRIzol. To see the minimum number of cells required for reliable RNA extraction, we serially diluted unsorted muscle cells and checked their RNA quality. We learned that even 100,000 muscle digest cells are not enough to ensure high quality RNA extraction (Table 3.5). As we could only obtain about 20,000 cells of interest with two mice, this meant that we would have to pool 100 mice to get enough of the rare cell types.

Dilutions	Cell Counts	RNA conc.	RIN
2:3	~1,000,000	112.1 ng/ml	8.6
2:30	~100,000	31.7 ng/ml	N/A
2:300	~10,000	<20 ng/ml	N/A
2:3000	~1,000	<20 ng/ml	N/A

Table 3.5. Muscle digest before FACS is serially diluted before RNA extractions. When there was 100,000 or less cells of the muscle digest, we did not get good RNA extraction out of the sample.

The RNAscope HiPlex Assay

Five cell type specific markers were chosen and we ordered stock HiPlex probes with appropriate channels as shown in Table 3.6. To note, we had initially tried CD45 to mark the immune cells, but we were not able to detect the signals and changed to CD74.

Cell Types	Markers	Channels
Muscles	Acta1	T1 (488)
FAPs	PDGFRα	T3 (650)
Leukocytes	CD74	T4 (488)
Endothelial cells	PECAM1	T5 (550)
Satellite cells	Pax7	T6 (650)

Table 3.6. Muscle resident cell types investigated with corresponding markers. Representative marker chosen for each cell type and assigned 488, 550, or 650 channel.

29 months old mouse quadriceps sample was fixed and stained with HiPlex probes and the first set of images were taken before any signal amplification to obtain the background noise for 488, 550, and 650. 488 had the most autoflourescence with our muscle samples (Fig. 3.3). The signals for T4, T5, and T6 were developed and imaged. The signals were then cleaved by supplied chemical cleavage reagent. The signals for T1, T2, and T3 were developed and image.

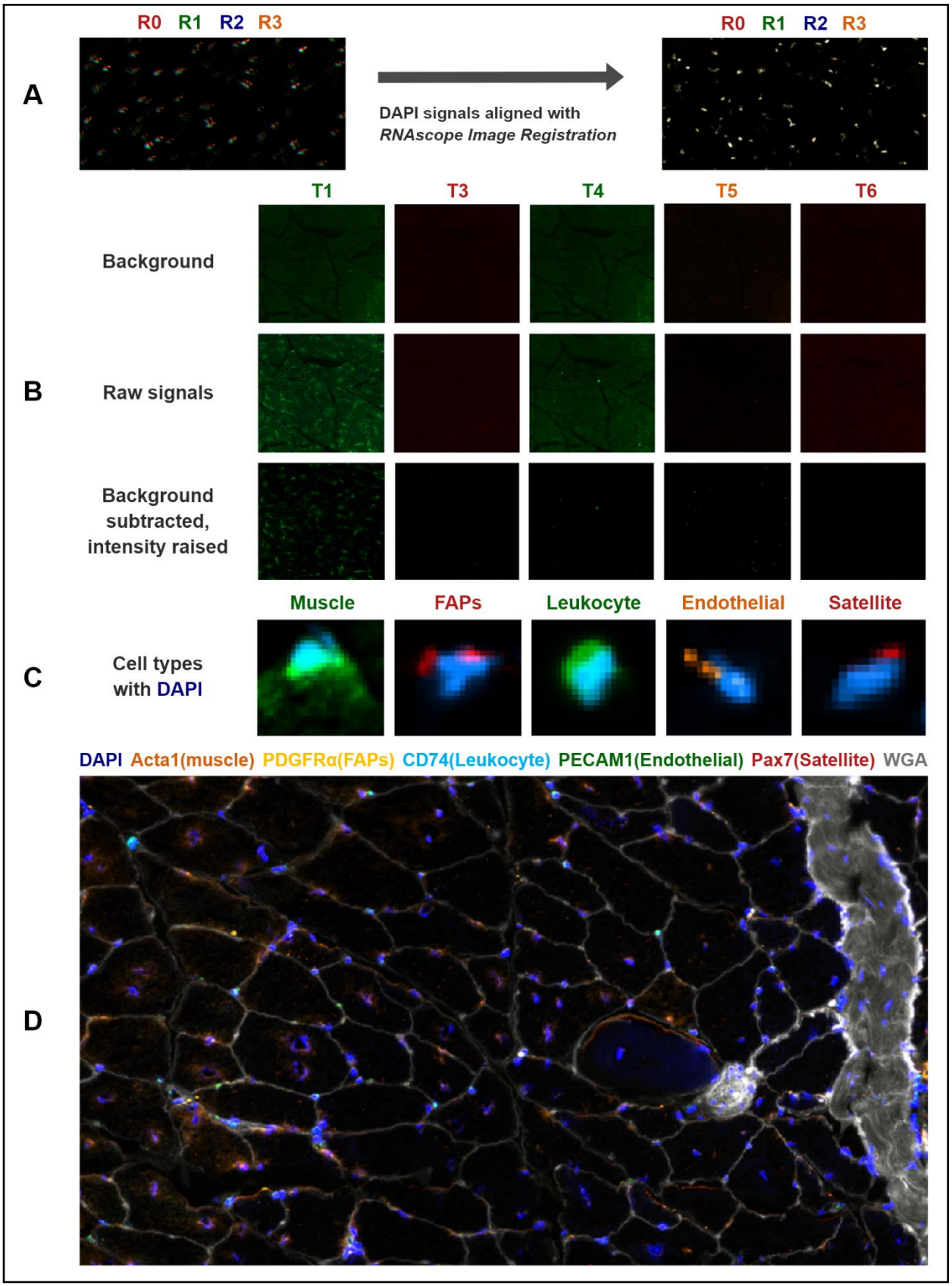
A
R0 R1 R2 R3
DAPI signals aligned with
RNAscope Image Registration
R0 R1 R2 R3
B
T1 T3 T4 T5 T6
Background
Raw signals
Background subtracted, intensity raised
C
Muscle FAPs Leukocyte Endothelial Satellite
Cell types with DAPI
D
DAPI Acta1(muscle) PDGFRα(FAPs) CD74(Leukocyte) PECAM1(Endothelial) Pax7(Satellite) WGA

Figure 3.3. RNAscope HiPlex Assay on 29 months mouse quadriceps muscles. (A) DAPI signals from 4 imaging rounds (R0 – R3) are plotted together (left). The misalignment is corrected by provided *RNAscope Image Registration* software (right). (B) Background noise from each channel is collected prior to any signal development. The backgrounds are subtracted from the raw image of each channel to get the final product (signal raised after removing the background to reveal distinct dots). (C) Representative image for each cell type identified from above images and zoomed for better visualization. (D) A portion of the field of view zoomed to show various cell types and WGA (myofibers) at once.

The signals were cleaved once again and WGA staining was performed. Although we tried to image the identical region each time, some misalignments are unavoidable across the imaging sessions. To correct the misalignment, HiPlex image registration software was used and its result is showing in Figure 3.3A. Next we used the background image we took from the three channels to subtract the noise from the raw images (Fig. 3.3B). Representative image of each cell type is shown in Figure 3.3C. Acta1 is the only diffused signal type we have. It strongly stains the muscle cell the proximal edge of the myofiber and the signal weakens as it gets further from the nucleus. Central muscle nucleus is stained most strongly along the contour of the nucleus and quickly fades further from the nucleus. The signals for the FAPs cells are noted with one or more small dots on or next to the nucleus. They are very similar to the signals of the satellite cells and some signals do appear in both FAPs and Satellite cells. We thought this may be a spill over signal and tried switching the order of the signal development but we still saw some cells having both signals. There seems to be a considerable population of Pax7+ and PDGFRa+ cells in mouse muscles. Leukocytes were few in number but they were easily detectable with characteristically large blob of signals covering most of the nucleus and more. Endothelial cells are marked with multiple small signals near and on nucleus and several endothelial cells are often found together, forming a line. Figure 3.3D shows all cell types along with WGA to show the myofibers. We counted each cell type specific signal for each nuclei in three random field of views for total of 1977 nuclei (Fig. 3.4). Myofibers made up about half of the total nuclei and FAPs and endothelial cells made the other half. Not many leukocytes were observed. We saw almost 10% satellite cells with our initial

analysis, but this may be due to generous counting of the signals. If we apply more strict counting criteria (signals occurring far from the nucleus or extremely dim dots dismissed as noise), we get under 3% satellite cells. We did a couple of pilot experiment with younger muscle samples which had noticeably less noise. We got around 2% satellite counts with the young muscles and took note of the ideal Pax7 staining patterns. We decided to apply new, more strict counting criteria for all cell types in proceeding HiPlex analysis.

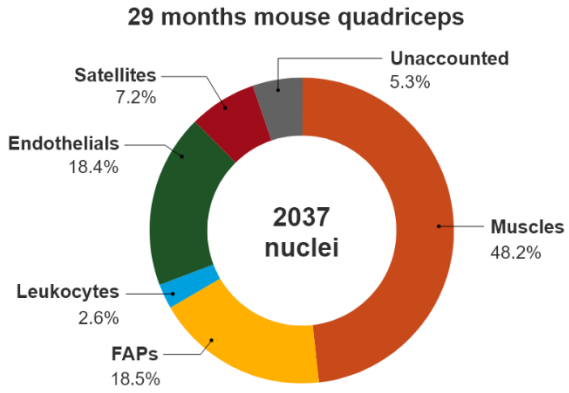

	Markers	FOV1	FOV2	FOV3	Total	%
Cell count	DAPI	562	578	561	1701	83.50515
Muscle	T1-Acta1	362	289	330	981	48.15906
FAPs	T3-PDGFRα	131	118	127	376	18.45852
Leukocyte	T4-CD74	23	22	8	53	2.601865
Endothelial	T5-PECAM1	124	116	134	374	18.36033
Satellite	T6-Pax7	30	59	57	146	7.167403
Unaccounted	No mark	45	34	28	107	5.252823
	Sum	715	638	684	2037	100

Figure 3.4. Initial muscle distribution data with HiPlex on 29 months muscles. Cell type distribution data from average of three fields of view for total of 1997 nuclei. Generous scoring criteria applied for this initial study; all signals taken as positive hits even though some suspected to be staining artifacts and false positives.

Discussion

We formulated our gating strategies based on the literature search and got results comparable to what others reported (Table 3.2). However, this does not mean that this gating strategy is perfect. The distribution percentage of the collected cell types also do not reflect the actual distributions in muscles. For instance, we were not able to collect much FAPs cells. This may be due to especially poor gating strategy for FAPs collection. As this is a relatively newly recognized muscle resident cell type, the best FACS selection strategy is still being investigated. We used CD45-, CD34+, CD31-, Sca1+ as the FAPs indicators. Ling et al., (2015) used Sca1+, CD31-, CD45- as the mesenchymal stem cells (MSC), which is thought to be the larger category of the FAPs cells[7]. The difference between FAPs and MSC in FACS in gating is with CD34. Traditionally MSC is selected with negative staining of CD34 while FAPs are selected with positive staining of CD34. More recently, however, some reports presence of CD34+ MSC in mouse samples, suggesting that CD34 shouldn't be used as a gating criterion in identifying the progenitor cells. In support of this opinion, MSC isolation protocol by *R&D System* also just use Sca1+, CD31-, CD34-. If we change our FAPs criteria to include both CD34 positive and negative groups, we expect to get a population of 3-4% which is the same number reported by others who use the same criteria[7]. Note that these numbers are still only with the FACS of digested mouse muscle samples and not the real representation of the actual physiological distribution. Many cells are lost during sample preparation and FACS is expected to skew the result for certain types of cells. Also, the gating strategy for each cell type is not perfect. We choose to lose much of the actual population to ensure a homogeneous population. One cell type might require more stringent criteria than another, leading to the reduction of the total cells collected. FAPs cells for instance, may make much larger proportion of the muscle tissue but with FACS, we only got 3-4% of the total viable, single cells.

Another problem we found with the muscle FACS was the rapid decline of the RNA quality. We worried our muscle digest procedures are too harsh for the cells but the single cell muscle digests showed surprisingly high viability according to the PI stain (about 75 to 80% viable). TRIzol extraction of the RNA from the muscle digest returned high RIN scores as well (Table 3.4). However, once these cells go through the FACS, the RNA quality drastically decline and no further analysis could be performed (Table 3.3). We have tried different FACS instruments at different locations, but we couldn't retrieve quality RNAs. It seems like the combined stress of the tissue digest and FACS greatly compromise the RNA integrity.

RNAscope HiPlex offered an alternate approach to the problem. It allows the analysis of multiple RNA expressions while keeping the tissue intact. No cell is lost during the sample preparation, and the spatial information of various cells of interests is preserved. Autofluorescence in muscles had been a big challenge in visualizing the tissue with IF, but the background subtraction tool of the RNAscope Image Registration Software was extremely effective in removing the noise and revealing the signals (Fig. 3.3B). We would even recommend applying this tool in normal IF experiments to eliminate the autofluorescence of geriatric muscles.

Although signals from the HiPlex experiments were clean, interpretation of the data had some ambiguity. As cells in the muscles do not have a clearly visible cell boundaries, it was often difficult to assign the signal to a nucleus when the signal is found between multiple nuclei. Also, even though the software does very good job removing almost all noise, geriatric muscles tended to show some noise. As HiPlex signals are usually fine dots near nuclei, some of the tiny dots caused by the noise look very similar to the true signals. To avoid making the bias, for the earliest HiPlex experiments, I had opted for extremely generous selection criteria, counting any signal near a nucleus to be a true signal. The distribution data shown in Figure 3.4 represents the results of this generous selections. This is however, not the true reflection of the actual distribution, because we could identify quite many signals that were clearly from the noise. For instance, one

region of the field of view could be dotted with background noise that extends to places outside the tissue. All nuclei in that region would be scored positive for the signal but that is clearly not depicting the actual cell distribution. As we gained more experience looking and identifying the distinctive features of the positive signals (Fig. 3.3C), we eventually adopted more stringent and accurate scoring system to better reflect the actual distributions.

REFERENCE

1. Frontera, W.R. et al. Skeletal muscle: a brief review of structure and function. Calcif. Tisue Int. 96, 183-195 (2014).

2. Chal, J. et. al. Making muscle: skeletal myogenesis in vivo and in vitro. Development. 144, 2104-2122 (2017).

3. Criswell, T.L. et. al. The role of endothelial cells in myofiber differentiation and the vascularization and innervation of bioengineered muscle tissue in vivo. Biomaterials. 34, 140-149 (2013).

4. Relaix, F. et. al. Perspectives on skeletal muscle stem cells. Nat. Comm. 12, 692 (2021).

5. Giordani, L. et. al. High-dimensional single-cell cartography reveals novel skeletal muscle-resident cell populations. Mol. Cell. 74, 609-621 (2019).

6. Zhang, X. et. al. Characterization of cellular senescence in aging skeletal muscle. Nat. Aging. 2, 601-615 (2022).

7. Liu, L. et. al. Isolation of skeletal muscle stem cells by fluorescence-activated cell sorting. Nat. Protoc. 10, 1612-1624 (2015).

CHAPTER 4:

Identifying Aged Cell Types in Muscles

Background

The cells age with time, but different cells exhibit different aging phenotypes. For instance, endothelial cells are known to show SA-β-gal activity with age[1], but muscle cells do not show SA-β-gal activity with age. This does not mean muscles do not age. It simply means the aging phenotypes of muscles do not include the SA-β-gal activity. In order to properly dissect various cell types in muscles and recognize how they age, we need to explore various aging markers and see which ones best demonstrates the aging of each cell type. Some cell types have known aging markers from studies in other tissue contexts. For instance, a subset of memory T cells are shown to have increased CD57 and KLRG1 expressions with age[2]. However, it's necessary to test if the known aging markers are also suitable for the cells residing in the muscles. Previously mentioned endothelial cells were shown to have SA-β-gal activity when they are studied from retinal blood vessels[1], but endothelial cells in skeletal muscles have not been shown to have the SA-β-gal activity. We could start with the known aging marker for each cell type from other tissue environments, but ultimately, we need to find the best aging marker for the cell types in the context of the skeletal muscles. The very fact that these cells exhibit different aging phenotypes when in skeletal muscles hint at the mysterious mechanism of the muscle aging and advocates the necessity of this study.

Our first strategy in determining the best aging marker for each cell type is to combine the cell type identification with the HiPlex and the known IF based aging markers in aged muscles. We can compare the distributions of the cell types for each aging marker to see what cell types are most abundantly expressing the tested marker. Once we obtain the list of promising aging markers for each cell type, we can further test them by comparing the results from the young and

old muscles. A good aging marker for the cell type would have a noticeable increase in the frequency of the cells positive for the marker, nicely correlated with the increased age.

We had explored a few ways to combine a RNA FISH technology with IF. We reasoned that all probes should be applied right away when the sample is at its best condition, so we don't lose any signal due to the various sample processing. As for the development of the signals, we tried different orders (RNA FISH first or IF first) with a fixation step in between, and saw that either one works (data not shown). It then came to our attention that the company selling the RNAscope supplies also sells a co-detection kit for simultaneous detection of the RNA and protein. The kit instructs us to stain the sample with all probes and develop the RNA signal first. Fixation is then performed and the IF development is done. The procedure was not very different from what we had done, but the buffers included with the kit is supposed to help preserve the RNA signals throughout the process and so we decided to use them.

Another way of combining two different assays is to perform consecutive cryosections. An average diameter of a nucleus is 10 um and RNA originating from a muscle nucleus is always found near the nucleus. Even though muscles have gigantic multinucleated cell bodies, RNAs do not travel across the entire cell body. Instead, they are known to occupy a small area proximal to the nuclei known as the zone of influence[3]. If a section is made at a thickness less than the width of this zone of influence, we would expect to find the cell split between the two consecutive sections. The exact size of the zone of influence is unclear but we can empirically determine the right thickness to preserve the signals from most cells.

Methods

Co-Detection

Co-detection was performed according to the manufacturer's instructions. In short, cryosectioned muscle samples were fixed with 4% PFA for 30 minutes at room temperature and dehydrated with

50, 70, and 100% ethanol, 1 minute each. The samples were stored in fresh 100% ethanol for at least a day at -20°C. The sample was retrieved and air dried. Hydrophobic barrier was drawn and the primary antibody was applied, diluted with supplied Antibody Diluent 1:100. The slide was incubated overnight at 4°C. The sample was washed in PBST for 2 minutes, twice and fixed with 4% PFA for additional 30 minutes. The sample was washed with PBST for 2 minutes, twice and Protease IV was applied for 30 minutes at room temperature. The sample was washed with distilled water twice. Normal Basescope protocol was performed at this point. The sample was then blocked with Co-Detection Blocker and incubated for 15 minutes at 40°C. The sample was washed twice with 1X Wash Buffer, 2 minutes each. The secondary antibody was diluted in Co-Detection Antibody Diluent 1:1000 and applied for 1 hour at room temperature. The sample was washed with PBST for 2 minutes, twice and counterstained with 50% hematoxylin and DAPI.

Consecutive cryosections and thickness optimization

Snap frozen murine muscles were cryosectioned at 3 to 8 µm thicknesses and HiPlex Assay was performed with just one HiPlex probe: T3-PDGFRa (FAPs marker). The percentage of FAPs positive cells was determined from the samples and plotted on thickness vs. percentage graph. Average FAPs percentage from previous HiPlex experiments with 10 µm sections was calculated and marked on the graph. The minimum thickness required to reach the average FAPs percentage with 10 µm section was identified.

Analysis of the triplet assays

Three consecutive cryosections of 7 µm thickness were made. If any of the three sections had obvious deformities or folds, three new consecutive sections were prepared. The sections were placed on different slides but at similar orientation as rotations across the sections make it extremely difficult to identify the same regions. The middle section was always chosen for the HiPlex assay while first and third sections were used for ORF1 or p21 Basescope staining. All

three assays were performed as described previously. To quantify, entire muscle section was examined to count and locate every ORF1 positive cell and cross referenced with HiPlex data of the identical region (using the notable DAPI pattern recognition method previously described) to determine its cell type. The frequency of ORF1 positive cells was normalized to the total number of nuclei found in the entire cross section of the muscle. p21 signals were quantified by manually counting every p21 signal in the entire cross section of the muscle. As the signals were tiny, the examination was done by viewing at 50% magnification in NIS-Element software and taking the screen shot of what's visible on the screen. Total of 11 screenshots were taken for the entire cross section of the muscle and each screen shot was opened in ImageJ to utilize the cell counting tool. p21 signals were also normalized to the total number of nuclei. HiPlex analysis was done in three random fields of view and p21 data of the same three field of views were cross referenced to get distribution of p21 cell types as well. ORF1 positive cells were individually tracked and referenced with p21 data to check whether ORF1 positive cell was also positive for p21.

Results

RNAscope integrated Co-Detection Assay

The co-detection of the immunofluorescence (IF) targets by traditional antibodies and the ISH targets by *RNAscope* is done with *ACD*'s co-detection kit. In short, the sample is fixed and stained with the primary antibodies. It is then fixed once more and permeated for the normal *RNAscope* protocol. After developing the RNA signals with *RNAscope*, The sample is blocked and stained with the secondary antibodies for the development of the IHC signals.

Figure 4.1A shows the co-detection of p16 mRNA through the *Basescope* assay and p16 protein detection through IF on etoposide treated LF1. *Basescope* is a colorimetric assay but the signals from the brightfield had been overlaid and given an inversed color for the better visualization.

We tried to combine IF markers for different cell types and p16 mRNA Basescope probe to see which muscle cell types exhibit the aging phenotypes. As we already had the IF markers from the FACS study (Table 3.1), we simply applied the co-detection protocol with the newly developed p16 mRNA *Basescope* probe. For the satellite cell detection, however, we chose to use the well established Pax7 antibodies instead. The results for p16 mRNA co-staining with Pax7 are shown in Figure 4.1B. We could detect Pax7 signal from the 8 months or younger muscles, but the frequency of p16 mRNA at this age group was very low and we couldn't find a satellite cell that expresses p16 mRNA. For the geriatric muscles (25-36 months) we saw more p16 mRNA signals but this time we had difficulty developing Pax7 signals. We tried using different Pax7 antibodies and signal retrieval protocols but nothing worked very well in our hands. This was quite unfortunate as the satellite cells were our primary interest at the time. We had slightly better outcomes with co-staining of the other cell types but they were also very inconsistent. The frequencies of the detected cells were much lower than expected and it seemed like each IF

requires different, optimized protocols to ensure a high detection rate. We needed an alternate method where every cell type in the muscle can be detected at once, without the need to fine tune each detection. We had to get a consistent result from all cell types of interest so their phenotypes

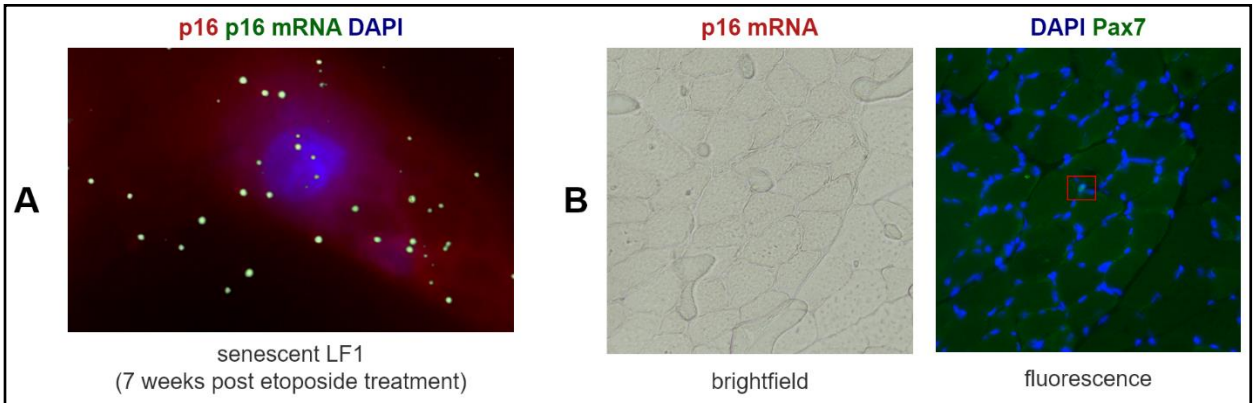

Figure 4.1. Co-detection of RNA and proteins. (A) 7 weeks post etoposide treatment LF1 is stained for p16 protein and p16 mRNA through RNAscope co-detection kit. (B) 8 months mouse muscles stained for p16 mRNA and Pax7 protein. Pax7+ cells are occasionally detected but no p16 mRNA seen at this age group.

Combining ORF1 IF with the HiPlex

After a successful HiPlex assay on young and old muscles, we decided to try combining the HiPlex with the IF. The Co-detection protocol is not meant to be used with the HiPlex assay, but with a slight modification they can be used. After trying different modifications we had some promising results combining HiPlex with the ORF1 IF to identify ORF1 expressing cell types in the muscles. Figure 4.2A shows an example of ORF1 IF performed with the HiPlex assay. As this was to test if the combination works, we just used one HiPlex probe which marks the FAPs cells (PDGFRa). Because this probe was conjugated with a far red (*Dylight 650*), ORF1 signal was developed with *Alexa Fluor 546.* We observed large blob or green signals indicative of the ORF1 on some nuclei of the 29 months old gastrocnemius. We also saw red dots indicative of the FAPs marker on some nuclei. Indeed, some cells were positive for both ORF1 and PDGFRa. However, the quantification of the ORF1+ FAPs cells proved challenging because many signals from both were dim and hard to distinguish from the abundant background noise. It seems like our attempt to combine both

assays led to suboptimal staining results. We may be able to improve the outcome with further tweaking of the protocols, but as the HiPlex assay is still relatively new, we wanted to get more reliable data using unmodified protocols. One way to achieve this is to perform a consecutive cryosectioning and using one section for the HiPlex and the other for the IF. As most cells are preserved across the two sections, this method will allow us to perform two different assays on the same set of cells while adhering to the original protocols. We first performed cryosections of 29 months old quadriceps at various thicknesses and checked how different thicknesses affect ORF1 staining. From 10 um to 20 um thicknesses, we observed same high ORF1 signal intensities (Fig. 4.2B). As using a 10 um thick section as opposed to the thicker sections did not result in less staining, we decided to do two consecutive cuts of 10 um thicknesses.

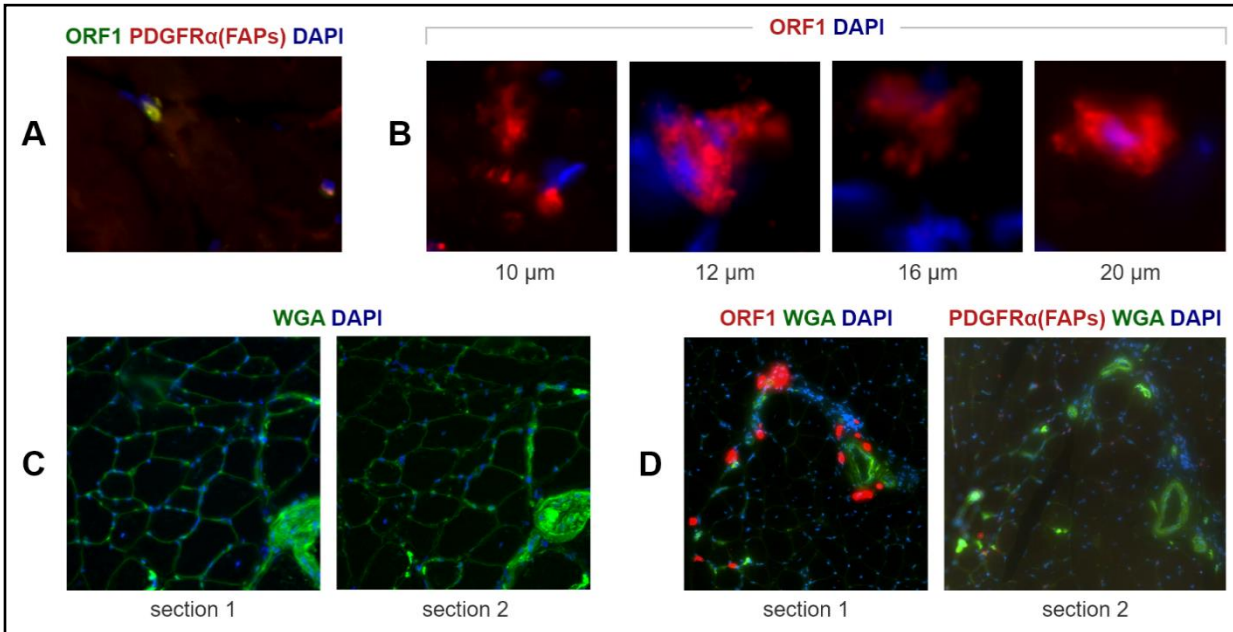

Figure 4.2. Combining ORF1 protein detection with HiPlex. (A) Using the co-detection kit allows some ORF1 and HiPlex co-staining on 29 months old mouse gastrocnemius muscles, but the signals are dim and infrequent. (B) ORF1 staining is as strong in 10 um section as in 20 um muscle cryosection. (C) Consecutive 10 um muscle sections allows most nuclei and myofibers to be conserved across two sections. (D) Performing ORF1 staining in one and HiPlex on the other of the two consecutive muscle sections of 10 um thickness allows identification of ORF1+ cell types.

To see how well cells are preserved across two 10 um thick sections, we prepared the sections and stained both with DAPI and WGA to see nuclei and myofiber patterns. Figure 4.2C compares the two consecutive sections and we confirmed that the cells are mostly preserved

between the sections. Finally we made a pair of consecutive sections and stained one with ORF1 and the other with PDGFRa HiPlex for the FAPs cells. Figure 4.2D shows the results from the comparable regions of the two sections side by side. We could recognize some FAPs cells exhibiting ORF1 signals.

Combining p21 Basescope Assay with the HiPlex

If we could combine IF with the HiPlex by utilizing consecutively cut sections, it means we could combine other methods on these sections as well. We had learned p21 could be very useful aging marker in the muscles and wanted to try combining p21 Basescope assay with the HiPlex. Figure 4.3 shows the result of this combination on two consecutively cut 29 months old quadriceps. In the displayed example, we identified one group of p21 signals to be from the FAPs cells and the other group of p21 signals from cells of unknown origin as the cell did not show any of the tested cell type specific marker.

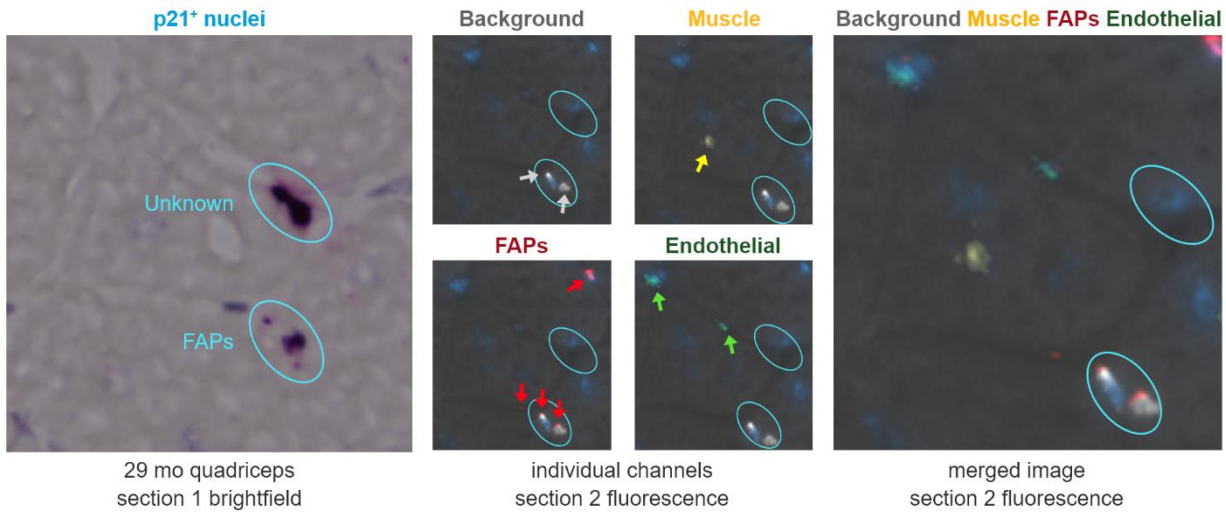

Figure 4.3. Combining p21 mRNA detection with Basescope and the cell type identification with HiPlex. Two consecutive cuts of 10 um thickness made with 29 months quadriceps. One is stained for p21 mRNA using Basescope (left). Another is stained for cell type markers with HiPlex (right). Each of the p21+ nuclei is cross referenced with individual cell type marker on the consecutive section to determine the identity (middle). In the example shown above, one group of p21 signals originated from FAPs cells while another group of p21 signals originated from undetermined nuclei that were negative for all markers we tested.

Combining p21 Basescope Assay and ORF1 IF with the HiPlex

7 μm thickness was determined to be the optimal thickness for three consecutive cryosections (Fig. 4.4A). Figure 4.4B illustrates the combination experiment to perform three different assays on the same set of cells. The thickest portion of the mouse quadriceps was cut into three consecutive sections of 7 μm thick and each section was used for either ORF1 IF, cell typing HiPlex, or p21 Basescope assay. Using these assays on a 29 months old mouse quadriceps, we determined cell type distribution, p21 positive cell type distribution and ORF1 positive cell type distribution (Fig. 4.4C).

DAPI counts were estimated using ImageJ particle analysis tool, but they were only used as a reference to check our total counts are within expected range. The total count is calculated by adding all individual cell count to represent each count in percentages. This inevitably accumulates overcounting errors due to false positive in each cell type which is about 2% per probe for a total of about 10% overcounting.

It was already expected that not all p21 positive cells would be ORF1 positive because p21 is much more abundant of the two, but we were not sure whether all ORF1 positive cells would be p21 positive as well. Cross referencing p21 and ORF1 data revealed that although some aged cells expressed both p21 and ORF1, some cells only expressed ORF1 (Fig. 4.5D).

In young (2 months) vs old (29 months) mouse quadriceps, there wasn't any noticeable difference in the cell type distribution (Fig. 4.5A), but the frequencies of the muscle aging markers p21 and ORF1 greatly increased with the aged sample (Fig. 4.5B, C).

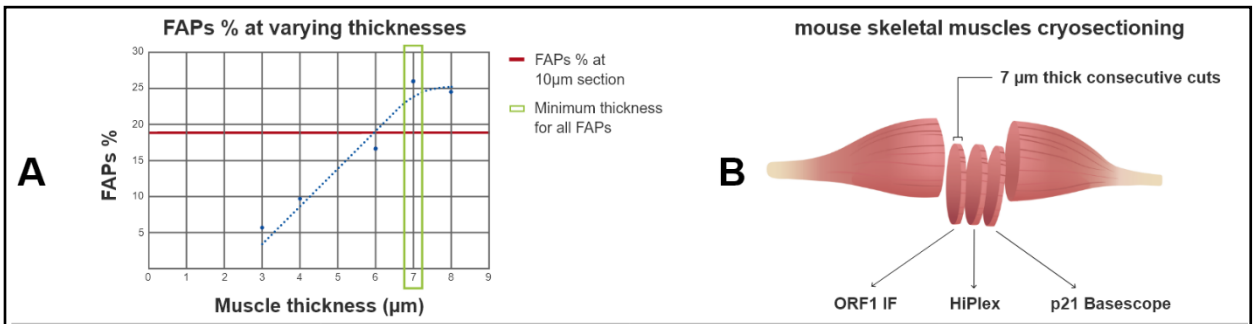

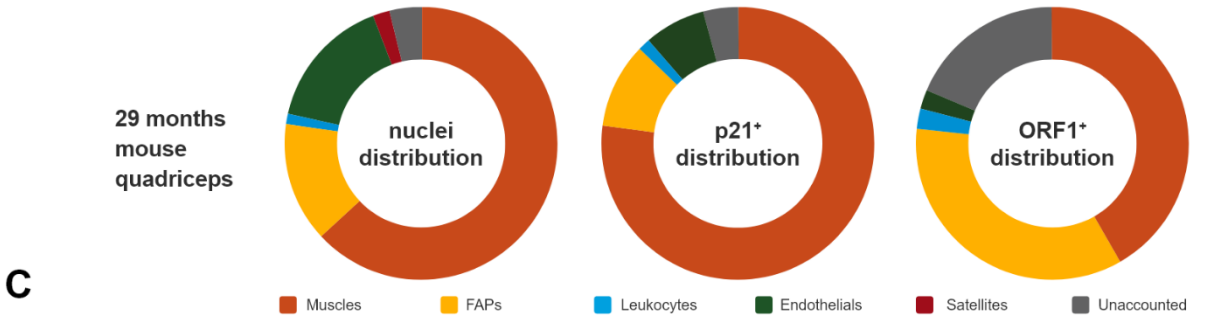

	All		p21		ORF1	
	count	%	count	%	count	%
Muscles	1558	63.1	169	77.2	18	41.7
FAPs	350	14.2	22	10.0	15	34.9
Leukocytes	30	1.2	3	1.4	1	2.3
Endothelials	389	15.7	16	7.3	1	2.3
Satellites	50	2.0	0	0	0	0
Unaccounted	93	3.8	9	4.1	8	18.6
Sum	2470	100	219	100	43	100

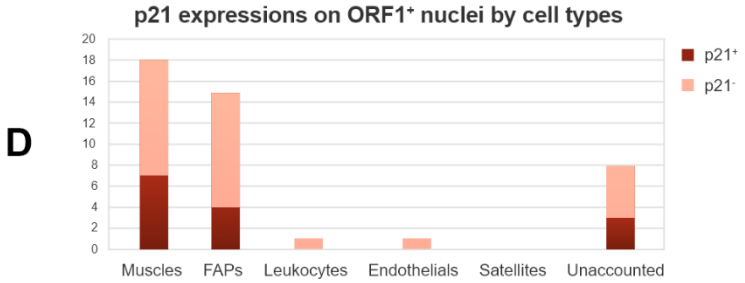

	p21⁺	p21⁻
Muscles	7	11
FAPs	4	11
Leukocytes	0	1
Endothelials	0	1
Satellites	0	0
Unaccounted	3	5

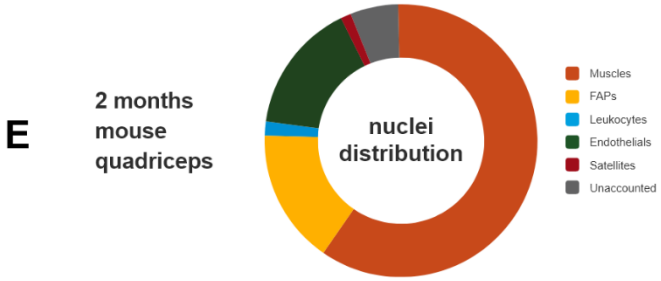

	Count	%
Muscles	1197	60.1
FAPs	315	15.8
Leukocytes	35	1.8
Endothelials	312	15.7
Satellites	21	1.1
Unaccounted	113	5.7

Figure 4.4. Cross referencing HiPlex results with p21 and ORF1 staining of the same cells. (A) 7 µm determined to be the optimal thickness of muscle sections as they are the smallest necessary to preserve the signals from the assays. (B) The combination experiment schematics (C) Distribution data by cross referencing HiPlex results with p21 and ORF1 staining. (D) p21 expressions of ORF1 positive cells by cell types (E) HiPlex analysis on 2 months old mouse quadriceps.

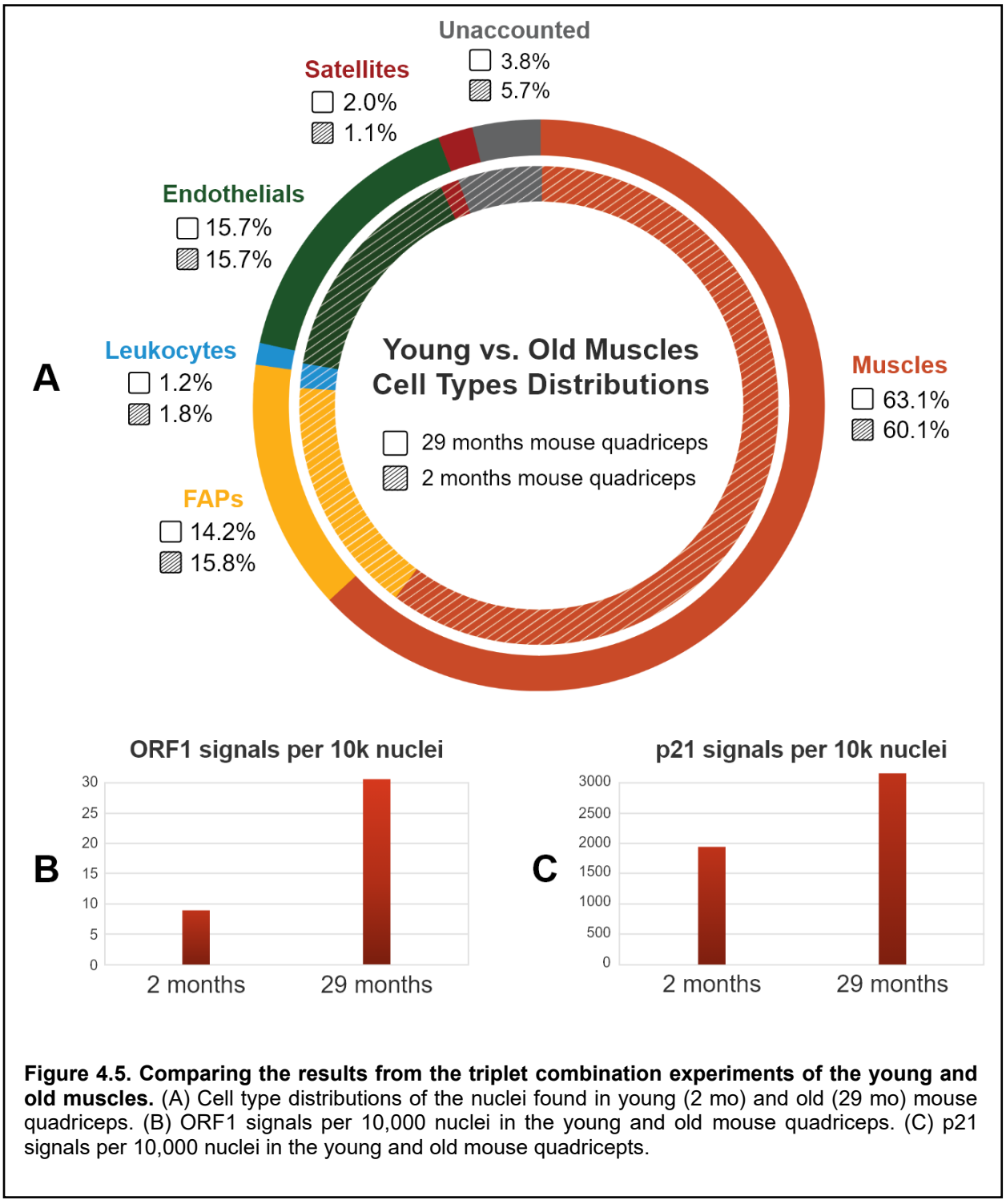

Figure 4.5. Comparing the results from the triplet combination experiments of the young and old muscles. (A) Cell type distributions of the nuclei found in young (2 mo) and old (29 mo) mouse quadriceps. (B) ORF1 signals per 10,000 nuclei in the young and old mouse quadriceps. (C) p21 signals per 10,000 nuclei in the young and old mouse quadricepts.

Discussion

When combining the three assays, we first attempted three consecutive cryosections of 10 μm thickness. This was not successful as only 20 – 30% of the nuclei were preserved across the three sections (data not shown). Using three 3 um thick sections to get combined total of 9 μm was also unsuccessful as all three assays showed decline in performance (frequency of positive cells decreased by about 50%). We had to use minimum possible thickness for the three sections that still preserved the signals. The assay most affected by decreased section thickness was the HiPlex, and so we used the HiPlex assay to set the minimum necessary thickness. We decided to use just one HiPlex probe to test the performance change by the section thickness. 647 has the best signal to noise ratio, and we had two probes utilizing the 647 channel: T3-PDGFRa and T6-Pax7. As T6-Pax7 marks for the rare satellite cells, we decided to use T3-PDGFRa for our tests. Cryosections of varying thicknesses were made and stained with T3 HiPlex probe (Fig. 4.4A). With our previous HiPlex experiments with 10 μm sections, we had about 19% of the cells as FAPs positive. It was only with 7 μm or greater sections that we observed comparable FAPs percentage. We already knew two consecutive cryosections of 10 μm each could be cross referenced without problem, and they have 20 μm thickness in total. Three consecutive 7 μm sections would have 21 μm thickness in total and should be usable as cross references.

The distribution data obtained from these sections employed the new, stringent selection criteria which slightly changed the distribution pattern compared to our initial analysis in Figure 3.4. To note, we found about 60% of the nuclei to be myofibers. This is not to be interpreted as 60% of the cells are myofibers as each myofiber is expected to contain multiple nuclei. If strictly determining the cell count distribution, we expect much smaller percentage of myofibers. However, it is also true that each myofiber has unusually large cell body. If we are to think about the percentage by mass or volume, muscle tissue would be mostly composed of myofibers.

p21 counts also does not accurately represent p21 positive cell counts. There is no way of accurately associating p21 mRNA signal to the originating nucleus. We have investigated a method of estimating p21 positive nuclei based on the signal count and the distance to the closest nuclei (Appendix B), but this estimation was not applied to the data in Figure 4.4C. Instead, the data simply shows the total number of signals observed and what were the cell type identity of the closest nucleus, to get a crude depiction of p21 expressions. We observed that most of the p21 signals had a nearby myofiber nucleus. This may be because myofibers are the most abundant cell type in the tissue, but the fact that the percentage of myofibers associated p21 signals is greater than the percentage of myofiber nuclei in the same tissue means that the myofibers are indeed more likely to produce p21 signals with age than other cell types.

ORF1 on the other hand was extremely rare aging phenotype and part of the reason may be because this is not highly expressed in old muscles. Even though myofibers make up 63% of the total nuclei, only 42% of the ORF1 positive cells were from myofibers (Fig. 4.4C). FAPs cells on the other hand, make up only 14% of the total nuclei but accounted for 35% of the ORF1 positive cells. This means that the FAPs cells have high tendency to develop ORF1 expression with age. Another interesting population was the unaccounted cells. These make only 4% of the total nuclei but they accounted for almost 20% of the ORF1 positive cells. An uninvestigated cell type may be highly expressing ORF1 with age, or ORF1 positive cells may be losing its cell type characteristics and not getting detected by our HiPlex probes. In either case, a further study is needed to clarify the origin of ORF1 and its implication in muscle aging.

As ORF1 positive cells were very rare, we couldn’t get much data on ORF1 and p21 positive cells. We speculated same cells may be exhibiting ORF1 and p21, but our data revealed that many ORF1 positives cells were negative for p21. It seems like these are two different aging markers and aged cells in muscles do not necessarily express both markers. Some cells seem to be expressing one type of aging marker while other cells express different type of aging marker.

This is actually in accordance with our cell type distribution data, as different cell types demonstrated enhanced expressions of different aging markers.

We had also performed this analysis with the young muscles (2 months mouse quadriceps). We expected to find different cell type distributions (more satellite cells, for instance) but we did not find much difference in our data from the two age groups of mice (Fig. 4.5A). As for the ORF1 and p21 expressions, however, there was a clear increase in the expressions with the aged group (4.5B).

REFERENCE

1. Han, Y. et. al. Endothelial senescence in vascular diseases: current understanding and future opportunities in senotherapeutics. Exp. & Mol. Med. 55, 1-12 (2023).

2. Rodriguez, I. J., et. al. Immunosenescence study of T cells: a systematic review. Front. Immunol. 11 (2020).

3. Nevalainen, M. et. al. Distribution of mRNA transcripts and translation activity in skeletal myofibers. Cell Tissue Res. 353, 539-548 (2013).

CHAPTER 5:

Discussions

Summary

We have explored various markers and tools to study aged cell types in skeletal muscles. The myofibers are post-mitotic, multinucleated cells with large protein structures. These features make analyzing myofibers extremely challenging. We attempted isolating single myofiber nuclei for RNA analysis but a lot of cells were lost during the digestion process, and RNA extracted from the sorted cells were too damaged to obtain useful information from a reasonable number of mice (Table 3.3). Analyzing the intact tissue by immunofluorescence labeling was also difficult due to the autofluorescence in aged muscle tissues (Appendix A). This forced us to look for alternative approach that can perform various RNA analysis in intact tissue which utilizes colorimetric assays or somehow handle the autofluorescence of the muscles.

The Basescope Assay is a hypersensitive and specific RNA FISH technology that utilizes colorimetric assays to detect up to two RNA targets. The technology only requires ~50 nt sequences to hybridize and was suitable for detecting p16 mRNA. p16 mRNA has splice variants of almost identical RNA sequences, but we designed a Basescope probe that targets the unique sequence found at its exon junction (Fig. 2.4A). We demonstrated successful differentiation between proliferative and senescent LF1, and between young and old mouse muscles, with p16 Basescope Assays (Fig. 2.4 & 2.5). We have also shown limited success in distinguishing aged human muscles, but we don't expect this probe to be very useful in analyzing the human muscles, as the frequency of p16 signals were too low and only seen with the oldest human muscle samples (Fig. 2.5). Instead, our recommended aging marker in muscles is p21 mRNA. Unlike p16 mRNA found in few of the aged cells, p21 is found in young, proliferative cells as well, and its expression is greatly increased with age (Fig. 2.5).

Another interesting aging marker we explored was ORF1 proteins. ORF1 is one of the two proteins encoded by LINE-1 retrotransposable elements which are shown to increase with age in muscles. We found EPR21844 ORF1 antibody to be very effective in staining ORF1 signals; the

results were consistent, easy to distinguish, and clear in showing the increased expressions with age or a diseased state (Fig. 2.6). ORF1 seems to be expressed in only certain cells, but it would be very interesting to track these ORF1 expressing cells to see how they contribute to the muscle aging.

In exploring various muscle aging markers, it came to our attention that some markers seem to be expressed by only certain types of cells. The skeletal muscles are mostly composed of the functional proteins of the myofibers, but the tissue also contains a number of other cell types. Studies from other tissue environments suggest that different cells demonstrate different progression of aging and exhibit different aging markers. The best aging marker for one type of cell may not be the best aging marker for another cell type of the same tissue. In order to understand the mechanism of aging in skeletal muscle, we need to grasp the full picture of the various aging progressions and mechanisms intertwined by multiple cell types in the tissue. The very first step in this endeavor is to identify the best aging marker specific for each cell type in the muscle. This would allow us to readily identify the aged cells no matter what type it is, and not miss the crucial players in studying the muscle aging.

The RNAscope HiPlex Assay provided a way to study multiple cell types at once through its simultaneous RNA detections. We began by identifying suitable cell type marker for muscle, endothelial, satellite, leukocyte, and fibroadipogenic progenitor (FAPs) cells (Fig. 3.4). Staining a mouse geriatric muscle with these markers showed cell type distribution comparable to what are reported on the literature through RNA sequencing. Although our approach is limited to identifying well known cell types of the established RNA markers, it can be performed on intact muscles and avoid the problem of incomplete digestion often found with the single cell RNA sequencing. The HiPlex Assay also preserves the spatial data which are completely lost with usual RNA analysis. We are able to locate the aged cells which express the RNAs of interest and survey its neighbors to gain an insight on how different cells interact to drive the muscle aging.

Overlaying the HiPlex data on p21 or ORF1 stained muscle samples revealed the identity of p21 or ORF1 expressing cells. We report that most of the p21 signals in aged skeletal muscles originate from the myofibers (Fig. 4.4C). This was a surprising finding because we thought mitotic cell types in the muscles would be the ones entering the senescence and expressing various known aging markers. At least with p21, however, myofibers were responsible for the increased expression with age. ORF1 on the other hand was largely expressed by FAPs and unknown cell types. As FAPs are also known to be responsible for the p16 signals in myofibers, we had already expected to find other aging markers expressed by this cell type. What we didn't expect was the large number of ORF1 positive cells with unknown cell identity. There are some minority cell types we omitted from our study such as tenocytes and neuronal cells, and some of these cell types may be highly expressing ORF1 with age. Another explanation is that the aged cells with ORF1 expression is losing its cell identity and not being detected by the HiPlex probes.

Limitations

One of the biggest limitations of our assays is inability to track the RNA signal to its originating nucleus. For quantification, we assigned the signals to the closest nucleus, but it's possible that the signal came from a further nucleus. Additional staining could better define the boundaries of certain cell bodies but because cells are squeezed in between the peripheral spaces of the myofibers, some cell bodies are overlapped when looking through the triplet lateral sections spanning 21 μm. We accept that not all of our signal assignment would be accurate but expect most to be correctly assigned and is sufficient to depict the general trends of RNA expressions.

Another major limitation of the RNA FISH approach is that it can only be used with known RNA markers. We can't learn what RNAs are expressed in the tissue. We can only locate RNAs that are already known or suspected to be found in the tissue. Some well-known cell type or aging markers are detected by antibodies but the RNA counterparts for these protein markers may not

be as good. CD45, for instance, was a good immune cell marker when detected with the antibodies but targeting RNA sequence of CD45 did not reliably identify the immune cells.

Performing multiple assays over two or three consecutively cut muscle sections raises inaccuracy and lowers the efficiency of the assays. Although most cells seem to be preserved across the three sections, some nuclei are clearly absent or newly introduced in a section. Even for the nuclei that seem to be present in all three sections, it's possible that the rare RNA molecule of interest happened to reside on one side of the cell that we did not look at. All of the RNAscope based assays are very tedious and time-consuming procedure. Stacking multiple of these assays for an analysis limits how many samples we can process in a reasonable window of time. We would have liked to look at more mice and more age groups to get better quantification data, but the time and resource it takes to process each sample deters any attempt of high throughput analysis.

Future directions

We have done extensive studies with mouse and human muscles, but our analysis can very well be applied to other tissue types. In our pilot experiments, we saw promising results of the Basescope Assays with mouse lungs, brain, heart, and kidney tissues (data not shown). Depending on the tissue type, the optimal fixation and protease digestion time changes, but otherwise identical procedure is applied to all tissue types.

So far, we found p21 RNA to be a good aging marker for myofibers and ORF1 to be interesting marker to investigate further. p16 RNA was an acceptable marker for mouse samples but in our limited testing with the human muscle samples, it did not have high enough frequency for any useful analysis. However, for human p16, there are already well established antibodies that are routinely used in clinical settings. CINtec® p16 Histology is one that we found to work very well with the human samples. Figure 5.1A shows 1 month senescent LF1 staining brown with

the CINtec p16 antibody staining. This staining was actually too strong with the manufacturer's recommended 8 minutes incubation, so for the 4 months senescent LF1 staining, we only incubated for 5 minutes. We also confirmed that the assay is sensitive enough to show the changes in p16 expression. In Figure 5.1B, 4 months senescent LF1 treated with 3T3 showed reduced brown staining compared to the non-treated senescent LF1. It would be interesting to overlay the p16 staining of the geriatric mouse muscle with the HiPlex Assay we developed.

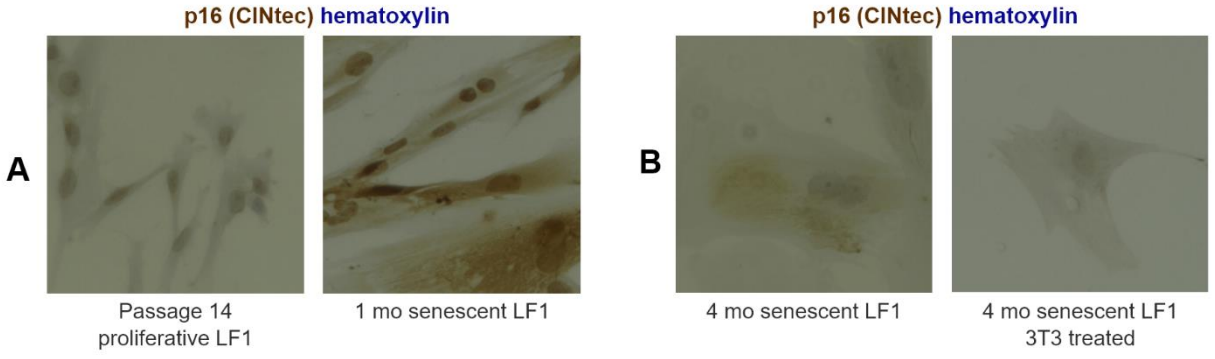

Figure 5.1. CINtec p16 Histology for human p16 protein detection. (A) p16 staining on proliferative (left) and senescent (right) LF1 using p16 CINtec Histology, 8 minutes incubation. (B) p16 staining on senescent LF1 with (right) and without (left) 3T3 treatments using p16 CINtec Histology, 5 minutes incubation.

Ultimately, we could create a comprehensive reference of various known aging markers and show which cell types exhibit which set of markers at what stage of aging (Fig. 5.2). This would require making a list of promising RNA aging markers through literature search and designing appropriate HiPlex probes. If we can find the working HiPlex probes for the aging markers, we can simply run one HiPlex assay with various cell type and aging markers and see which cell types exhibit the tested markers with age. This would not only guide us through the complex mechanisms of muscle aging, but also help any laboratory interested in studying the role of specific cell types at specific stages of muscle aging to quickly identify the relevant markers. From what we know so far, we can create a smaller reference: p21 mostly from the myofibers at early stages of aging, followed by p16 and ORF1 from FAPs at later stages of aging.

Finally, we would like to highlight the usefulness of the background subtraction tool built in the RNAscope Image Registration Software. Our early efforts in studying the intact geriatric muscles were often hurdled by the persistent autofluorescence. We had tried physical and chemical methods of quenching this autofluorescence, but nothing really worked (Appendix A). The background subtraction tool of the Image Registration Software, however, work extremely well. For younger muscles, there is absolutely no autofluorescence left and for the oldest muscles, the noise is rare and usually negligible. We think this tool can be applied for other IF assays and greatly enhance the quality of the analysis. Markers that we previously decided not to use because they were too weak and dim, can now be employed again using the background subtractions. Together with signal amplification strategies (Fig. A1.1C), the incorporation of the background subtraction should greatly increase the number of tools we can utilize in studying intact muscles.

RNA Marker	RNA Expression by Age	2 - 3 months	6 - 9 months	12 - 16 months	20 - 25 months	30 - 36 months
A						
B						
C						
D						
E						

Figure 5.2. Speculated look of the reference data. Made up data that can be used as a reference page to quickly identify set of RNA markers to use for studying specific cell type and stage of muscle aging. Pie charts show cell type distribution of the cells expressing the RNA marker of interest.

Appendix A:

Addressing the Autofluorescence

Muscles are notorious for high autofluorescence in the green channel. In addition to this inherent autofluorescence of the muscles, we had to deal with the increased autofluorescence with aged cells. Senescent cells are known to accumulate lipofuscin and lipofuscin like compounds in the cytoplasm. Under oxidative stress, these compounds aggregate and create dotted fluorescence at a wide spectrum of wavelengths (Fig.A1.1B). In Figure A1.1A, we have recorded these autofluorescence from etoposide induced senescent LF1 using all available channels of the Nikon Ti2-Eclipse Fluorescence Microscope. The autofluorescence peaked at 488, and was high between 546 and 568. We tried keeping the samples out under the light for few days before staining, and also letting the sample getting bleached by lasers before amplifying the signals, but nothing seemed to help much. To see if using different cell line mediates the problem, we used etoposide treatment to induce senescence of the IMR90 cells. Figure A1.1C shows etoposide induced senescent IMR90 stained with p16; we amplified the p16 signal using Tyramide Signal Amplification Kit (Thermo Fisher Scientific). The autofluorescence of senescent IMR90 cells was even worse, producing high autofluorescence in all tested channels. We tried using FFPE autofluorescence quenching solution from Advanced Cell Diagnostics on senescent IMR90 and saw noticeable reductions in the autofluorescence (Fig. A1.1D). Signals persisted at weaker intensity in 488 channel, but were almost completely eliminated from the red channels. Applying this to the muscle sections did seem to dim the overall autofluorescence from the young and old samples (data not shown) but by this time, we have learned about the background subtraction tool of the RNAscope Image Registration Software. The use the software quickly and efficiently removed all signals from the background. The tool allows modifying the parameters of its algorithm and we found that the optimal results for the muscle samples were obtained within ±0.2 value of the default. As the default values did just as good job in removing the background, we performed our analysis without modifying the values.

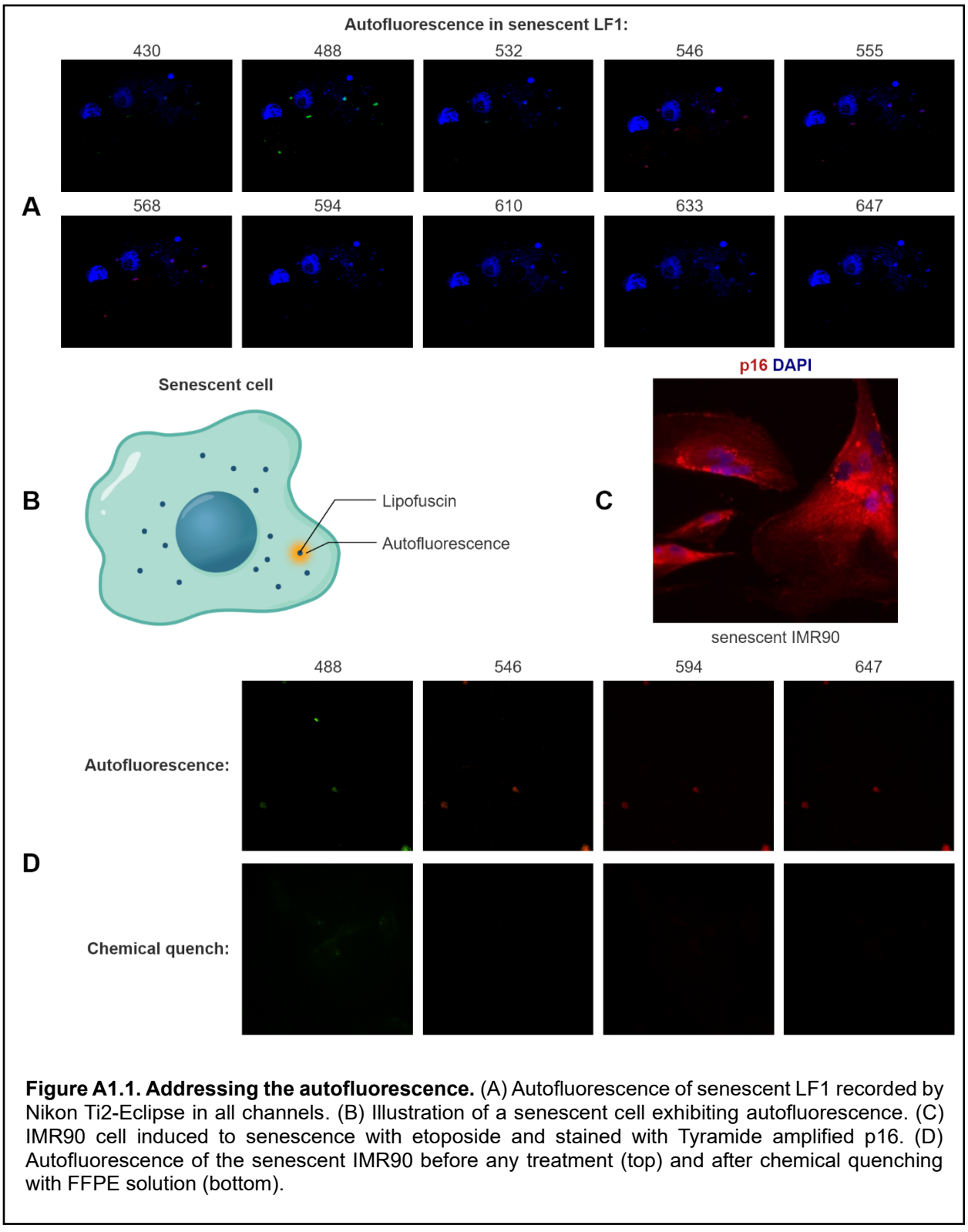

Figure A1.1. Addressing the autofluorescence. (A) Autofluorescence of senescent LF1 recorded by Nikon Ti2-Eclipse in all channels. (B) Illustration of a senescent cell exhibiting autofluorescence. (C) IMR90 cell induced to senescence with etoposide and stained with Tyramide amplified p16. (D) Autofluorescence of the senescent IMR90 before any treatment (top) and after chemical quenching with FFPE solution (bottom).

Appendix B:

Quantifying Basescope Results in Muscles

One of major limitations of the Basescope Assay is with the uncertainty of assigning RNA signal to its originating nucleus. This means we are able to count actual numbers of RNA signals in the sample, but we can never assess the accurate number of the RNA expressing cells. To estimate the number of cells expressing RNAs of interest, we formulated an algorithm that can be used in a bulk analysis. As we are working with myofibers which have multi nucleated cell bodies, finding the number of RNA producing nuclei is not technically finding the number of RNA producing cells. However, for the simplicity of the explanation, we will just say each nucleus is an individual cell for any cell type here, as this algorithm may be applied to any tissue assessed with Basescope Assay.

The rationales of this algorithm are shown in Figure A2.1A. The first rationale is that each RNA signal can only be associated with maximum of one nucleus. It's not possible for the RNA molecule to be made by multiple nuclei. This means that the maximum number of the RNA producing nuclei is equal to the number of RNA signals counted from the sample.

The second rationale is that each nucleus may be associated with more than one signal. If there are multiple signals in a small area, they could all be originating from one nucleus or from multiple nuclei. But there must be a limit to how far a signal can be associated with a nucleus (rationale 3). And this maximum distance between a signal and its nucleus would eventually be observed when we look at enough data (rationale 4). We can take the conservative approach and assume that the RNA came from the closest nucleus, which may be 50 pixels away or 200 pixels away. If we take enough measurements, we will accumulate thousands of the minimum distances between a signal and a nucleus and they will form a bell-shaped curve. The greatest distance we find in the data would be the best approximation of the maximum distance RNA can travel from the nucleus. If this value changes with added data, it narrows down the estimation further and give even better estimation. Even when using a distance much smaller than the actual maximum distance, our estimation is not wrong; it just provides the wider range of possible cell counts.

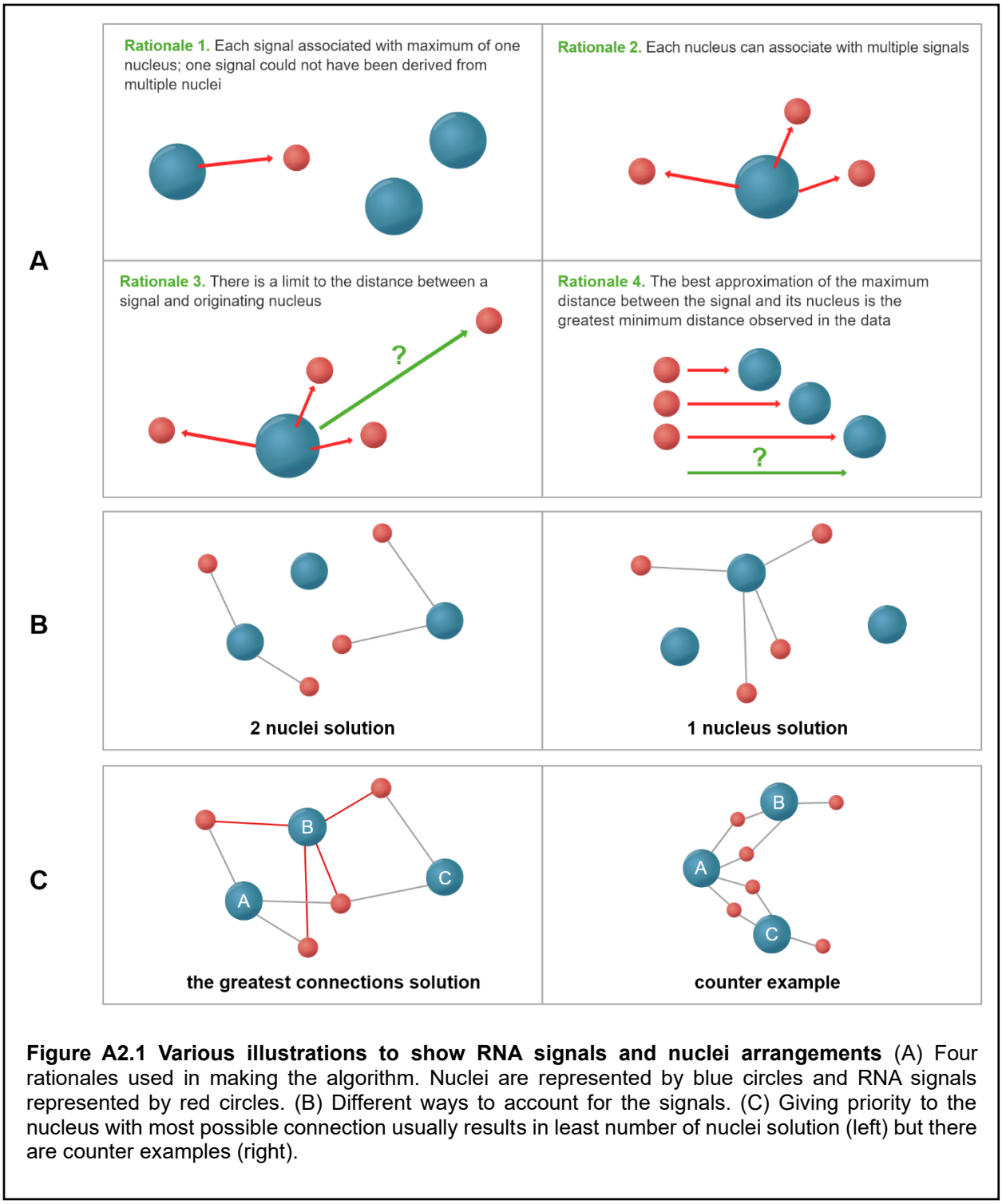

Figure A2.1 Various illustrations to show RNA signals and nuclei arrangements (A) Four rationales used in making the algorithm. Nuclei are represented by blue circles and RNA signals represented by red circles. (B) Different ways to account for the signals. (C) Giving priority to the nucleus with most possible connection usually results in least number of nuclei solution (left) but there are counter examples (right).

To narrow down the lower range of the estimation (the minimum possible cell count responsible for the RNA signals), we have to think about different ways in which signals can be associated with the nuclei within the distance maximum identified. Figure A2.1B illustrates two examples where different numbers of responsible nuclei are determined from the same arrangement of signals and nuclei. Since we have to find the smallest possible cell count that can produce all signals, the best solution for the example is one in Figure A2.1C, where all signals originate from nucleus B. Finding the smallest number of nuclei responsible for the signal can be achieved by trying all combination of signal and nuclei and selecting for the one that involved least number of nuclei. However, this calculation quickly becomes impractical and often impossible with how many nuclei and signals we observe in each field of view. An alternative approach is to find a general pattern of the best solution and try making the estimate using the pattern. We realized that the best solution for most sets of arrangements was when a nucleus with most signals within its maximum distance was allowed to be associate with those signals first. Figure A2.1C left image, for example, had nucleus B surrounded by 4 signals all within its reach. When we allowed nucleus B to be associated with those 4 signals before considering the involvement of other nuclei, we arrived at the best solution. However, this approach is not always correct. In Figure A2.1C right image, we illustrated a counter example where nucleus A can be associated with 4 signals, nuclei B and C can each be associated with 3 signals. If we let nucleus A to associate with the 4 signals, we also require B and C to take care of the signals in the far right. We end up needing all three nuclei to take account of the observed signals. However, if we choose to associated nuclei B and C, they would each take 3 signals and complete the solution. This time, it only involved two nuclei to take care of all observed signals. Despite being able to think of a counter solution, we saw giving priority to the nuclei with most associations to generally work and decided to employ this to our scripts.

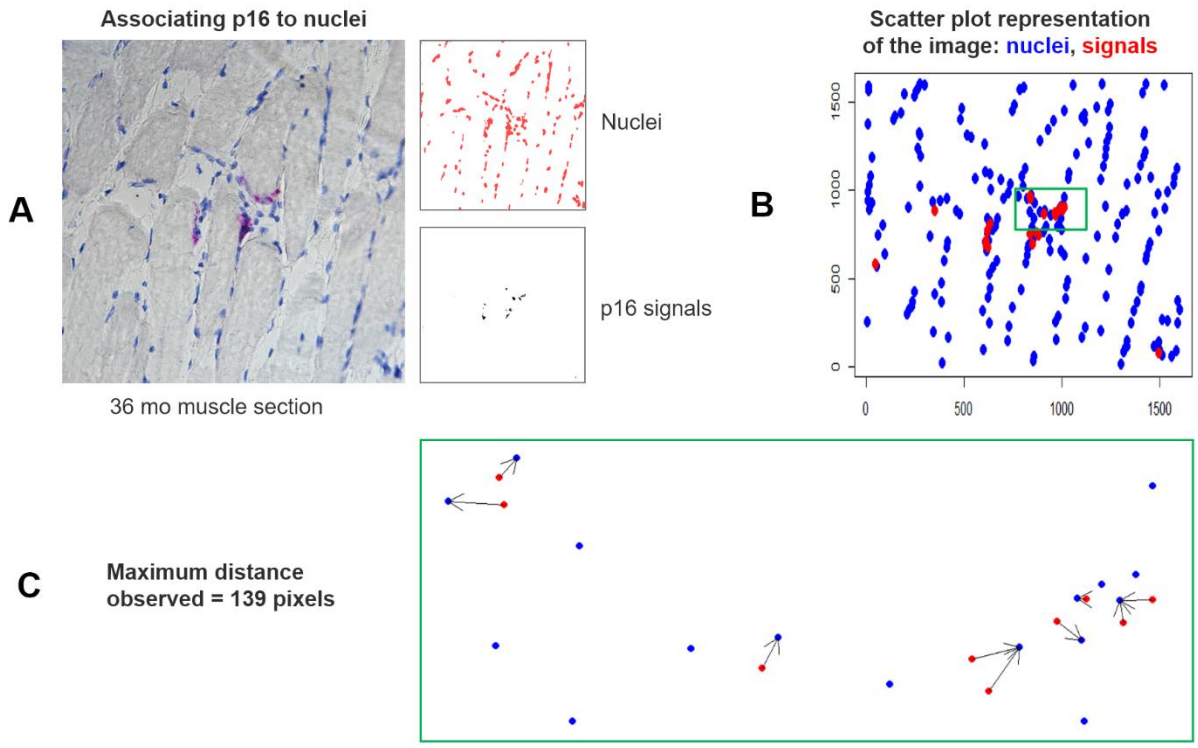

Figure A2.2. Working with the real data to find the distance maximum (A) The result from a Basescope p16 staining on 36 months mouse muscle. Using ImageJ, nuclei signals and p16 signals were separated and assigned different colors. (B) Center points of various signals determined, and coordinates assigned over a dot diagram. (C) Zoomed in view of an area showing arrows between a signal and its closest nucleus. The greatest minimum distance observed here was 139 pixels.

We took Basescope Assay data from p16 staining of 36 months mouse muscles to retrieve the nuclei and RNA signals (Fig. A2.2A). We found the center points of the signals and assigned coordinates over a dot diagram (Fig. A2.2B). We then calculated distance between each RNA signal and its closest nucleus and got 139 pixels as the greatest observed minimum distance. We then created a matrix of all RNA signals vs all nuclei signals found in the field of view (Fig. A2.3A). There were 21 RNA signals and 63 nuclei signals in total and whenever RNA signal was within 139 pixels of the nucleus, we assigned value of 1. If the distance was greater than 139 pixels, we assigned value of 0. The sums of the connection values are shown at the bottom of the matrix and can be interpreted as the number of possible connection each nucleus can make. The greatest connection in this example was made by nucleus 41, highlighted green (Fig. A2.3B).

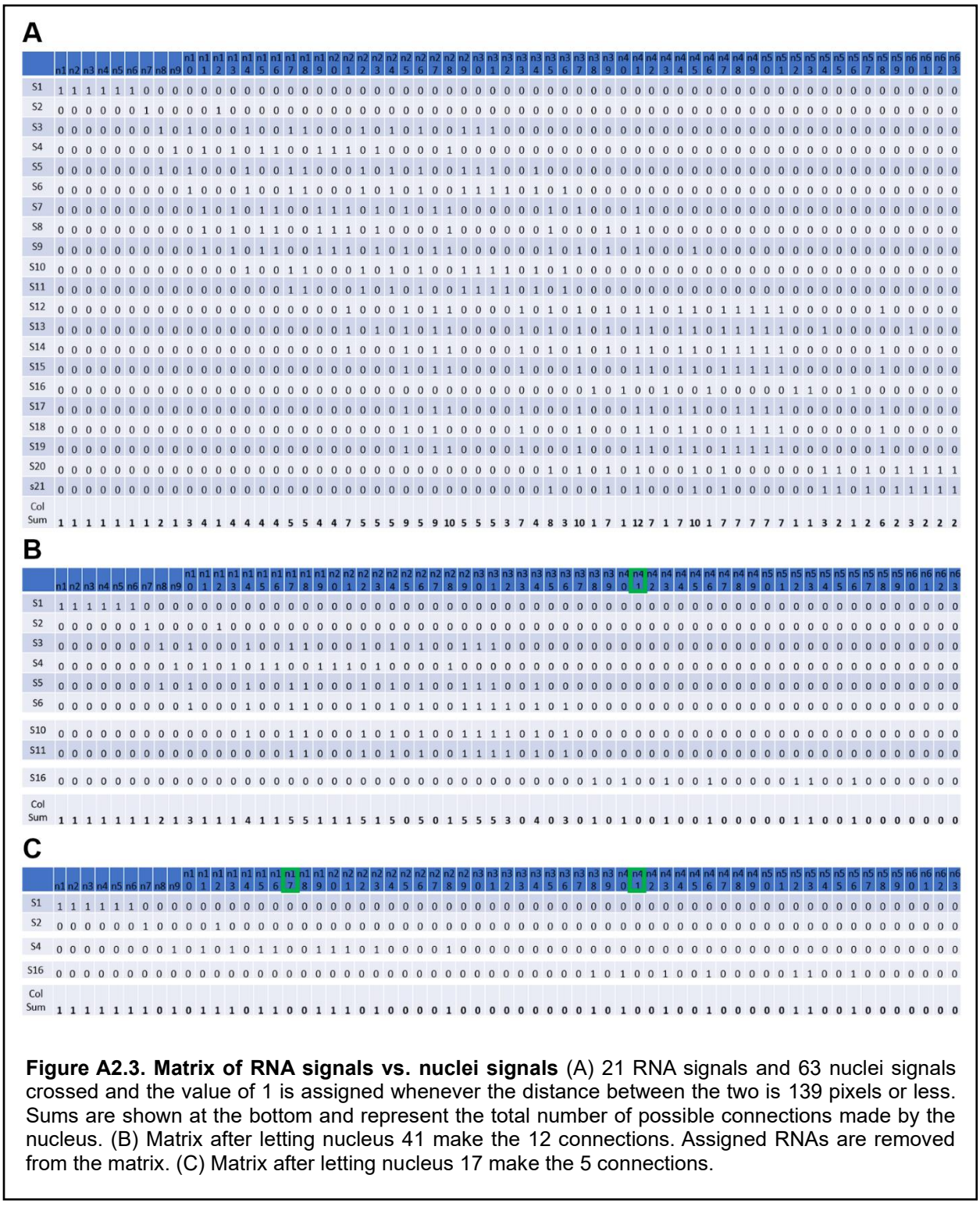

Figure A2.3. Matrix of RNA signals vs. nuclei signals (A) 21 RNA signals and 63 nuclei signals crossed and the value of 1 is assigned whenever the distance between the two is 139 pixels or less. Sums are shown at the bottom and represent the total number of possible connections made by the nucleus. (B) Matrix after letting nucleus 41 make the 12 connections. Assigned RNAs are removed from the matrix. (C) Matrix after letting nucleus 17 make the 5 connections.

Nucleus 41 was given the priority and allowed to make association with all RNA signals within 139 pixels. 12 RNA signals had been associated and removed from the matrix. The next greatest connection was now made by nucleus 17, highlighted green in Figure A2.3C. It was also allowed to associate with RNAs within 139 pixels and 5 RNA were removed. Note that multiple nuclei had 5 possible RNA associations but nucleus 17 came up first when scanning left to right and was given the priority. This process was repeated until no RNA is left in the matrix. The number of nuclei that was allowed to associate with one or more RNA is calculated.

We applied this script to ten other fields of view (Fig. A2.4A). We identified 264 as the greatest minimum distance between a RNA and a nucleus and updated our distance maximum value in the script. The range of possible p16 positive nuclei are shown in Figure A2.4B along with estimated frequency of senescent cells in muscle, which was comparable to known senescence frequency in other tissue environments.

A

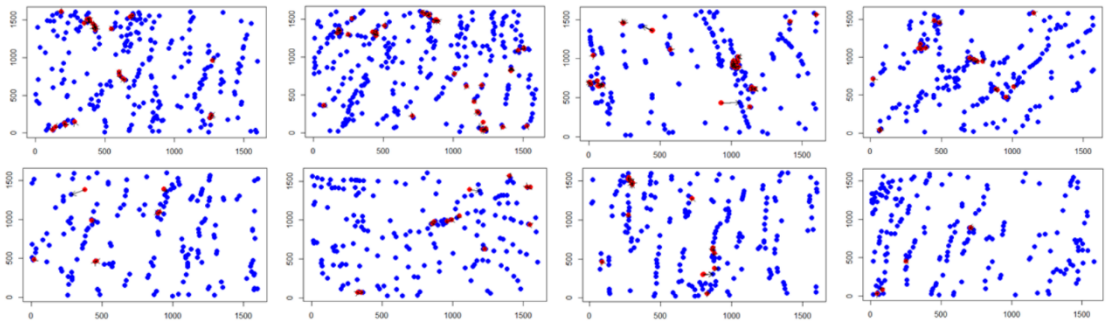

B

	i1	i2	i3	i4	i5	i6	i7	i8	i9	i10
Nuclei	214	239	266	474	189	173	171	193	186	207
Signals	21	29	43	42	20	8	13	17	5	10
Max distance (pixels)	139	235	264	154	188	145	169	183	109	195
P16+ nuclei	4-21	6-29	8-43	6-42	7-20	4-8	5-13	5-17	3-5	3-10
Frequency	1.87-9.81%	2.51-12.13%	3.01-16.17%	1.27-8.86%	3.70-10.58%	2.31-7.51%	2.92-7.60%	2.59-8.81%	1.61-2.69%	1.45-4.83%

Figure A2.4. Applying the script to ten fields of views. (A) Basescope data from 10 fields of view processed and shown over dot diagrams with minimum distances. (B) Results of the matrix analysis. The greatest minimum distance (the distance maximum) is now 264 pixels. The range of possible p16 positive cell counts are shown. Estimated frequencies of senescent cells in muscles are comparable to what are reported in the literatures.

Appendix C:

Detecting LINE-1 Polymorph Sequences

LINE-1 retrotransposable elements used to have a GAG sequence in its 3' UTR. These LINE-1s are still found in the primates including humans. In humans, we also have a mutant sequence where GAG is changed to ACA. This is the currently active version of LINE-1 sequence found in human. Distinguishing between the two sequences by RNA FISH had been impossible with traditional technologies. We worked closely with Advanced Cell Diagnostics to make Basescope probes that can distinguish LINE-1 polymorph sequences. These polymorph sequences are only different in three nucleotides (ACA vs GAG) and to distinguish the two is really pushing the limitation of the Basescope technology. We chose ~50 bp sequence surrounding the polymorph site and made probes for the ACA and GAG versions of the sequence and also for their reverse complement sequences (Supp. Data 2). These probes are referred to as L1-ACA, L1-ACAR, L1-GAG, or L1-GAGR.

We first tested our probes in human senescent cells (LF1). Figure A3.1A shows p16 staining of the normal and replicatively senescent LF1 cells; p16 Basescope showed positive signals only with the senescent cells. Figure A3.1B shows the results of L1-ACA and L1-GAG staining of the senescent LF1. In both cases, we see positive signals indicative of the L1 sequences in senescent LF1. We then tested baboon fibroblasts as our non-human primate samples. Figure A3.1C shows p16, L1-ACA, and L1-GAG staining on proliferative (passage 7) baboon fibroblasts on top and 2 weeks post etoposide treated senescent baboon fibroblasts on the bottom. Nothing was detected from the proliferative cells, while some p16 signals are detected with senescent baboon fibroblasts. L1-ACA did not detect anything from senescent baboon fibroblasts but L1-GAG detected some signals from senescent baboon fibroblasts. These data support our understanding that non-human primates only have the original GAG version of the LINE-1 and our probes are able to distinguish between the two polymorph sequences.

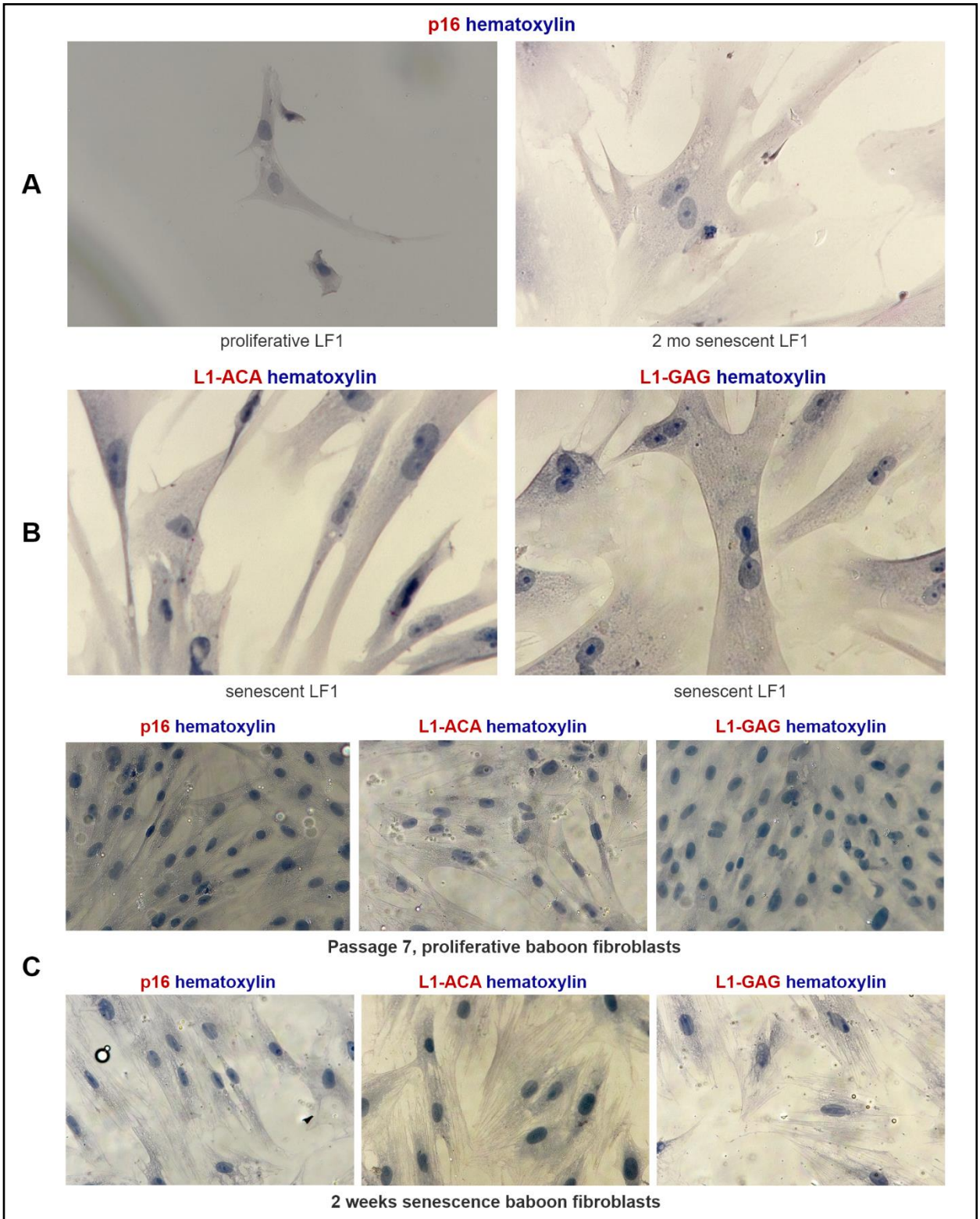

Figure A3.1. L1 polymorph sequences against human and baboon fibroblasts (A) Basescope p16 showing senescence of human LF1 (B) Basescope L1-ACA and GAG probes staining positive in senescent LF1 (C) Only L1-GAG and not ACA detected with senescent baboon fibroblasts.

To further analyze the distinguishing power of our L1 probes, we needed a model where we have the complete control over the expressed LINE-1 sequences. We chose to use the NIH 3T3 mouse fibroblast cell line. As this is a mouse cell line, there is no endogenous human LINE-1 expression. We made sure that our L1 probes do not detect anything from the mouse genome as well. This complete control over LINE-1 sequences also allows us to mathematically determine and distinguish between false positives that come from the probe mismatch and from general unspecific binding (Supp. Data 3).

To introduce LINE-1 sequence to the mouse cells, we performed FugeneHD transfection with plasmids containing the part of the LINE-1 sequence we are interested in. Figure A3.2A shows the transfection result of the 3T3. The plasmid had GFP reporter. Image on the left shows untransfected 3T3 without any green signal, the image at the center shows 48 hours post transfection result with ACA plasmid, and the image at the right shows 48 hours post transfection result with GAG plasmid. The transfected cells were then stained with the L1 probes and the results are shown in Figure A3.2B. For the most part, the greatest signals are seen when the tested probes matched with the transfected sequence. However, we did see that the probes also detected mismatched polymorph sequence at a reduced efficiency. Because these cells were expressing LINE-1 sequence at unusually high levels, the small chances of picking up the mismatch sequence had been amplified. In usual physiological settings, we expect most of the detected signals to be from the matching pair of probe and sequence. Nonetheless, we wanted to investigate whether the distinguishing power of our probes can be enhanced. The most obvious way of affecting probe hybridization and specificity is to adjust the hybridization temperatures. We set out to perform the assay on various temperatures to determine the most optimal hybridization conditions for the greatest distinguishing power. Figure A3.2C shows the result of this temperature tweaking. We observed that 48°C was the best temperature for most probes, although in certain cases, 46°C might be having better distinguishing powers. The mismatched false positives usually

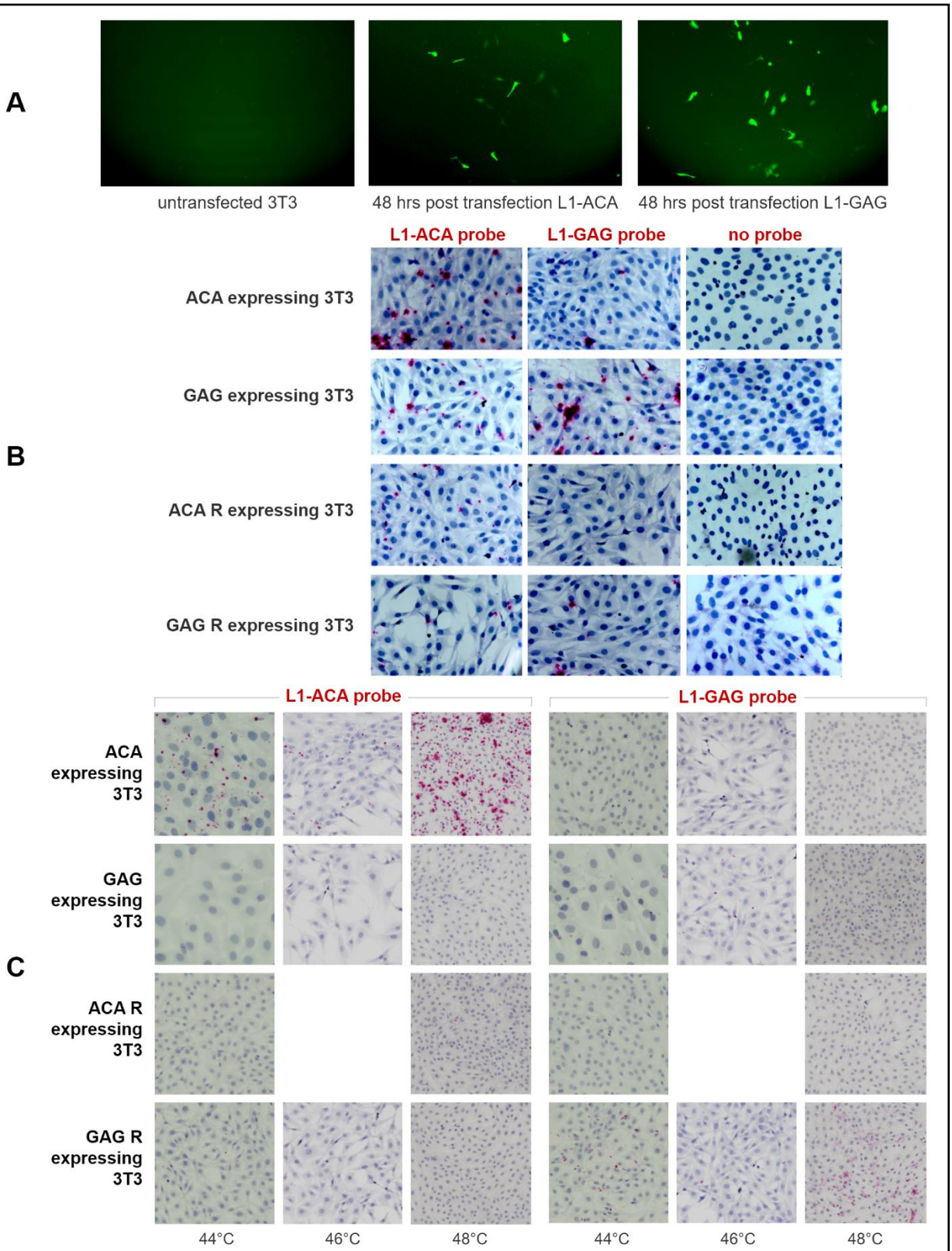

Figure A3.2. Testing distinguishing powers of L1 probes with L1 transfected 3T3. (A) 3T3 mouse fibroblasts transfected with partial L1 sequences. (B) L1 probes tested on transfected 3T3. (C) L1 probes tested at various hybridization temperatures with 3T3 transiently expressing L1.

occurred with the probe and its reverse complement sequence. We lost some data for the ACA reverse complementary sequence transfected 3T3.

The disparities in the results may be due to the varying transfection efficiency. We decided to create single cell clones stably expressing various LINE-1 sequences. We were able to produce some clones that stably expressed high level of LINE-1 sequence and also replicated without problem. Figure A3.3A shows one exemplary clone expressing L1-ACA. Here, we see every cell exhibiting GFP indicative of the successful transfection, we had no problem expanding the cultures, and they all consistently expressed L1-ACA as shown with the Basescope Assay. However, this was not the case with most clones. Figure A3.3B shows the typical result of the transfection. Here, we are showing cells transfected with GAG reverse complement sequence. Even though we picked out single cells of high GFP expression, when they were expanded we often found that only some cells were continuing to express the GFP. And for some reason, GFP expressing cells did not replicate well. We tried serial dilutions and multiple single cell selection attempts, but failed to find a clone that replicated well while maintaining LINE-1 expressions. One of the reasons we had hard time finding the perfect single cell to expand was the extremely low chance of the stable transfection. Figure A3.3C shows typical example of the cells selected for the stable transfection. Even though they are all resistant to the selection, only a dozen cell out of the entire 10 cm dish had had GFP expression, and most of these cells were not replicating. We had to go through many dozens of transfected cell cultures to find a couple of single cells that stably expressed LINE-1 sequence. To increase the transfection efficiency, we tried using 4D nucleofection, which claimed over 90% transfection rate. In our hands, however, only ~11% of the million cells were transfected and if we assume 0.01% of the transfected result in the stable expression, we only get about 10 potentially good single cells out of each transfection attempt. Since most of the 10 cells are not replicating, we end up having to go through multiple transfections to find one that works. This rate was not much better than FugeneHD transfection,

which had about half the efficiency of the 4D nucleofection but made up by being able to transfect two million cells at once in a 10 cm dish. As making good clones for all sequences took too much time, we decided to revisit this later.

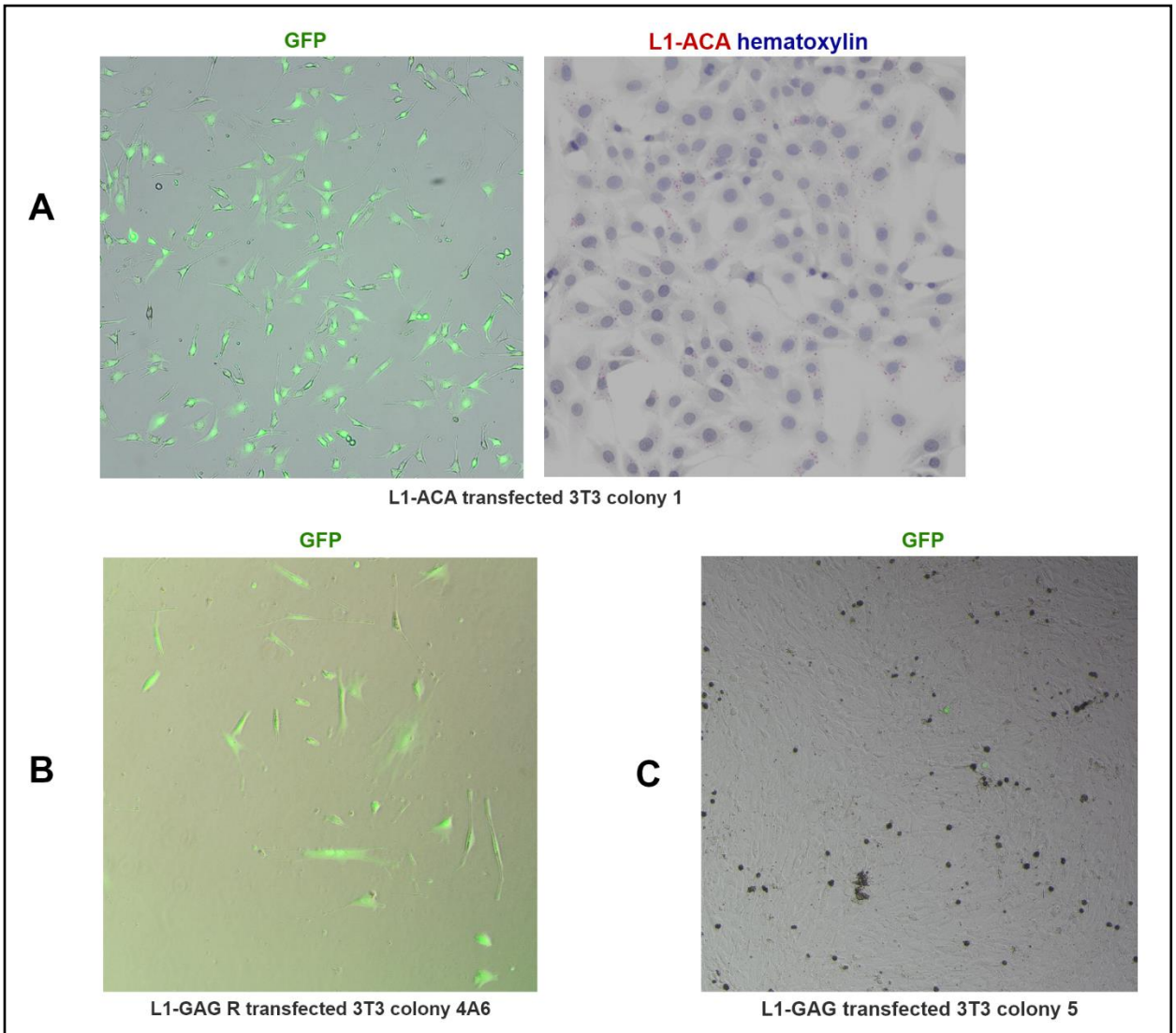

Figure A3.3. Attempts at making stably expressing 3T3. (A) An example of a good clone. All cells express GFP indicative of successful transfection and they all show L1 expression when tested with the probe. (B) Example of typical single cell expansion where not all cells end up being GFP positive. (C) Usual stable transfection rate was about 10 per 1 million cells transfected. Only few GFP positive cells remain in the dish as shown after the selection periods and they are often non-replicating.

Supplementary Data

probe 1	ggcttgcttaggtaaacaaa	probe 20	gaaggaaatagagacacaaa	probe 39	tatgcagccaaaaaacacat
probe 2	acagacaaacaaaaagacag	probe 21	aaattgatagaccgctagca	probe 40	tctcacaccagttagaatgg
probe 3	aacctctgcagacttaagtg	probe 22	tacaaacacctctacgcaaa	probe 41	acttttacactgttggtggg
probe 4	tctgacagctttgaagagag	probe 23	cagagacacaaccaaaaaag	probe 42	ccattgtggaagtcagtgtg
probe 5	catctacaccgaaaacccat	probe 24	atgcagaaaaagcctttgac	probe 43	cccattactgggtatatacc
probe 6	attcaaaccaaaggcaaaga	probe 25	gctatctatgacaaacccac	probe 44	tataaagacacatgcacacg
probe 7	accaatacagagaagtgctt	probe 26	aaaactggaagcattccctt	probe 45	tcacaatagcaaagacttgg
probe 8	cgagaactacgtgaagaatg	probe 27	agaaggaaataaagggtatt	probe 46	acccaaatgtccaacaatga
probe 9	gcaaagcctccaagaaatat	probe 28	gaggaagtcaaattgtccct	probe 47	aaaaaaccaaacaccgcata
probe 10	attatccaggagaacttccc	probe 29	caacttacaagggatgtgaa	probe 48	cgattacaaggatgacgatg
probe 11	ctaggaagaaactgcatcaa	probe 30	ccactgctcaaggaaataaa		
probe 12	agactttaacaccccactgt	probe 31	gacaaacaaatggaagaaca		
probe 13	tcccacacattaataatggg	probe 32	cctaagccaaaagaacaaag		
probe 14	acaccccactgtcaacatta	probe 33	gcatcacactacctgacttc		
probe 15	agcagacctaatagacatct	probe 34	tgaaactggatcccttcctt		
probe 16	accacagtgcaatcaaacta	probe 35	acctaggcattaccattcag		
probe 17	gagaacaaagacaccacata	probe 36	cagcatggcacatgtataca		
probe 18	agcaggaaagatccaaaatt	probe 37	acagcaaaagaaactaccat		
probe 19	aaagcaagagcaaacacatt	probe 38	aacaaccccatcaaaaagtg		

Supplementary Data 1. L1HS Stellaris Probes sequences. The sequences of 48 Stellaris Probes used for L1HS detection shown.

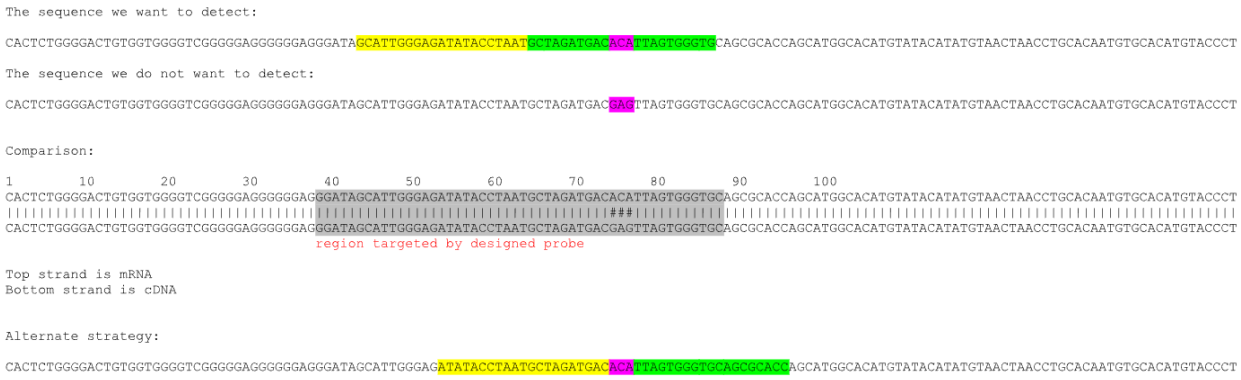

Supplementary Data 2. L1 polymorph specific Basescope probes design. 39-88 of the L1 sequence excerpt was targeted by the Basescope and screened against the mouse genome to make sure no other sequence is detected by the probe.

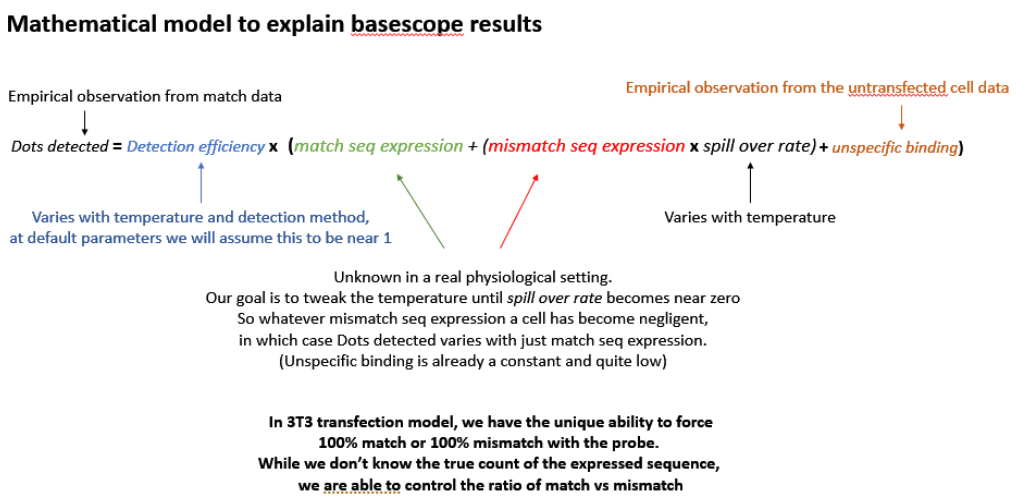

Supplementary Data 3. Mathematical determination of two sources of the false positives. Using L1HS expressing 3T3 mouse cell line allows us to control the variables to calculate false positives from mismatch vs unspecific binding. In real data example with ACAR stably expressed in 3T3 hybridized at 40C, a field of view containing 15.5 nuclei and 132 ACAR RNA signals demonstrates ACAR expression of 8.52 RNA per nucleus. Same probe used on untransfected 3T3 showed 1 signal per 29 nuclei, or 0.03 RNA unspecifically bound per nucleus. Assuming detection efficiency of 1, match sequence expression according to the equation comes out to be 8.49 per nucleus. Same ACAR expressing 3T3 tested with GAGR probe resulted in 1.92 signals per nucleus. We already know this cell is expressing 8.49 ACAR sequence per nucleus, which in this case act as the mismatch seq expression. The equation is now 1.92 signal/nucleus = 8.49 signal/nucleus x spill over rate. Solving for the spill over rate, we get 0.23. We can conclude that at 40C, for every mismatch sequence expressed (GAGR), our ACAR probe falsely detects as a positive match at 23% chance.